

NASA/TM-2012-217601



Algorithm for Simulating Atmospheric Turbulence and Aeroelastic Effects on Simulator Motion Systems

*Anthony V. Ercole and Frank M. Cardullo
State University of New York, Binghamton, New York*

*Lon C. Kelly
Unisys Corporation, Hampton, Virginia*

*Jacob A. Houck
NASA Langley Research Center, Hampton, Virginia*

August 2012

NASA STI Program . . . in Profile

Since its founding, NASA has been dedicated to the advancement of aeronautics and space science. The NASA scientific and technical information (STI) program plays a key part in helping NASA maintain this important role.

The NASA STI program operates under the auspices of the Agency Chief Information Officer. It collects, organizes, provides for archiving, and disseminates NASA's STI. The NASA STI program provides access to the NASA Aeronautics and Space Database and its public interface, the NASA Technical Report Server, thus providing one of the largest collections of aeronautical and space science STI in the world. Results are published in both non-NASA channels and by NASA in the NASA STI Report Series, which includes the following report types:

- **TECHNICAL PUBLICATION.** Reports of completed research or a major significant phase of research that present the results of NASA Programs and include extensive data or theoretical analysis. Includes compilations of significant scientific and technical data and information deemed to be of continuing reference value. NASA counterpart of peer-reviewed formal professional papers, but having less stringent limitations on manuscript length and extent of graphic presentations.
- **TECHNICAL MEMORANDUM.** Scientific and technical findings that are preliminary or of specialized interest, e.g., quick release reports, working papers, and bibliographies that contain minimal annotation. Does not contain extensive analysis.
- **CONTRACTOR REPORT.** Scientific and technical findings by NASA-sponsored contractors and grantees.

- **CONFERENCE PUBLICATION.** Collected papers from scientific and technical conferences, symposia, seminars, or other meetings sponsored or co-sponsored by NASA.
- **SPECIAL PUBLICATION.** Scientific, technical, or historical information from NASA programs, projects, and missions, often concerned with subjects having substantial public interest.
- **TECHNICAL TRANSLATION.** English-language translations of foreign scientific and technical material pertinent to NASA's mission.

Specialized services also include organizing and publishing research results, distributing specialized research announcements and feeds, providing information desk and personal search support, and enabling data exchange services.

For more information about the NASA STI program, see the following:

- Access the NASA STI program home page at <http://www.sti.nasa.gov>
- E-mail your question to help@sti.nasa.gov
- Fax your question to the NASA STI Information Desk at 443-757-5803
- Phone the NASA STI Information Desk at 443-757-5802
- Write to:
STI Information Desk
NASA Center for AeroSpace Information
7115 Standard Drive
Hanover, MD 21076-1320

NASA/TM-2012-217601



Algorithm for Simulating Atmospheric Turbulence and Aeroelastic Effects on Simulator Motion Systems

*Anthony V. Ercole and Frank M. Cardullo
State University of New York, Binghamton, New York*

*Lon C. Kelly
Unisys Corporation, Hampton, Virginia*

*Jacob A. Houck
NASA Langley Research Center, Hampton, Virginia*

National Aeronautics and
Space Administration

Langley Research Center
Hampton, Virginia 23681-2199

August 2012

Acknowledgments

We would like to thank Kirill Zaychik for his exceptional insight throughout the course of this research. Our appreciation is extended to Harry Verstynen of NASA Langley Research Center for piloting all experiments and for his exceptional contribution to the subjective analysis and tuning of the algorithms. Our gratitude also extends to all other members of NASA Langley Research Center who assisted in the on-site testing and tuning of these algorithms.

The use of trademarks or names of manufacturers in this report is for accurate reporting and does not constitute an official endorsement, either expressed or implied, of such products or manufacturers by the National Aeronautics and Space Administration.

Available from:

NASA Center for AeroSpace Information
7115 Standard Drive
Hanover, MD 21076-1320
443-757-5802

Abstract

Atmospheric turbulence produces high frequency accelerations in aircraft, typically greater than the response to pilot input. Motion system equipped flight simulators must present cues representative of the aircraft response to turbulence in order to maintain the integrity of the simulation. Currently, turbulence motion cueing produced by flight simulator motion systems has been less than satisfactory because the turbulence profiles have been attenuated by the motion cueing algorithms. There have been advances in motion cueing algorithm development at the Man-Machine Systems Laboratory, at SUNY Binghamton. In particular, the system used to generate turbulence cues has been studied. An investigation of this implementation indicated that the turbulence simulation produced inadequate cues and caused the simulator motion platform to diverge during long runs.

This report presents a new turbulence motion cueing algorithm, referred to as the augmented turbulence channel. Like the previous turbulence algorithms, the output of the channel only augments the vertical degree of freedom of motion. This algorithm employs a parallel aircraft model and an optional high bandwidth cueing filter.

Simulation of aeroelastic effects is also an area where frequency content must be preserved by the cueing algorithm. The current aeroelastic implementation uses a similar secondary channel that supplements the primary motion cue with aeroelastic oscillations. This particular model computes the pitch and yaw axes fuselage bending of a slender, high-speed, transport aircraft. Integration of the augmented turbulence channel and aeroelastic model was completed to allow high frequency motion from both sources to augment the cueing algorithm. Offline testing was performed to examine the frequency content of the augmented motion cues. Upon completion of this testing, the algorithm was implemented on two NASA Langley Research Center flight simulators: the Visual Motion Simulator and the Cockpit Motion Facility, and subjectively tuned to specifications detailed in the Federal Aviation Administration Airman's Guide to Turbulence Reporting.

Two studies were conducted to evaluate the effect of the turbulence channel and aeroelastic model on pilot control input. Quantitative results of the experiments indicate that while compensating for atmospheric turbulence, the pilot is better correlated with the aircraft

response, when the augmented channel is in place. During the severe turbulence runs, with the augmented channel, results indicate that the pilot is unable to compensate for the turbulence intensity. Subjective results of the studies show that during most runs, the augmented turbulence channel increased the necessary compensation to adequately perform the task. This demonstrates that the added motion induces more work from the pilot. It is recommended that a multi-pilot study be conducted to verify the turbulence algorithm and better support the subjective and quantitative results presented in this report.

Table of Contents

| | |
|---|------|
| Abstract | iii |
| List of Tables | viii |
| List of Figures | ix |
| Nomenclature | xi |
| Symbols | xii |
| 1. Introduction..... | 1 |
| 1.1 Introduction | 1 |
| 1.2 High frequency motion cueing | 2 |
| 1.3 Objectives and Scope of Research | 3 |
| 1.4 Atmospheric Turbulence | 5 |
| 1.5 Turbulence Models..... | 6 |
| 1.6 Aeroelasticity..... | 7 |
| 2. Literature Review of Current Motion Cueing Algorithms | 8 |
| 2.1 Introduction | 8 |
| 2.2 Classical Motion Cueing Algorithm..... | 9 |
| 2.3 NASA Coordinated Adaptive Washout Algorithm..... | 13 |
| 2.4 Modified NASA Adaptive Motion Cueing Algorithm..... | 14 |
| 2.5 SUNY Linear Optimal Motion Cueing Algorithm..... | 16 |
| 2.6 SUNY Nonlinear Motion Cueing Algorithm | 18 |
| 3. Higher Frequency Motion Cueing Algorithms | 21 |
| 3.1 Introduction | 21 |
| 3.2 Simulation of Atmospheric Turbulence | 22 |
| 3.3 Motion Cueing Due to Aeroelastic Effects | 24 |
| 4. Design of Atmospheric Turbulence Motion Cueing Algorithm and Integration with Aeroelastic Model | 32 |
| 4.1 Introduction | 32 |
| 4.2 Augmented Turbulence Channel Design | 33 |
| 4.3 Reduce Order Aircraft Model Development | 36 |
| 4.4 Parameter Identification Methods | 37 |
| 4.5 Large Civil Transport: Reduce Order Aircraft Model Development | 39 |
| 4.6 GH SCT: Reduced Order Aircraft Model Development..... | 43 |
| 4.7 Turbulence Cueing Filter..... | 48 |
| 4.8 Integration with Aeroelastic Model..... | 51 |
| 4.9 Testing: Offline Simulation of Algorithms | 52 |

| | | |
|-------|--|-----|
| 4.9 | Testing: Offline Simulation of Algorithms | 52 |
| 4.9.1 | Large Civil Transport: Offline Testing..... | 53 |
| 4.9.2 | Generic High-Speed Civil Transport: Offline Testing..... | 60 |
| 5. | Design of Experiments..... | 69 |
| 5.1 | Introduction | 69 |
| 5.2 | Background Information | 69 |
| 5.3 | Tuning the Augmented Turbulence Channel (ATC)..... | 72 |
| 5.4 | Design of Experiments | 75 |
| 6. | Results of Real-Time Experiments | 83 |
| 6.1 | Introduction | 83 |
| 6.2 | Large Civil Transport Study – Subjective Analysis | 83 |
| 6.2.1 | Large Civil Transport Experiment 1: Subjective Analysis | 84 |
| 6.2.2 | Large Civil Transport Experiment 2: Subjective Analysis | 86 |
| 6.2.3 | Large Civil Transport Experiment 3: Subjective Analysis | 90 |
| 6.3 | Large Civil Transport Study – Quantitative Results | 93 |
| 6.3.1 | Large Civil Transport: Experiment 1 – Quantitative Results | 93 |
| 6.3.2 | Large Civil Transport: Experiment 2 – Quantitative Results | 106 |
| 6.3.3 | Large Civil Transport: Experiment 3 – Quantitative Results | 115 |
| 6.4 | Generic High-Speed Civil Transport Study – Subjective Analysis | 116 |
| 6.4.1 | GHST Experiment 1: Subjective Analysis..... | 116 |
| 6.4.2 | GHST Experiment 2: Subjective Analysis..... | 121 |
| 6.4.3 | GHST Experiment 3: Subjective Analysis..... | 125 |
| 6.5 | Generic High-Speed Civil Transport Study – Quantitative Results..... | 130 |
| 6.5.1 | GHST: Experiments 1,2, and 3: Quantitative Results..... | 130 |
| 7. | Conclusions and Future Recommendations..... | 132 |
| 7.1 | Summary and Conclusions | 132 |
| 7.2 | Future Recommendations..... | 140 |

| | |
|---|-----|
| Appendices | 143 |
| Appendix A: Turbulence Spectrums Defined:..... | 143 |
| Appendix B: Fortran code for ATC; DASE model parameters..... | 145 |
| Appendix C: FAA Airman’s Guide to Reporting Turbulence Intensity (TBL 7-9-1)..... | 148 |
| Appendix D: Gain Tuning Test Plans..... | 149 |
| Appendix E: Cooper-Harper Rating Scale..... | 152 |
| Appendix F: Experiment Conditions and Run Order | 153 |
| References | 157 |

List of Tables

| | |
|--|-----|
| Table 5.4.1 – Run order and conditions for GHSCT experiments..... | 81 |
| Table 6.2.1 – Large Civil Transport Experiment 1, Turbulence Intensity and CHR..... | 84 |
| Table 6.2.2 – Large Civil Transport Experiment 1, FAA Turbulence Reporting Criteria | 86 |
| Table 6.2.3 – Large Civil Transport Experiment 2, Turbulence Intensity and CHR..... | 88 |
| Table 6.2.4 – Large Civil Transport Experiment 2, FAA Turbulence Reporting Criteria | 89 |
| Table 6.2.5 – Large Civil Transport Experiment 3, Turbulence Intensity and CHR..... | 90 |
| Table 6.2.6 – Large Civil Transport Experiment 3, FAA Turbulence Reporting Criteria | 92 |
| Table 6.3.1 – Mean Square of Pitch Stick Input, Large Civil Transport Experiment 1 . | 100 |
| Table 6.3.2 – Mean Square of Pitch Stick Input, Large Civil Transport Experiment 2 . | 109 |
| Table 6.3.3 – Mean Square of Pitch Stick Input, Large Civil Transport Experiment 3 . | 116 |
| Table 6.4.1 – GHSCT Experiment 1, Turbulence Intensity and CHR | 118 |
| Table 6.4.2 – GHSCT Experiment 1, FAA Turbulence Reporting Criteria | 120 |
| Table 6.4.3 – GHSCT Experiment 1, Turbulence Intensity and CHR | 122 |
| Table 6.4.4 – GHSCT Experiment 2, FAA Turbulence Reporting Criteria | 124 |
| Table 6.4.5 – GHSCT Experiment 3, Turbulence Intensity and CHR | 126 |
| Table 6.4.6 – GHSCT Experiment 3, FAA Turbulence Reporting Criteria | 128 |

List of Figures

| | |
|---|----|
| Figure 1.1 – NASA CMF with IFD on motion base (Courtesy of NASA LaRC)..... | 1 |
| Figure 2.2.1 – Classical Algorithm Block Diagram | 10 |
| Figure 2.3.1 – NASA Coordinated Adaptive Washout Algorithm Block Diagram (NASA Adaptive Algorithm)..... | 13 |
| Figure 2.4.1 – UTIAS Modified NASA Adaptive Motion Cueing Algorithm Block Diagram | 14 |
| Figure 2.4.2 – SUNY Binghamton Modified NASA Adaptive Motion Cueing Algorithm Block Diagram..... | 16 |
| Figure 2.5.1 – Linear Optimal Cueing Algorithm Optimization Structure..... | 17 |
| Figure 2.5.2 – Linear Optimal Cueing Algorithm Block Diagram..... | 18 |
| Figure 2.6.1 – Nonlinear Optimal Cueing Algorithm Optimization Structure | 18 |
| Figure 2.6.2 – Nonlinear Optimal Cueing Algorithm Block Diagram | 19 |
| Figure 3.1.1 – Reid/Robinson Algorithm with Turbulence Channel (Reid, 1990)..... | 22 |
| Figure 3.2.1 – Original SUNY Implementation of Turbulence Channel (Telban, 2005). | 23 |
| Figure 3.3.1 – Artist rendition of Generic High Speed Civil Transport (GHSCT) | 25 |
| Figure 3.3.2 – DASE Model, Flexible Aircraft Modes (Davis, 2009)..... | 27 |
| Figure 3.3.3 – DASE Model Block Diagram (Davis, 2009)..... | 30 |
| Figure 4.2.1 – Original SUNY Implementation of Turbulence Channel (Telban, 2005). | 33 |
| Figure 4.2.2 – Implementation 1 of Augmented Turbulence Channel | 34 |
| Figure 4.2.3 – Implementation 2 of Augmented Turbulence Channel | 34 |
| Figure 4.5.1 – Input and Output Data for Large Civil Transport ROAC Development ... | 39 |
| Figure 4.5.2 – Bode Diagram of Large Civil Transport ROAC | 41 |
| Figure 4.5.3 – PSD of Large Civil Transport ROACs and Aircraft Acceleration (NZ) ... | 42 |
| Figure 4.5.4 – Time Response of Large Civil Transport ROACs and Aircraft Acceleration (NZ) | 43 |
| Figure 4.6.1 – PSD of Large Civil Transport ROAC and GHSCT Aircraft Acceleration (NZ) | 44 |
| Figure 4.6.2 – Input and Output Data for GHSCT ROAC Development..... | 45 |
| Figure 4.6.3 – Bode Diagram of GHSCT ROACs..... | 46 |
| Figure 4.6.4 – PSD of GHSCT ROACs and Aircraft Acceleration (NZ)..... | 47 |
| Figure 4.6.5 – Time Response of GHSCT ROACs and Aircraft Acceleration (NZ) | 48 |
| Figure 4.7.1 – Bode Diagram of Turbulence Cueing Filter | 49 |
| Figure 4.7.2 – Step Response of Turbulence Cueing Filter | 50 |
| Figure 4.8.1 – Integration of DASE Model and Augmented Turbulence Channel | 51 |
| Figure 4.9.1 – Large Civil Transport Model GUI (courtesy of NASA LaRC)..... | 54 |
| Figure 4.9.2 – Large Civil Transport Implementation 1 of Augmented Turbulence Channel | 55 |
| Figure 4.9.3 – Large Civil Transport Implementation 2 of Augmented Turbulence Channel | 55 |
| Figure 4.9.4 – Large Civil Transport Testing, Time Response, ACT Off, Vertical Channel Only | 56 |
| Figure 4.9.5 – Large Civil Transport Testing, Time Response, Implementation 1 of ATC, Vertical Channel Only | 57 |

| | |
|--|-----|
| Figure 4.9.6 – Large Civil Transport Testing, Time Response, Implementation 2 of ATC, Vertical Channel Only | 58 |
| Figure 4.9.7 – Large Civil Transport Testing, Time Response, Comparison of Implementations 1 and 2..... | 59 |
| Figure 4.9.8 – GHSCT Implementation 1 of Augmented Turbulence Channel and DASE Aeroelastic Model..... | 60 |
| Figure 4.9.9 – GHSCT Implementation 2 of Augmented Turbulence Channel and DASE Aeroelastic Model..... | 61 |
| Figure 4.9.10 – GHSCT Testing, Time Response, ATC Off, Vertical Channel Only | 63 |
| Figure 4.9.11 – GHSCT Testing, Time Response, Implementation 1 of ATC, Vertical Channel Only..... | 64 |
| Figure 4.9.12 – GHSCT Testing, Time Response, Implementation 2 of ATC, Vertical Channel Only..... | 65 |
| Figure 4.9.13 – GHSCT Testing, Time Response, ATC Off, DASE Model On..... | 66 |
| Figure 4.9.14 – GHSCT Testing, Time Response, ATC On, DASE Model On..... | 67 |
| Figure 5.2.1 – Visual Motion Simulator (Courtesy of NASA LaRC) | 70 |
| Figure 5.2.2 – Visual Motion Simulator Flight Deck (Courtesy of NASA LaRC) | 70 |
| Figure 5.2.3 – Artist Rendition of Cockpit Motion Facility (Courtesy of NASA LaRC) | 71 |
| Figure 5.2.4 – Generic Flight Deck on CMF motion system (Courtesy of NASA LaRC)..... | 72 |
| Figure 5.4.1 – Large Civil Transport Experiment Configuration Block Diagrams | 78 |
| Figure 5.4.2 – GHSCT Experiment Configuration Block Diagrams..... | 79 |
| Figure 6.3.1 – Large Civil Transport Experiment 1, Normalized Mean Square of Vertical Velocity..... | 95 |
| Figure 6.3.2 – Large Civil Transport Experiment 1, Light Turbulence, PSD of Pitch Stick Input and Normalized PSD of Pitch Stick Input | 97 |
| Figure 6.3.3 – Large Civil Transport Experiment 1, Moderate Turbulence, PSD of Pitch Stick Input and Normalized PSD of Pitch Stick Input..... | 98 |
| Figure 6.3.4 – Large Civil Transport Experiment 1, Severe Turbulence, PSD of Pitch Stick Input and Normalized PSD of Pitch Stick Input | 99 |
| Figure 6.3.5 – Coherence Function of Vertical Velocity and Pitch Stick Input; PSD of Pitch Stick Input, Large Civil Transport Experiment 1, Level 2 Turbulence | 102 |
| Figure 6.3.6 – Coherence Function of Vertical Velocity and Pitch Stick Input; PSD of Pitch Stick Input, Large Civil Transport Experiment 1, Level 4 Turbulence | 104 |
| Figure 6.3.7 – Coherence Function of Vertical Velocity and Pitch Stick Input; PSD of Pitch Stick Input, Large Civil Transport Experiment 1, Level 6 Turbulence | 105 |
| Figure 6.3.8 – Large Civil Transport Experiment 2, Normalized Mean Square of Vertical Velocity..... | 107 |
| Figure 6.3.9 – Coherence Function of Vertical Velocity and Pitch Stick Input; PSD of Pitch Stick Input, Large Civil Transport Experiment 2, Turbulence Off..... | 110 |
| Figure 6.3.10 – Coherence Function of Vertical Velocity and Pitch Stick Input; PSD of Pitch Stick Input, Large Civil Transport Experiment 2, Turbulence Level 2 .. | 111 |
| Figure 6.3.11 – Coherence Function of Vertical Velocity and Pitch Stick Input; PSD of Pitch Stick Input, Large Civil Transport Experiment 2, Turbulence Level 4 .. | 113 |
| Figure 6.3.12 – Coherence Function of Vertical Velocity and Pitch Stick Input; PSD of Pitch Stick Input, Large Civil Transport Experiment 2, Turbulence Level 6 .. | 114 |

Nomenclature

| | |
|-------|--|
| ARMAX | Auto-Regressive Moving Average with External Input |
| ARX | Auto-Regressive with External Input |
| ASL | Above Sea Level |
| ATC | Augmented Turbulence Channel |
| BJ | Box-Jenkins |
| CHR | Cooper Harper Rating |
| CMF | Cockpit Motion Facility |
| DASE | Dynamic Aeroservoelastic |
| DME | Distance Measuring Equipment |
| DOF | Degree-of-Freedom |
| GFD | Generic Flight Deck |
| GHST | Generic High-Speed Civil Transport |
| GUI | Graphic User Interface |
| IFD | Integration Flight Deck |
| LaRC | Langley Research Center |
| LCT | Large Civil Transport |
| M | Mach Number |
| NLAC | Nonlinear Aircraft Model |
| OE | Output Error |
| Ref-H | Reference-H High Speed Civil Transport Configuration |
| ROAC | Reduced Order Aircraft Model |
| VMS | Visual Motion Simulator |

Symbols

| Symbol | Definition | Units |
|-------------------------|--|---|
| A | area | in ² |
| a | acceleration of a point | m/s ² |
| E | modulus of elasticity | psi |
| g | acceleration due to gravity | m/s ² |
| G | turbulence gust vector | m/s or ft/s |
| I | cross section area moment of inertia | in ⁴ |
| k _i | roots of the general solution of the wave equation | rad/in |
| L | length | in |
| R | radius | in |
| S | simulator centroid displacement | m |
| S _m | speed of sound in fuselage material | in/s |
| t | thickness | in |
| Z | vertical channel displacement | m |
| \ddot{Z} | vertical channel acceleration cue | m/s ² |
| $\overline{\ddot{X}}_A$ | aircraft state | ($\ddot{X}, \ddot{Y}, \ddot{Z}$) (m/s ²), (p,q,r) (rad/s) |
| $\overline{\ddot{X}}_M$ | motion system state | (x,y,z) (m), (φ,θ,φ) (rad) |
| $\overline{\ddot{X}}_M$ | acceleration cue | ($\ddot{X}, \ddot{Y}, \ddot{Z}$) (m/s ²), (p,q,r) (rad/s) |
| β | Euler angles β = [φ θ φ] ^T | rad |
| k _i | roots of frequency equation | rad |
| ρ | density | lbf/in ³ |
| ω | angular velocity ω = [p q r] | rad/s |
| ω _i | frequency | rad/s |
| Δ() | augmentation cue | m |

| Subscripts | Definition |
|-------------------|---------------------------------|
| () _A | relates to aircraft |
| () _{AE} | relates to aeroelastic bending |
| () _G | relates to turbulence wind gust |
| () _M | relates to simulator motion cue |
| () _S | relates to simulator |
| () _{SR} | relates to simulator rotation |
| () _T | relates to turbulence response |

Superscripts

$()^A$
 $()^I$
 $()^S$

Definition

aircraft reference frame

inertial reference frame

simulator reference frame

1. Introduction

1.1 Introduction

One of the most important objectives of any vehicle simulation is providing an environment in which the pilot or driver will sense the motion of the vehicle. The operator's perception of the vehicle motion affects his/her response and control strategy. In addition to out the window visual simulation and vehicle sensor displays, many simulators incorporate six degree-of-freedom motion platforms. These motion systems are intended to stimulate the body's motion sensing apparatus and provide a more immersive experience. Shown below is the NASA Cockpit Motion Facility, with one of the interchangeable flight decks on the motion system (Figure 1.1).



Figure 1.1 – NASA CMF with IFD on motion base (Courtesy of NASA LaRC)

Motion cueing algorithms are designed to handle a wide range of dynamic inputs to produce the most realistic motion at the pilot station. These include the aircraft response to pilot control inputs, atmospheric disturbances, and various other external inputs. This presents the designer with multiple issues, as the algorithm needs to provide the pilot with realistic cues while keeping the simulator within its geometric limitations and the constraints of the hardware. Because of this, within the algorithm, there are various filters and mathematical operations that can mute certain characteristics of the aircraft motion. One main area of focus is in the simulation of high frequency cues.

1.2 High frequency motion cueing

Conventional motion cueing algorithms do not produce satisfactory results when generating cues in high frequency scenarios, i.e. simulating atmospheric turbulence or aeroelastic effects. This is due to the presence of motion cueing washout filters designed to washout the cue arising from pilot control, along with various operations designed to scale and limit the outputs. Iteration rate smoothing filters also present a problem in this regard. At the Man-Machine Systems Laboratory, SUNY Binghamton, Cardullo and Ellor developed an approach whereby the turbulence state bypassed the cueing algorithm and the iteration rate filter, directly porting the turbulence model output to the motion system.

Other advancements were pioneered by Lloyd Reid and Paul Robinson. In their implementation, a second channel was used in parallel with the primary cueing channel. This second channel employed a reduced order model of the aircraft response to turbulence along with a high-pass filter. The filtered output was then integrated twice and summed with the output of

the primary cueing algorithm, augmenting the motion in just the vertical channel. This output is then sent to the cueing hardware which drives the motion base. See chapter 3 for a more in depth explanation of the Reid Robinson algorithm.

A version of the Reid Robinson approach was later implemented by Telban (a) at the Man-Machine Systems Laboratory to the nonlinear cueing algorithm, improving the turbulence simulation. In this implementation, the overall turbulence simulation was improved, however, further investigation led to the revision of this algorithm. Chapter 4 goes into greater detail on the changes implemented to the algorithm to produce the new algorithm that is used in the offline and on-site testing.

Aircraft with long and slender fuselages have a tendency to bend, deflecting the pilot station. This aeroelastic bending can be excited by various pilot inputs or atmospheric loads. When providing cues for the flexural vibrations of an aircraft, it is necessary to prevent attenuation or distortion by the cueing algorithm. There have been advancements in this regard, using both complex finite element models and more simplified linear models. Both approaches will be discussed and assessed in Chapter 3; also detail will be provided on the integration with the augmented turbulence channel in Chapter 4.

1.3 Objectives and Scope of Research

Providing pilots with appropriate turbulence simulation is quite desirable. Whether it is training exercises or analysis of the added workload of flying through moderate or severe turbulence, the motion cues must be realistic or the legitimacy of these studies can be

compromised. The state of the art with regard to augmented motion cueing, specifically for atmospheric turbulence, produces acceptable results augmenting the amplitude of the simulator excursions, but does not do much to address the frequency content. This report looks at the shortcomings of the current algorithms and presents new augmented motion cueing algorithms.

There is also investigation as to whether it is necessary to use complex or finite element models when producing aeroelastic motion cues. Calculations of aeroelastic bending typically utilize very complex structural models. Recent advances in the simulation of flexible aircraft have implemented much simpler models to provide the pilot with aeroelastic motion cues in real-time.

It is also desirable to provide the pilot with aeroelastic motion cues while flying through atmospheric turbulence as the gusts cause significant loads on the aircraft, contributing to the bending. The current aeroelastic cueing algorithm augments the primary aircraft motion cue in a similar fashion to the augmented turbulence motion cueing channel. Integrating the two algorithms will provide pilots with realistic cues for a wide range of scenarios.

In the final chapter of this report, conclusions are drawn from the real-time experiments conducted at the NASA Langley Research Center. Even though these are not standard multi-pilot evaluations, verdicts can be drawn from the analysis of the data and subjective pilot evaluation. The future work section also presents possible multi-pilot experiments to be conducted in the verification process of the augmented turbulence channel. There is also room for investigation into the change in pilot workload when maintaining level flight or performing any number of tasks while flying through atmospheric turbulence.

Main objectives of this research:

- Investigate the issues with the current turbulence cueing algorithm
- Develop a new turbulence motion cueing algorithm
- Verify the turbulence cueing algorithm offline
- Implement the turbulence cueing algorithm on six degree of freedom flight simulators and tune the algorithm
- Integrate the turbulence cueing algorithm with existing aeroelastic cueing algorithm and verify through real-time simulation
- Develop and run real-time piloted experiments; set up for future multi-pilot experiments

1.4 Atmospheric Turbulence

The phenomenon of atmospheric turbulence is characterized by small-scale, irregular air motions caused by winds that vary in speed and direction. The mixing of warm and cold air in the atmosphere by wind causes clear-air-turbulence. Jet streams can cause severe turbulence due to high wind shear. This is also a problem at lower altitudes and near mountains as the conditions usually allow for wind shear.

Thunderstorms commonly cause aircraft to buffet upward, downward, and laterally; they are the most common source of severe turbulence. These situations can be extremely hazardous

and subject the aircraft to the possibility of lightning strikes which can lead to structural damage and disruption of electrical systems. Because of the many hazards, pilots are urged not to fly through thunder storms.

1.5 Turbulence Models

There are multiple models within the industry that are used to simulate atmospheric turbulence. Two of the more common models are the von Karman and Dryden turbulence spectra. Both of these turbulence spectrums are defined in the Terrestrial Environment Criteria Handbook²⁰. Simulating turbulence using the von Karman spectrum is not a simple process as it is quite computationally burdensome. Because of this, most simulations implement the Dryden turbulence model. To add rotational turbulent gust inputs to the simulation, the MIL STD disturbance model can also be implemented. Details on both the von Karman and Dryden turbulence models are provided in MIL-STD-1797A⁸.

The von Karman model is an analytical representation of turbulence spectra and is usually generated using a sum-of-sinusoids method (Houbolt, 1964). There are variations designed to reduce computation time, but each is developed off of this original model. One of the main advantages to these spectra is the physical accuracy of the gusts. It may be desirable to use the von Karman model to perform a more accurate structural analysis, but for the purposes of simulating turbulence in real-time, the Dryden spectrum has proven more than adequate.

The Dryden turbulence model was developed using in-flight data, acquired by flying through atmospheric turbulence in an aircraft equipped with various sensors. The data acquired

by the sensors was used to develop the Dryden spectrum. This spectrum was later used to develop the more commonly used turbulence model known as the simplified Dryden disturbance model⁸. Instead of using a prerecorded set of data, band limited white noise is passed through appropriate linear filters to produce the spectrum. This eliminates any repetitious nature of using a prerecorded dataset. T. R. Beal (1993) goes into great detail on the development of the necessary filters to convert the white noise input into turbulence wind gusts within the Dryden Spectrum.

The Military Standard, MIL-F-8785B, includes definitions for rotational turbulence inputs. Since atmospheric turbulence is not a uniform field, uneven gust gradients will cause the aircraft to rotate about its axes. This model defines gust in the form of angular velocity. Typically, these terms are applied to the aircraft equations of motion, through the aerodynamic terms. Each of the Large Civil Transport real-time experiments was conducted using both translational and rotational turbulence models. Discussion is also provided to support the use of the rotational turbulence model to provide the pilot with realistic turbulence cues. Definitions for each turbulence model spectra are detailed in Appendix A.

1.6 Aeroelasticity

Aeroelasticity is a phenomenon associated with structural deformations in the aircraft, which lead to changes in the aerodynamic forces. In 1947, Arthur Collar defined aeroelasticity as; “the study of the mutual interaction that takes place within the triangle of the inertial, elastic, and aerodynamic forces acting on structural members exposed to an airstream, and the influence of this study on design.” Aeroservoelasticity represents a combination of several theories, each

related to aircraft dynamics. According to Dinu (2006), the main focus of aeroservoelasticity includes the interaction between the flexible structure, aerodynamic forces, and the control laws acting on it.

Flexing of the aircraft structure can cause very undesirable results; including substantial reduction of control effectiveness as well as aircraft stability. Both of these effects are compounded when dealing with supersonic flight as certain maneuvers result in higher aerodynamic loads on the control surfaces. Aeroelasticity can also cause the pilot station to accelerate periodically, sometimes with high enough amplitude to cause involuntary pilot input. This involuntary input known as bio-dynamic coupling (BDC) also leads to an increase in difficulty controlling the aircraft. Some conceptual aircraft designs take advantage of wing flexibility to aid in maneuverability. These concepts only drive the need for more complex and accurate aeroelastic models.

2. Literature Review of Current Motion Cueing Algorithms

2.1 Introduction

Research regarding the development and verification of motion cueing algorithms has been conducted since vehicle simulator motion platforms were driven by them. It has been shown in the past that proper motion cueing and a robust motion system allow for a more realistic overall simulation. Not all simulation tasks justify the use of a motion system, but with the added fidelity, a more immersive experience can be provided to the pilot and his/her performance in the simulator improves.

Motion systems employed by flight simulators cannot duplicate aircraft motion; therefore, it is necessary to employ a set of algorithms to maximize the performance of the motion base. The basic mathematical operations done in these algorithms include limiting and scaling the motion commands, and washing out the motion commands with filters. The complexity of the cueing algorithms can vary quite a bit. With advances in computational power, the number of mathematical operations that can be completed during each time step grows continuously.

A literature review was conducted in order to become familiarized with the various motion cueing algorithms used at the NASA Langley Research Center and their bases. The first algorithm discussed is one of the least complex cueing algorithms; known as the Classical Algorithm. The Coordinated Adaptive Washout Algorithm (also known as the NASA Adaptive Algorithm), along with two modified versions, are also discussed. Finally, two other algorithms developed at SUNY Binghamton, the Linear Optimal and Nonlinear Optimal cueing algorithms are presented.

The major thrust of this research is to enhance cues arising from specific atmospheric conditions or aircraft dynamics. The reader will find a lengthy discussion of this specialized topic in Chapter 3.

2.2 Classical Motion Cueing Algorithm

The classical algorithm was first published by Conrad (1970); a block diagram of this algorithm is shown in Figure 2.2.1. It typically uses linear scaling and limiting on the

translational acceleration and angular velocity inputs (a_A^A and ω_A^A). Like the other cueing algorithms discussed here, there are two separate channels for the translational and rotational degrees of freedom, each with separate washout filters (Reid, 1985)

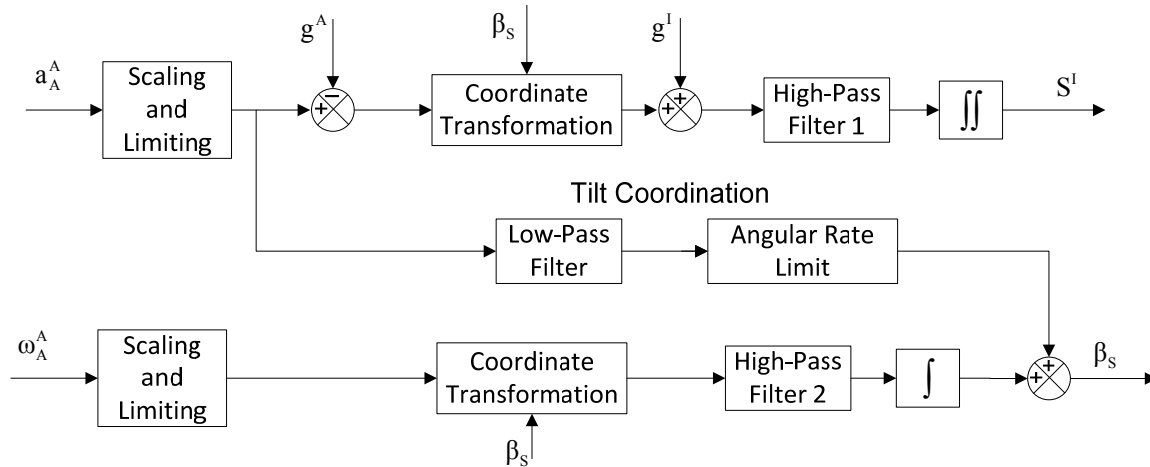


Figure 2.2.1 – Classical Algorithm Block Diagram

High-pass filters 1 and 2 are designed to wash out motion cues. In order to provide the reader with a better understanding of this washout process, time domain and frequency analyses are provided. Equation 2.2.1 represents a typical second order high-pass filter. Figure 2.2.2 shows the frequency response of the high-pass filter and Figure 2.2.3 shows the step response. Referring to the Bode Diagram, this filter passes all frequencies over 10 rad/s, anything below that frequency is attenuated. The step response indicates that the input signal will be washed out after about 0.5 seconds.

$$\text{High-Pass Filter} = \frac{s^2}{s^2 + 6.283s + 9}$$

Eq. 2.2.1

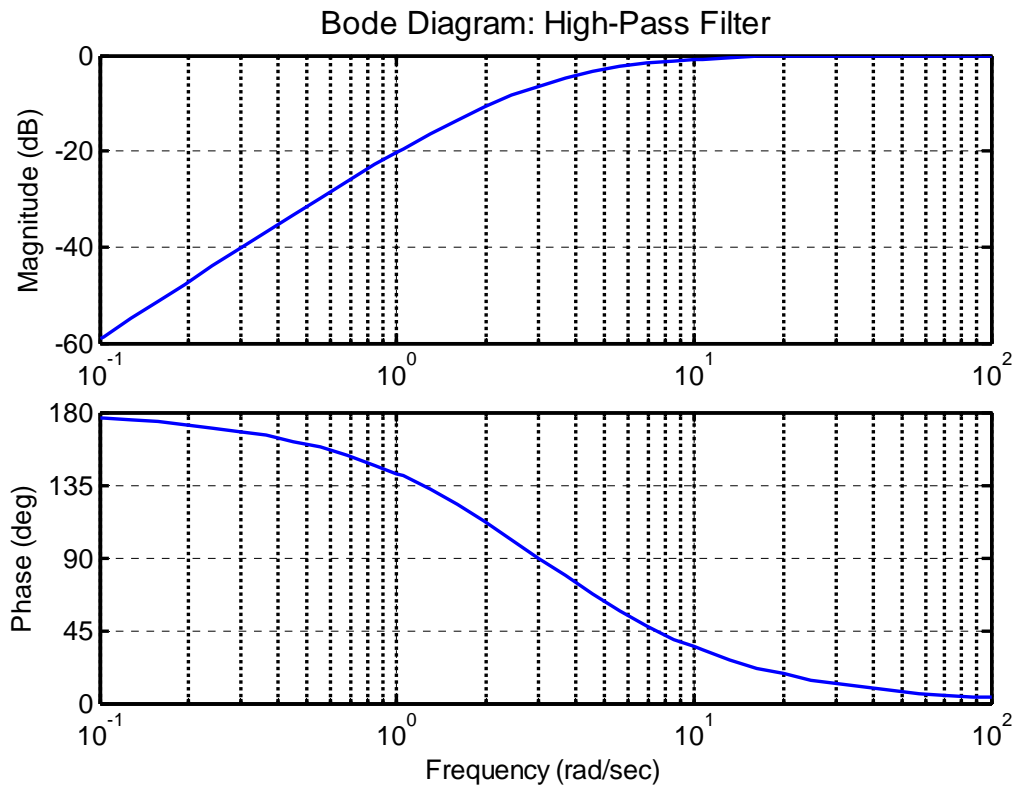


Figure 2.2.2 – Bode Diagram: Second Order High-Pass Filter

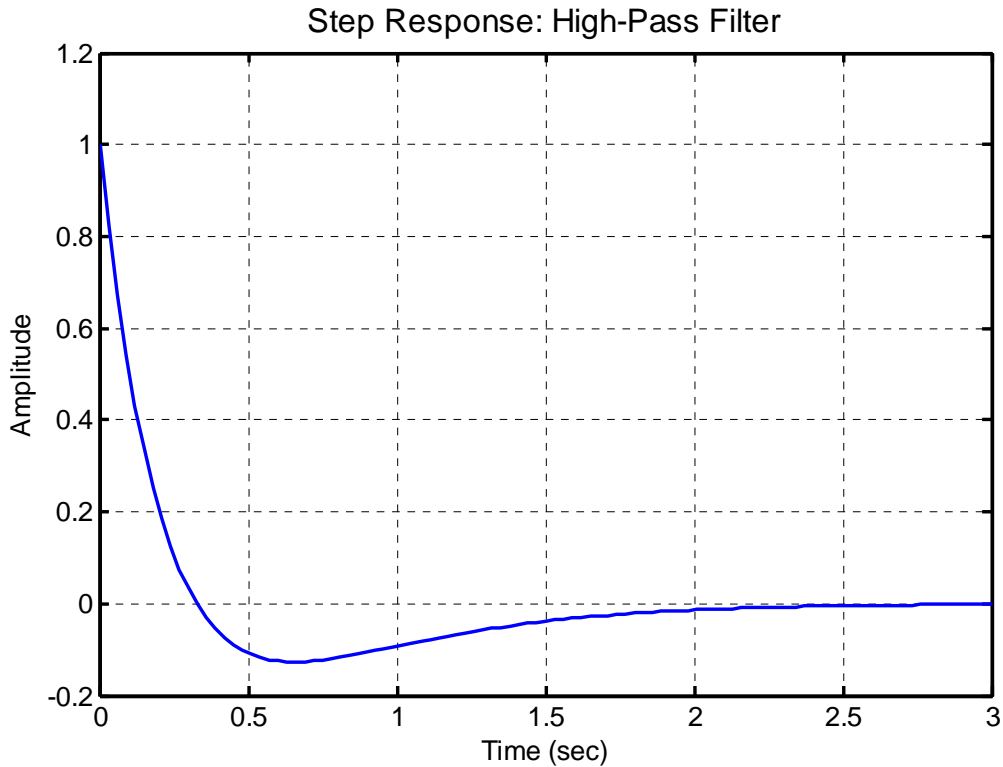


Figure 2.2.3 – Step Response: Second Order High-Pass Filter

Referring back to the block diagram (Figure 2.2.1); there is a crossover path to provide the pilot with the sensation of sustained acceleration. Because of the limitations of a typical motion base, translational acceleration cannot be sustained for very long. This is overcome by using a method known as tilt coordination, which takes advantage of the inability of the otoliths to distinguish between acceleration and tilt and consequently to rotate the motion platform and alter the direction of the steady-state specific force. In most cases, the algorithm will provide an “onset” cue with actual translational acceleration, and then tilt the platform as the translational motion is washed out. As long as this transition is done under the pilot’s angular velocity indifference threshold, the tilting will be unnoticeable.

2.3 NASA Coordinated Adaptive Washout Algorithm

This algorithm, also referred to as the NASA Adaptive Algorithm, was developed at NASA Langley Research Center by Parrish (1973). The architecture is similar to that of the classical algorithm; there are separate channels for the translational and rotational motion cues, and a crossover path for steady-state translational acceleration cues (Figure 2.3.1). The adaptive feature of this algorithm is applied using variable gain parameters which are based on the current state of the simulator. They are designed to minimize a cost function, and adapt constantly throughout the simulation.

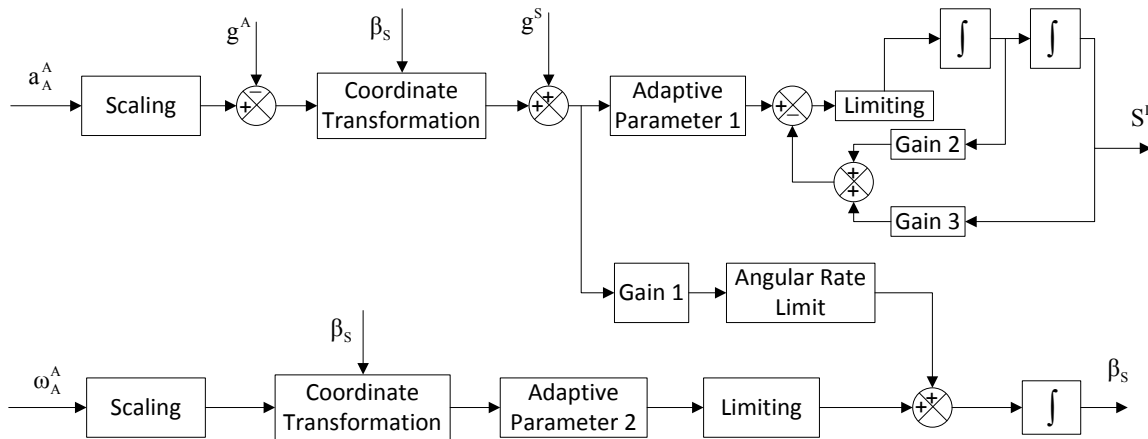


Figure 2.3.1 – NASA Coordinated Adaptive Washout Algorithm Block Diagram (NASA Adaptive Algorithm)

A set of two adaptive parameters are used in this algorithm; one for the translational channel and one for the rotational channel. These parameters directly impact the severity of the washout filters, with the intent of maximizing the available geometry of the motion base.

2.4 Modified NASA Adaptive Motion Cueing Algorithm

The NASA Adaptive Algorithm went through modifications conducted at both the University of Toronto (Reid, 1985) and SUNY Binghamton (Telban, 2000). The modified algorithms included a third adaptive parameter, along with the original two (Figure 2.4.1). Modifications were also made to the cost function; terms were added to the function to improve the effect of the adaptive parameters on the washout filters. Detailed descriptions of the changes are shown in Reid (1985).

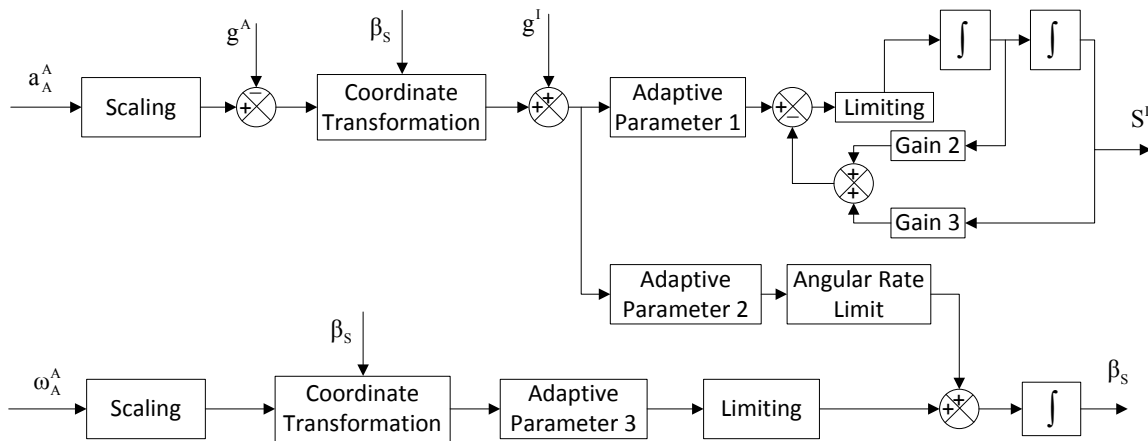


Figure 2.4.1 – UTIAS Modified NASA Adaptive Motion Cueing Algorithm Block Diagram

The new adaptive parameter (adaptive parameter 2) is a part of the crossover path that calculates the necessary rotation for the sustained translational acceleration cue. As with the original NASA Adaptive Algorithm, each adaptive term is updated constantly throughout the simulation.

Further modifications were made at SUNY Binghamton in order to rectify an instability in the algorithm. Reid et al. (a) discussed the unstable characteristics, and suggested limiting the adaptive parameters as a possible solution. This would also impede the ability of these parameters to adapt as they were intended, furthermore, the algorithm could still remain unstable under certain conditions.

The instability in the rotational channel was apparent when the simulator attempted to reach the neutral position. The algorithm is designed to force the simulator to continue moving and remain out of the neutral position. But, the adaptive washout algorithm, like all washout algorithms, attempts to bring the simulator to the neutral position under steady state conditions. According to Telban (2000), once the simulator reached the neutral position, it would begin to oscillate.

The changes to the algorithm include using g^{SR} , which is g in the imaginary reference frame Fr_{SR} (Figure 2.4.2). When the simulator responds to an angular input, the simulator frame is defined as Fr_{SR} . When dealing with a purely rotational case, $Fr_{SR} = Fr_S$ and $g_{SR} = g^S$. Under pure rotational input, in the original algorithm, the algorithm employed an active translational and tilt channel. This also led to stability issues; in the revised algorithm, a null translational channel is used when dealing with pure rotational input. This version of the Modified NASA Adaptive Algorithm is stable under both translational and rotational inputs, and any combination of the two.

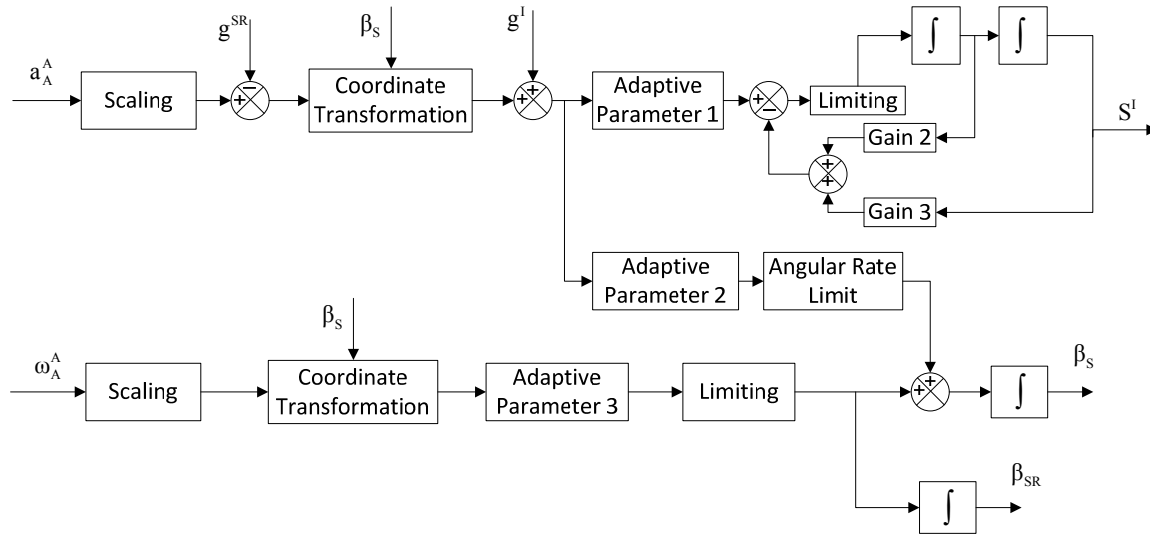


Figure 2.4.2 – SUNY Binghamton Modified NASA Adaptive Motion Cueing Algorithm Block Diagram

2.5 SUNY Linear Optimal Motion Cueing Algorithm

The Linear Optimal Cueing Algorithm, developed at the SUNY Man-Machine Systems Lab, is designed to optimize parameters of the different washout filters. The optimization takes place offline in MATLAB. This is done using a mathematical model of the human vestibular system, shown in Telban, et al. (b). The washout filter design is based on minimizing sensation error. These filters, $W(s)$, relate the simulator motion states to the aircraft states, as do the classical washout filters. The difference is the criterion against which the filter is designed. The operations used to calculate the components of $W(s)$ are shown in figure 2.5.1.

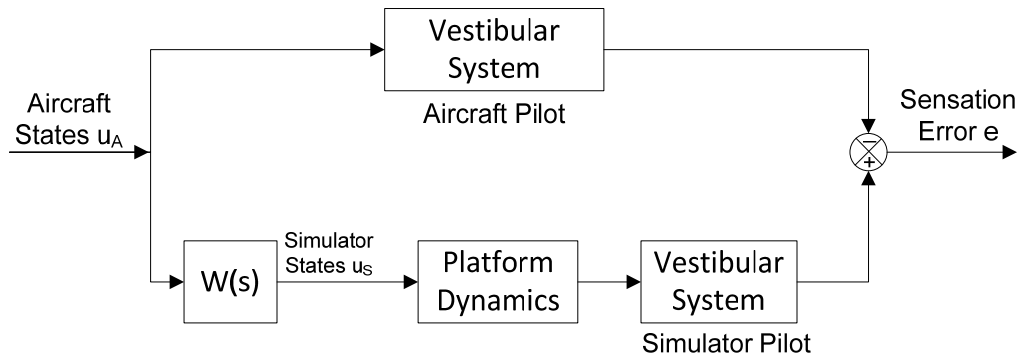


Figure 2.5.1 – Linear Optimal Cueing Algorithm Optimization Structure

The structure of the algorithm itself is quite similar to the Classical Algorithm. There are two separate channels for the translational and rotational cues, and just like the other algorithms discussed, a crossover path is used to provide the tilt coordination cue to the rotational channel (Figure 2.5.2). One main difference in this algorithm is the use of nonlinear scaling and limiting. W_{22} , W_{11} , and W_{12} are each 6th or 7th order filters. They are computed by adjusting weighting parameters in the cost function and using the Riccati equation to evaluate the terms.

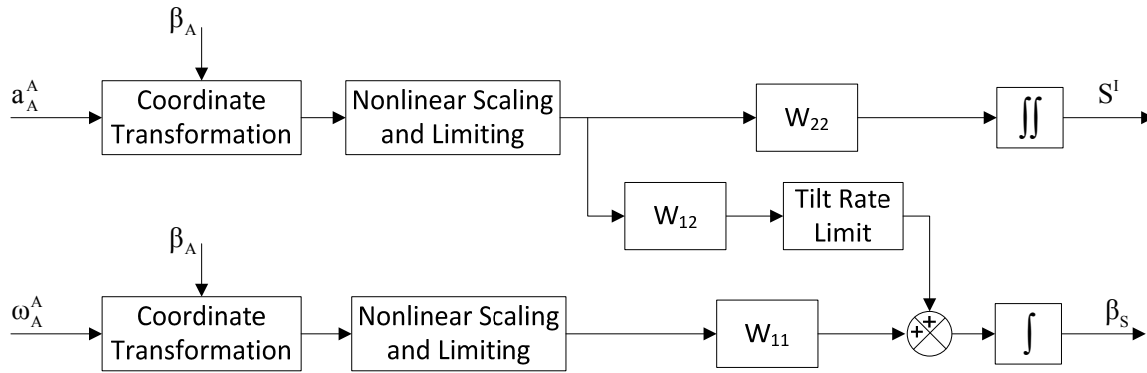


Figure 2.5.2 – Linear Optimal Cueing Algorithm Block Diagram

2.6 SUNY Nonlinear Optimal Motion Cueing Algorithm

The nonlinear optimal motion cueing algorithm incorporates models of the human vestibular system, similar to the linear optimal algorithm. This algorithm takes sensor modeling a step further by implementing semicircular canals and otolith models, as well as a visual-vestibular perception model and the optimization, all in real-time (Telban, et al (b)). Figure 2.6.1 shows the structure of the algorithm that calculates perceptual error.

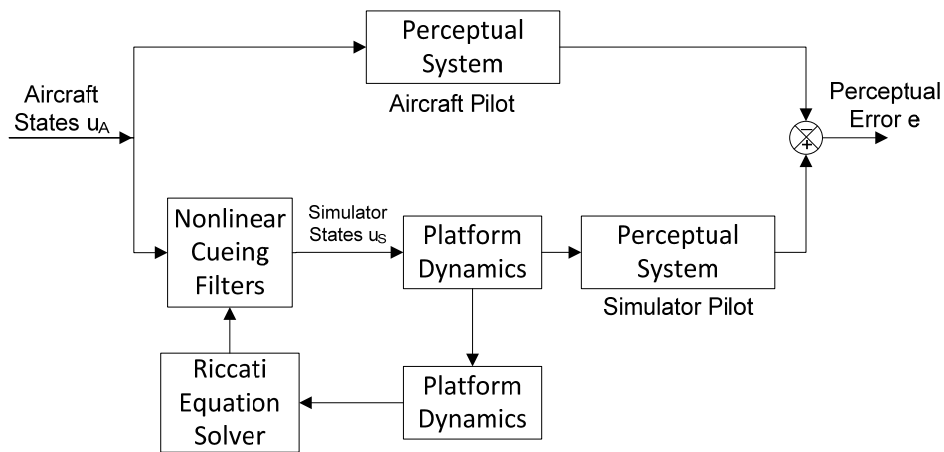


Figure 2.6.1 – Nonlinear Optimal Cueing Algorithm Optimization Structure

The top level block diagram of the algorithm is quite similar to the linear optimal algorithm (Figure 2.6.2). Since this algorithm solves the Riccati equation in real-time, it optimizes the filters before each iteration. This allows the algorithm to take advantage of the full geometry of the simulator. The filters have nonlinear characteristics; smaller motion cues are sustained for longer periods of time, and larger excursions are washed out quicker to make more motion available to the pilot.

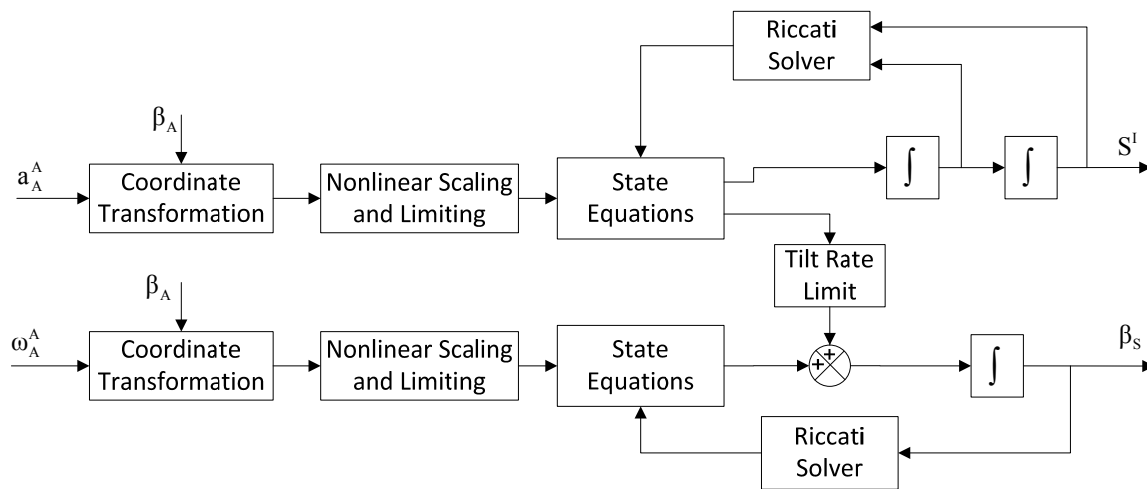


Figure 2.6.2 – Nonlinear Optimal Cueing Algorithm Block Diagram

This implementation solves two separate Riccati equations; one for the translational motion cue, and one for the rotational motion cue. The development of a real-time solution to the Riccati equation was quite challenging. Each iteration used the previous solution as initial conditions when computing the current solution. This algorithm used the offline computed solutions used in the Linear Optimal Algorithm for the first iteration. In order to continue

updating the filters in real time, a structured neural network is used to solve the Riccati equation.

The final version of this algorithm ran at 60 Hz; all real-time requirements were met.

3. Higher Frequency Motion Cueing Algorithms

3.1 Introduction

The objective of this area of research is to ensure high frequency motion cues are preserved by the cueing algorithm. Typical motion cueing algorithms apply limiting and scaling along with a set of washout filters to calculate the motion cue. These washout filters are low bandwidth and not able to preserve turbulence cues; furthermore, it is not necessary to wash out turbulence motion as it produces smaller excursions than most pilot inputs.

In these cases, the aircraft state includes an appropriate response to turbulence, however the motion cue does not. Rather than modifying the primary motion cueing algorithm to improve the simulation, an augmentation channel can calculate the lacking high frequency cues and combine them with the primary cue. The various motion cueing algorithms discussed in Chapter 2 are affected by this problem and can benefit from the addition of an augmentation channel that preserves high frequency cues. Augmenting motion cueing algorithms to improve atmospheric turbulence simulation has been attempted previously. One approach was developed by Cardullo and Ellor⁴; the high frequency effects bypassed the primary motion cueing algorithm, and were directly ported to the motion system. This augmentation was implemented on the USAF Undergraduate Pilot Training Simulators for the T37 and T38 aircraft.

Another method to improve turbulence simulation was developed by Lloyd Reid and Paul Robinson (1990). In their approach, there is a secondary channel that uses a reduced order aircraft model to calculate the aircraft response to atmospheric turbulence. This output is then scaled and filtered before being integrated twice. The integrated output is summed with the output of the primary flight channel in degree-of-freedom space (Figure 3.1.1).

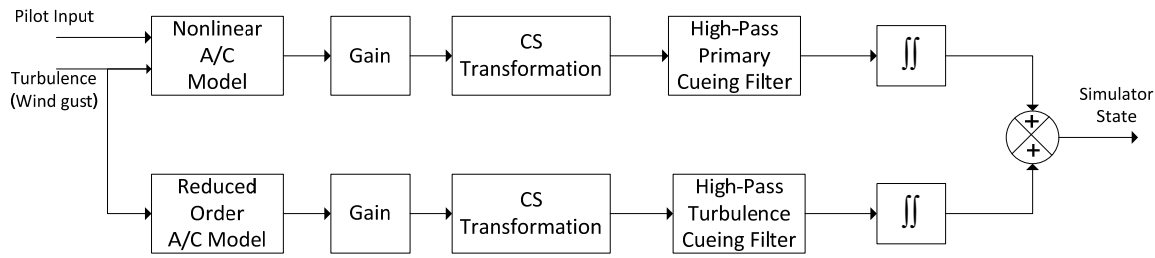


Figure 3.1.1 – Reid/Robinson Algorithm with Turbulence Channel (Reid, 1990)

An algorithm similar to the Reid/Robinson algorithm was implemented on the Nonlinear Motion Cueing Algorithm discussed in Chapter 2. The implementation produced more distinguishable turbulence cues, however when run for long periods of time, the output of the vertical channel would begin to diverge. The following sections in this chapter discuss the implementation. Chapter 4 describes a modified version, which was tested offline and implemented in real-time.

3.2 Simulation of Atmospheric Turbulence

The first algorithm discussed is the implementation on the Nonlinear Motion Cueing Algorithm, developed by Telban et al. (b), at SUNY Binghamton (Figure 3.2.1). This algorithm, like the Reid/Robinson approach, comprises a secondary flight channel to calculate the aircraft response to atmospheric turbulence. A transfer function (H_w) represented the aircraft dynamics in the vertical channel, specifically the response to turbulence. In this case, this was modeled as a high-pass filter. The turbulence input, G , is a gust vector with the units of velocity. The output of H_w is \ddot{X}_{A_T} ; the acceleration of the aircraft due to turbulence. This is then augmented by a

gain term and summed with the scaled and limited acceleration output of the primary flight channel.

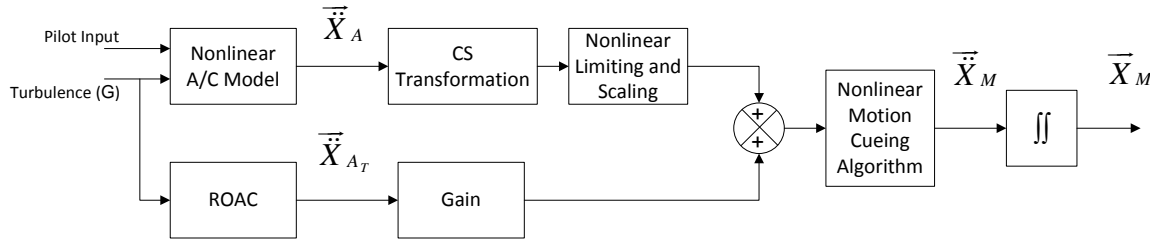


Figure 3.2.1 – Original SUNY Implementation of Turbulence Channel (Telban, 2005)

Unlike the secondary flight channel, the primary flight channel uses a nonlinear aircraft model. This nonlinear model calculates the dynamic aircraft response to all external inputs and pilot control. This includes the response to turbulence. This design is based on the ability to amplify simulator motion system response to turbulence by calculating it in the secondary channel and then summing it with the primary output. Both terms being summed are in the units of acceleration.

This summed output is then put through a cueing filter, to washout the cue, and integrated twice to generate the displacement of the simulator, in degree-of-freedom space. One issue with performing this summation before the cueing filter is applied is that the cueing filter was designed to generate cues which are optimized to the pilot. As discussed in Chapter 2, this algorithm continuously optimizes the filters, in a nonlinear fashion, with the intent of reducing

the pilot's perceptual error. This filter is designed for cues of a much lower frequency range than atmospheric turbulence.

Another area of concern is the two consecutive integrations. The aircraft response to atmospheric turbulence is not necessarily a zero mean process; therefore, double integrating that term can cause the amplitude of the displacement to grow with time. It is also noted that integrations naturally smooth high frequency inputs as they effectively average the magnitude. The integrations deteriorate the high frequency content of the cue before it is sent to the motion base and also cause the divergent tendency of the algorithm.

Each of these issues was taken into account when designing the turbulence channel. Discussion on the new algorithm, along with the results of offline testing, is presented in Chapter 4. The verification of the real-time implementation of the turbulence channel is conducted at length in Chapter 5.

3.3 Motion Cueing Due to Aeroelastic Effects

Aeroelastic motion cues tend to be in a higher frequency range than cues from pilot control input. Preserving the aeroelastic cue presents similar hurdles to simulating atmospheric turbulence. For these reasons, it is desirable to augment the primary motion cue to provide the pilot with the aeroelastic motion cues. This research was done with an aircraft model known as the Generic High-Speed Civil Transport (GHSCT). Raney (2002) describes the aircraft (Figure 3.3.1) as having a slender fuselage and delta wing design based on the Reference H Supersonic Transport (Ref H). It is supplemented with an aeroelastic bending model to simulate the flexibility of the fuselage.

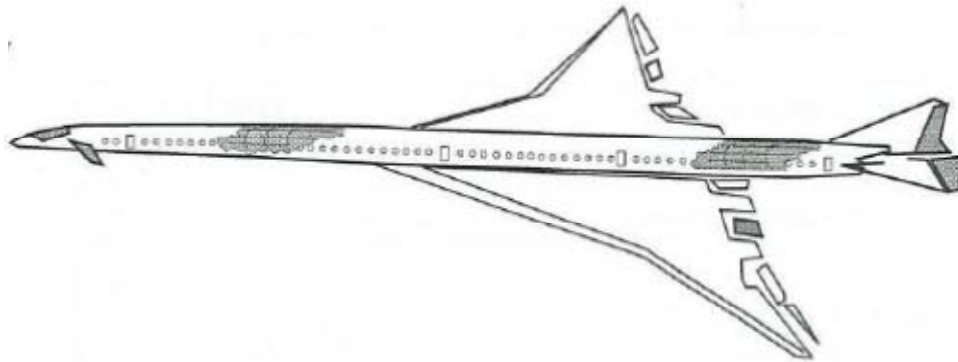


Figure 3.3.1 – Artist rendition of Generic High Speed Civil Transport (GHSCT)

The specific model described in Raney (2002) comprises improved-fidelity models for aerodynamics, inertia, engines, landing gear, and actuation systems. The model includes quasi-elastic flexible aerodynamics and the ability to calculate actuator hinge moments. It also has engine inlet models that predict and illustrate the supersonic inlet unstart phenomena, described in Jackson (1999). The aircraft model is based on wind tunnel and computational fluid dynamics studies. These studies included experiments at low sub-sonic speeds, as well as runs at up to Mach 2.4. High fidelity finite-element models were based on multi-material structural designs (Raney, 2002). These finite-element structural models were refined to evaluate the overall strength and rigidity of the aircraft, and to formulate flutter dynamic predictions.

This iteration of the model also included aeroservoelastic structural modes. The purpose of this extension of the model is to reproduce the effects of structural flexibility and gauge their impact on the pilot's flying abilities. As mentioned before, the aeroelastic bending provides the

pilot station with additional high frequency motion, and in turn, can change the dynamics of the pilot's control inputs. A specific portion of this study focused on the increase in high frequency motion from both turbulence and aeroelasticity, and the overall effect on the pilot control inputs.

The GHSCT was developed with the intent of implementing an aeroelasticity model that could be easily modified and used in real-time simulations. Data from the complex finite element model of the aircraft was used to verify the flexural frequencies of the Generic High-Speed Civil Transport Aircraft (Davis, 2009). As with the complex aeroelastic model; the flexibility of this new model could be excited by both atmospheric turbulence and pilot control input.

Oscillatory excitation of the pilot station not only provides the pilot with aeroelastic cues, it can also induce an involuntary response to the vibration. These control inputs may also be oscillatory; and can cause divergent vibrations in the fuselage. This phenomenon is known as bio-dynamic coupling. The primary objective of the GHSCT study is to determine the specific frequency range and structural characteristics that induce bio-dynamic coupling.

This particular Dynamic Aeroservoelastic Model, or DASE Model, comprises six flexible aircraft modes, described in Davis (2009) (Figure 3.3.2). Three of which are symmetric, and three anti-symmetric. The symmetric modes represent the bending in the pitch axis; the anti-symmetric modes represent the bending in the yaw axis. Each of these aeroelastic modes can be excited by pilot control input, atmospheric turbulence, or other external inputs. With the DASE model activated, the pilot is provided with both lateral and vertical cues, each representative of fuselage bending.

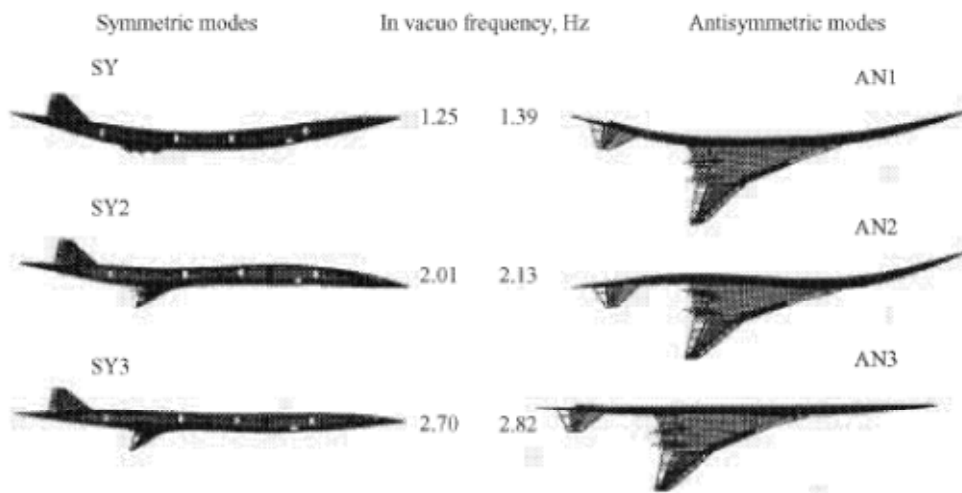


Figure 3.3.2 – DASE Model, Flexible Aircraft Modes (Davis, 2009)

Because the DASE Model is linear, this allows for easy modification of parameters between runs. This meets the requirements of the study while still maintaining necessary fidelity in the cues. The first DASE model was designed to mimic the bending modes of the complex aircraft. This simplified model was developed using the complex aircraft dimensions and mass properties. The modes were identified by conducting beam analysis and defining the aircraft fuselage as a thin hollow tube. The simplified model was compared with the complex model. Once they were verified, it became possible to scale the linear model to represent different sized supersonic jets. Details on the development of the simplified model, derived in Davis (2009), are shown below.

The first two equations (Eq. 3.3.1 and Eq. 3.3.2) represent the cross sectional area of the hollow tube and the cross sectional stiffness inertia; where A is the area (in^2), R is the radius (in), and t is the thickness (in) of the tube.

$$A = 2\pi Rt$$

Eq. 3.3.1

$$\frac{I}{A} = \frac{1}{2}R^2$$

Eq. 3.3.2

The lateral vibration of a beam with free ends is determined by the wave equation (Eq. 3.3.3); k_i represents the roots of this equation. Dividing by L obtains κ_i ; the roots of the frequency equation (rad). κ_1 , κ_2 , and κ_3 are the first three fundamental bending modes; representing the mode shapes shown in Figure 3.3.2. The frequencies of free vibration (ω_i) of a simple prismatic beam are shown in Eq. 3.3.4. They are proportional to the square root of the bending stiffness (K), and the distributed mass (M). This equation can be simplified to Eq. 3.3.5, where S_m represents a material property of the fuselage. S_m is defined in Eq. 3.3.6, where E represents the Young's modulus of the material and ρ is the density.

$$k_i L = \kappa_i = 0, 4.73, 7.853, 10.996, \dots$$

Eq. 3.3.3

$$\omega_i = (k_i^2) \sqrt{\frac{K}{M}}$$

Eq. 3.3.4

$$\omega_i = S_m \left(\frac{k_i^2}{\sqrt{2}} \right) R = S_m \left(\frac{\kappa_i}{\sqrt{2}} \right) \frac{R}{L^2}$$

Eq. 3.3.5

$$S_m = \sqrt{\frac{Eg}{\rho}}$$

Eq. 3.3.6

The block diagram of the linear DASE model is shown in Figure 3.3.3. This figure illustrates the different parameters used to calculate the fuselage bending of the aircraft. Inputs to the model are derived from the aircraft state, which is provided by the generic aircraft model, or GHSCT. Since this version of the DASE model is designed to provide the pilot with bending in both the pitch and yaw degrees-of-freedom (DOF), the rotational acceleration in those DOF are used as inputs. The pitch bending modes are combined with the static sag of the aircraft. This represents the neutral vertical position of the pilot station when the aircraft is in flight.

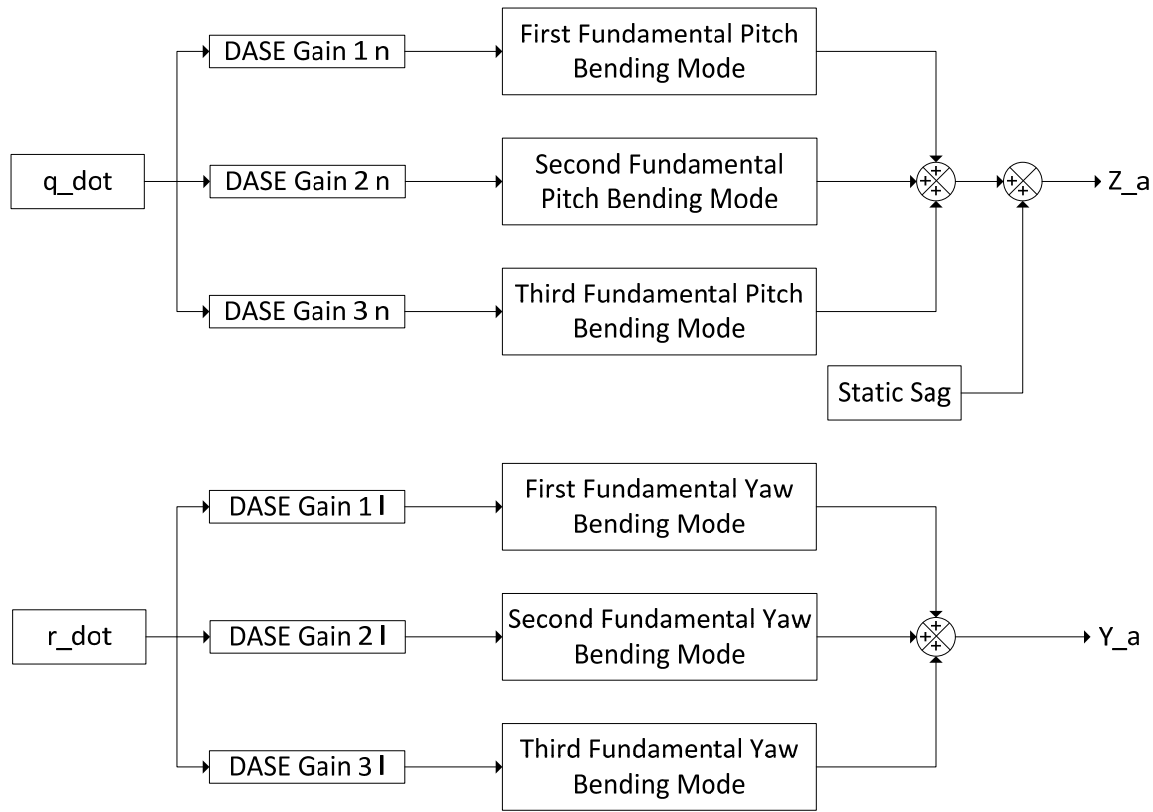


Figure 3.3.3 – DASE Model Block Diagram (Davis, 2009)

One component of the bending modes model that is not included is the flexibility of the wings, and the impact these forces have on the dynamics of the aircraft. Since this aircraft is designed for supersonic flight, the wings are configured with a delta design and are much more rigid than a conventional wing design. If the aircraft had a conventional or swept wing design, such as a Large Civil Transport, there would be much greater presence of flexibility in the roll axis and would merit the design of a model for these aeroelastic effects.

Chapter 4 presents the implementation of the DASE model along with its integration with the turbulence channel. Results of offline testing are provided there as well. Real-time

experiments are discussed in Chapter 5, the results of the experiments are presented and analyzed in Chapter 6. See Appendix B for details with regard to the different parameters in the DASE models.

4. Design of Atmospheric Turbulence Motion Cueing Algorithm and Integration with Aeroelastic Model

4.1 Introduction

The Augmented Turbulence Channel, or ATC, is executed in parallel with the primary motion cueing algorithm. An advantage to this setup is that it enables the ATC to be implemented with most cueing algorithms without much trouble. By design, the only portion of the primary motion cueing algorithm being augmented is the degree-of-freedom (DOF) output that drives the motion base. The visual displays and instruments are not augmented by the channel. The Augmented Turbulence Channel went through many revisions before its real-time implementation (discussed in Chapter 5). This chapter details the algorithm design and provides analysis of the offline testing of the algorithm.

Integrating this ATC with the Dynamic Aeroservoelastic Model was also a convenient operation from a programming standpoint. Since the DASE Model output also augments the DOF output of the primary motion cueing algorithm, the two cues could be combined before this operation takes place. Verification of the integration of the two augmented cueing algorithms (ATC and DASE) was conducted offline in MATLAB and Simulink. The version of the motion cueing algorithm (NASA Adaptive) was implemented in Fortran. To test the implementation, an offline version of this algorithm was executed in batch mode. The results of this analysis are presented in Chapter 4; results from the real-time implementation are detailed in Chapter 5.

4.2 Augmented Turbulence Channel Design

Two implementations of the Augmented Turbulence Channel were tested offline. Each design is based off the original turbulence channel implemented on the Nonlinear Cueing Algorithm (Figure 4.2.1). The nonlinear cueing algorithm summed the output of the turbulence channel with the primary motion cue before sending them through the nonlinear cueing filter. This filter is designed to wash out motion that arises from pilot control input and would filter out cues representing the aircraft response to turbulence.

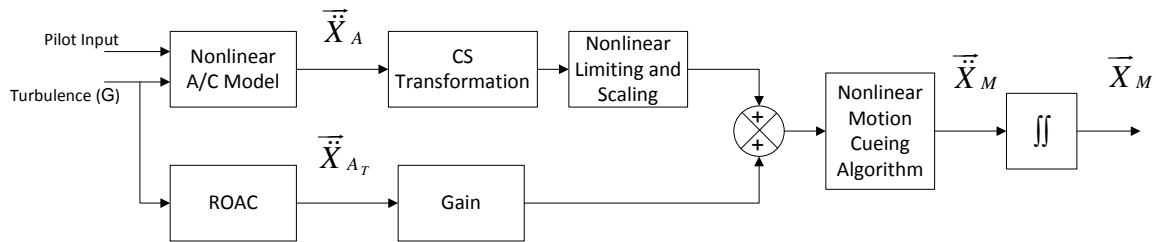


Figure 4.2.1 – Original SUNY Implementation of Turbulence Channel (Telban, 2005)

The original implementation was only applied to the heave channel. It is noted in Reid 1990, that the heave channel appears to be the most attenuated by the motion cueing algorithm. The implementation in the Nonlinear Algorithm produced somewhat more defined turbulence cues, but had severe issues with divergence. During long runs, up to 5 minutes, the motion base would begin to diverge. Possible explanations for this are in the configuration of the different components of the algorithm. By sending the turbulence cue through the same nonlinear washout filter as the primary motion cue, they are treated in the same fashion. In most cases, the

turbulence cue is going to drive the base at a higher frequency than the pilot. Consequently, this nonlinear filter is not capable of preserving the cue that is produced by the turbulence channel.

Another contributing factor to the divergence is the two integrations of the turbulence channel output. This operation will not only amplify the divergence of the signal, but also smooth the turbulence cue. In the end, the final cue had more amplitude, but the frequency content was deteriorated. The two new implementations of the turbulence channel used in the offline testing are shown in Figures 4.2.2 and 4.2.3 (Ercole, (2009)).

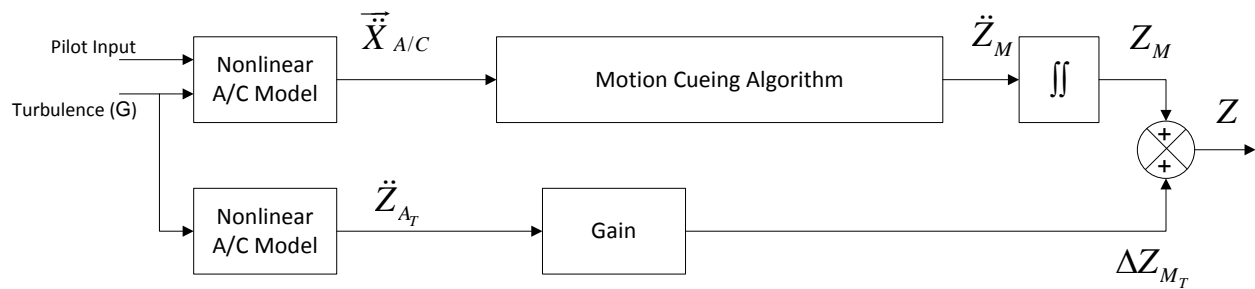


Figure 4.2.2 – Implementation 1 of Augmented Turbulence Channel

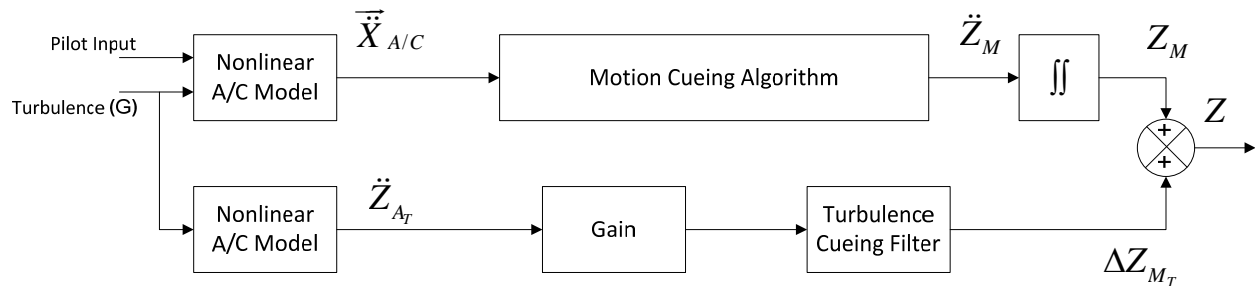


Figure 4.2.3 – Implementation 2 of Augmented Turbulence Channel

The Nonlinear Aircraft Model (NLAC) in the top channel calculates the aircraft state ($\vec{\bar{X}}_A$). This is then sent through a coordinate transformation, limiting and scaling, and the filters of the cueing algorithm. The output of the cueing algorithm comprises the entire state of the simulator, however, this figure only shows the vertical channel output (\ddot{Z}_M). \ddot{Z}_M is then integrated twice to obtain the simulator vertical displacement provided by the primary motion cueing channel (Z_M).

The second aircraft model is designed to calculate the aircraft response to turbulence alone (\ddot{Z}_{A_T}). In implementation 1 of this algorithm, the output of the aircraft model is scaled by a gain to become the turbulence augmentation cue (ΔZ_{M_T}). This output is technically a scaled acceleration; however, it is treated as a position cue.

When testing had first started on this ATC, the output of the primary motion cueing algorithm (\ddot{Z}_M) was summed with ΔZ_{M_T} . The combined signal was then integrated to form the vertical displacement of the simulator (Z_M). It became apparent very quickly that the two consecutive integrations were causing a great deal of divergence in the output. Further testing performed the integrations before summing the signals (similar to the Reid/Robinson approach). The turbulence channel output was always divergent.

Numerical integration is a process that will smooth a signal, something that is not desirable when preserving motion due to turbulence. The aircraft response to turbulence is not a zero-mean process. This is part of the reason why the signal diverges after being integrated twice. For these reasons, the output is just scaled.

In implementation 2, \ddot{Z}_{A_r} is scaled and sent through a specially designed cueing filter. The cueing filter conditions the turbulence motion cue before it is combined with the primary flight cue. The filter is designed to wash out the long period motion that is generated by the aircraft model in the turbulence channel. The high frequency motion of the primary flight cue is the portion that is most attenuated by the cueing algorithm. The purpose of the turbulence channel is to recover what is lost by the primary motion cueing algorithm. Since the long period motion of the aircraft is preserved by the cueing algorithm, there is no need to add more long period motion with the turbulence channel. With the turbulence cueing filter in place, the long period motion will be washed out of the turbulence channel output.

In Figures 4.2.2 and 4.2.3, the ATC uses a nonlinear aircraft model. This is done to ensure all the offline testing only examines the structure of the algorithm, and is not impacted by an inaccurate aircraft model. Details on the development of a Reduced Order Aircraft Model, for use in the real-time experiments, are presented in sections 4.5 and 4.6. Since the ATC was implemented along with two different aircraft models, two reduced order models were developed. Discussion on each component of the channel is conducted at length in the following sections of this chapter.

4.3 Reduced Order Aircraft Model Development

For real-time implementation, it was necessary to use a Reduced Order Aircraft Model, or ROAC, in the turbulence channel. The turbulence channel utilizes the aircraft response to turbulence alone. It was not possible to access this specific output from the nonlinear model because it is treated as a black box system. Only the aircraft state information is available as an

output; the aircraft response to turbulence alone had to be computed from a separate aircraft model.

In order to run the simulation in real-time with a high sampling rate (at least 50 Hz), only one Nonlinear Aircraft Model (NLAC) could be executed per iteration. Theoretically, if the computational power was high enough, two NLAC models could run in parallel. The aircraft model in the ATC represents the vertical aircraft response to turbulence wind gusts in the vertical direction. Since the ATC is implemented on two very different aircraft, it was necessary to design two ROAC models.

Multiple models were developed for each aircraft, the best were chosen based on an assessment of their accuracy. The models were evaluated in both the frequency and time domains. Since atmospheric turbulence is defined as a spectrum, the model cannot be verified using time response alone. Furthermore, the frequency response analysis of the ROAC output holds much more value than time domain analysis because the frequency content of the turbulence is what must be preserved in the cue.

4.4 Parameter Identification Methods

There are many methods available for parameter identification. Some which are built into the MATLAB – Simulink environment including: Auto-Regressive with External Input (ARX), Auto-Regressive Moving Average with External Input (ARMAX), Box-Jenkins (BJ), and Output-Error (OE), among others. There are desirable qualities for each of these methods, however the ARX tool was chosen because of its versatility.

Like most parameter identification methods, ARX allows the user to choose the order of the polynomial. One of the shortcomings when working with ARX is the need to use large datasets. When using small samples of a time response, ARX tends to produce unstable models. The only way to avoid this is by using longer runs or decreasing the time step to add more data points.

Another method known as Automatic Parameter Identification, or APID, was developed here at SUNY Binghamton by Dr. Kirill Zaychik. For developing the ROAC, this parameter identification method is superior to ARX as it determines the most accurate model based on the Power Spectrum Density (PSD) of the output. Before outputting a model in polynomial form, multiple polynomials are evaluated. Each model is examined in the frequency domain until the error between the input and output signals is reduced as much as possible. The accuracy of the model is also dependent on whether the user has selected the most applicable polynomial order.

The technique was originally developed by Zaychik (2009) to identify subject specific parameters that represent a human operator. It uses a bit climbing genetic algorithm. Verification of the ROACs developed in this chapter proves it can be applied to various single-input, single-output, scenarios. The only noted disadvantage to this algorithm is the time it takes to run. The models are identified using an algorithm coded in MATLAB, which can take 10 times longer than running ARX.

Both APID and ARX were executed to identify parameters of both aircraft models. The implemented models were both developed by APID because the results of the frequency response in each APID developed model showed better performance. The following sections (4.5 and 4.6) detail the ROAC development for each aircraft.

4.5 Large Civil Transport: Reduced Order Aircraft Model Development

For research purposes, we have been provided with an aircraft model representing a Large Civil Transport. This full nonlinear model operates in a black box form. There is no access to the parameters affecting the aircraft dynamics; however, we do have full control over initial conditions, pilot control input, and atmospheric conditions, along with other settings. In order to develop a ROAC, the Large Civil Transport was trimmed at 30,000 ft ASL at M 0.8, and flown through severe turbulence (level 5), with altitude hold on. Since no pilot control input is applied to the aircraft, the response in the vertical channel is primarily due to atmospheric turbulence. With this input/output data, parameter identification software can be used to identify a linear model. See Figure 4.5.1 for the input/output data used to develop the model.

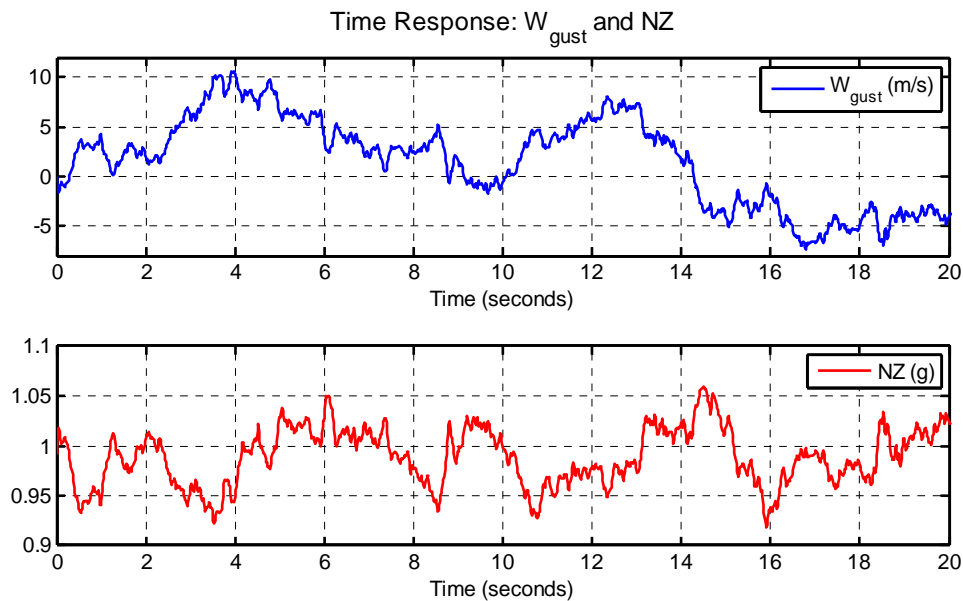


Figure 4.5.1 – Input and Output Data for Large Civil Transport ROAC Development

The first model was developed using ARX. The data was from running the NLAC at 60 Hz for about 5 minutes. Smaller datasets caused issues with developing unstable models; using 5 minute datasets eliminated this issue. The most accurate ROAC from ARX (Eq 4.5.1) is shown below. It is a 4th order transfer function. Verification was done by comparing the PSD of each model, and varying the polynomial order up to 6th.

$$\frac{\ddot{Z}_{A_T}(s)}{G} = \frac{.2422s^3 + 34s^2 - 845.5s + 2829}{s^4 + 126.7s^3 + 9762s^2 + 3.855*10^5s + 8.964*10^4}$$

Eq. 4.5.1

The model developed using APID was 2nd over 4th order transfer function (Eq. 4.5.2). Multiple polynomial orders were tested here, also up to 6, to determine the best format. The frequency response of both of these models is quite different. Figure 4.5.2 shows increased gain across most frequencies in the APID developed model. The APID developed model also has much less phase shift throughout all frequencies.

$$\frac{\ddot{Z}_{A_T}(s)}{G} = \frac{7s^2 + 2.94s + 0.63}{s^4 + 28.84s^3 + 423.6s^2 + 336.9s + 12.8}$$

Eq. 4.5.2

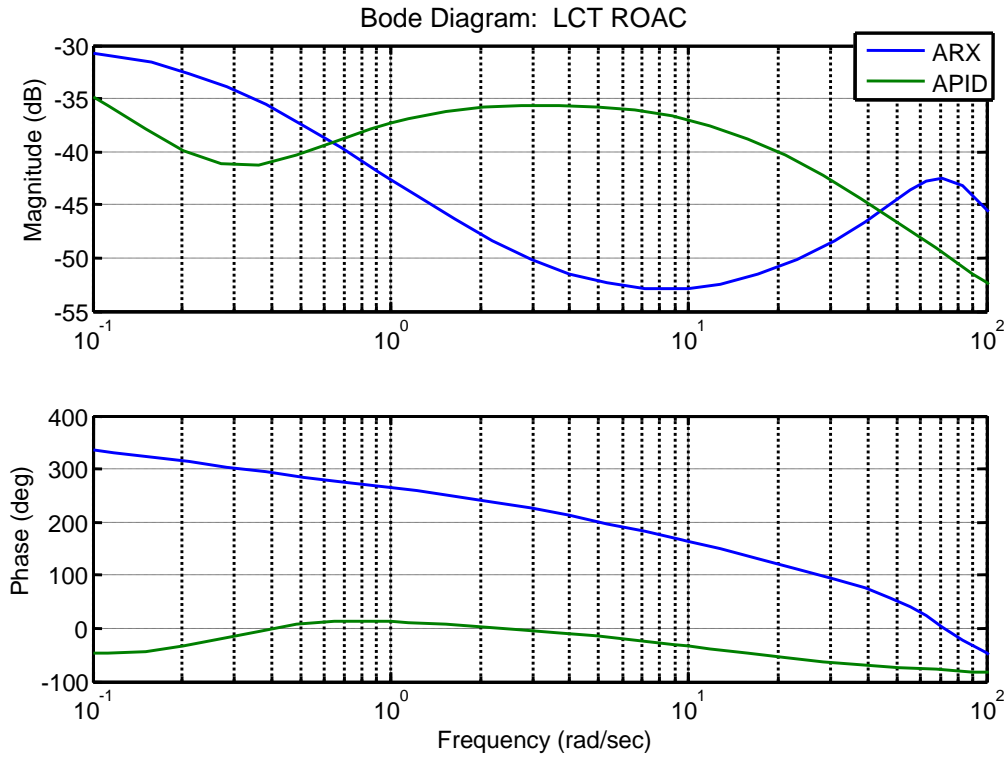


Figure 4.5.2 – Bode Diagram of Large Civil Transport ROAC

Plots comparing the PSD of each model are shown below (Figure 4.5.3). Since each aircraft model was developed with data representing the aircraft vertical response to turbulence (NZ), the output PSD of the ROACs is compared to the PSD of NZ. The units of Power in the following PSD plots are $\frac{(\text{Aircraft Vertical Acceleration (m/s}^2\text{)})^2}{\text{Hz}}$. The ARX developed model shows considerably higher power in very low frequencies, under 0.15 Hz. After this frequency, there is quite a bit of underestimation of the power. Comparing the APID developed model with NZ, the power is more aligned with that of the actual response of the full aircraft model in

frequencies over 0.1 Hz. Even though the APID ROAC shows less power in the low frequencies, the model is sufficient to produce appropriate turbulence cues.

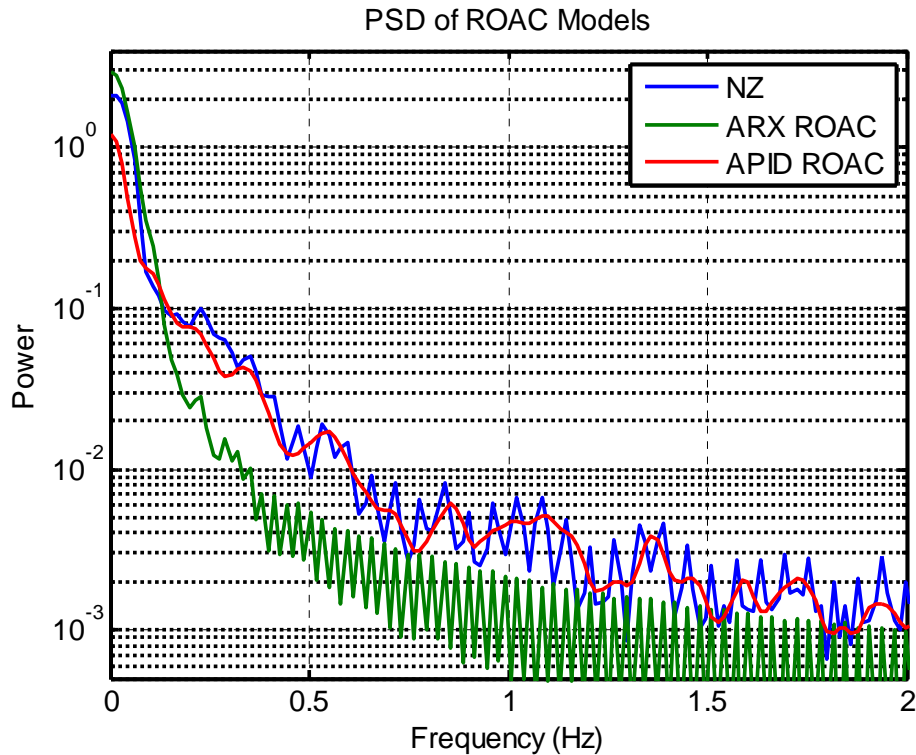


Figure 4.5.3 – PSD of Large Civil Transport ROACs and Aircraft Acceleration (NZ)

The high frequency content is also apparent in the time response plot of each model. In the time response, Figure 4.5.4, the majority of the 20 second sample shows more similarity in the frequency content of the APID ROAC and the response of the NLAC (NZ). The ARX developed model has very little amplitude in the short period oscillations. This characteristic was anticipated by the lack of power in frequencies above 0.2 Hz.

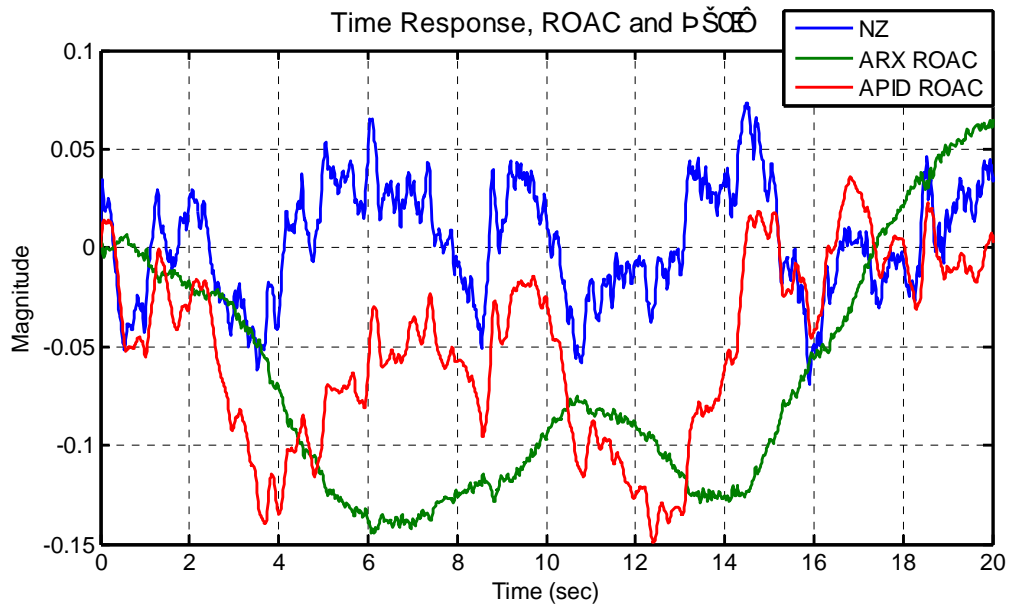


Figure 4.5.4 – Time Response of Large Civil Transport ROACs and Aircraft Acceleration (NZ)

4.6 GHSCT: Reduced Order Aircraft Model Development

Testing was conducted to see whether or not the Large Civil Transport ROAC could be used to represent this aircraft. The results of frequency analysis showed large differences in the performance of each model (see Figure 4.6.1). This shows the PSD of the vertical acceleration of the GHSCT (NZ) due to severe turbulence (level 6). This is compared to the simulated ROAC that was developed for the Large Civil Transport (Eq. 4.5.2). Based on the response in the lower frequencies, under 0.15 Hz, the PSD shows a great deal of error between the ROAC and NLAC response. For this reason, a new model was developed to better represent the dynamics of the GHSCT.

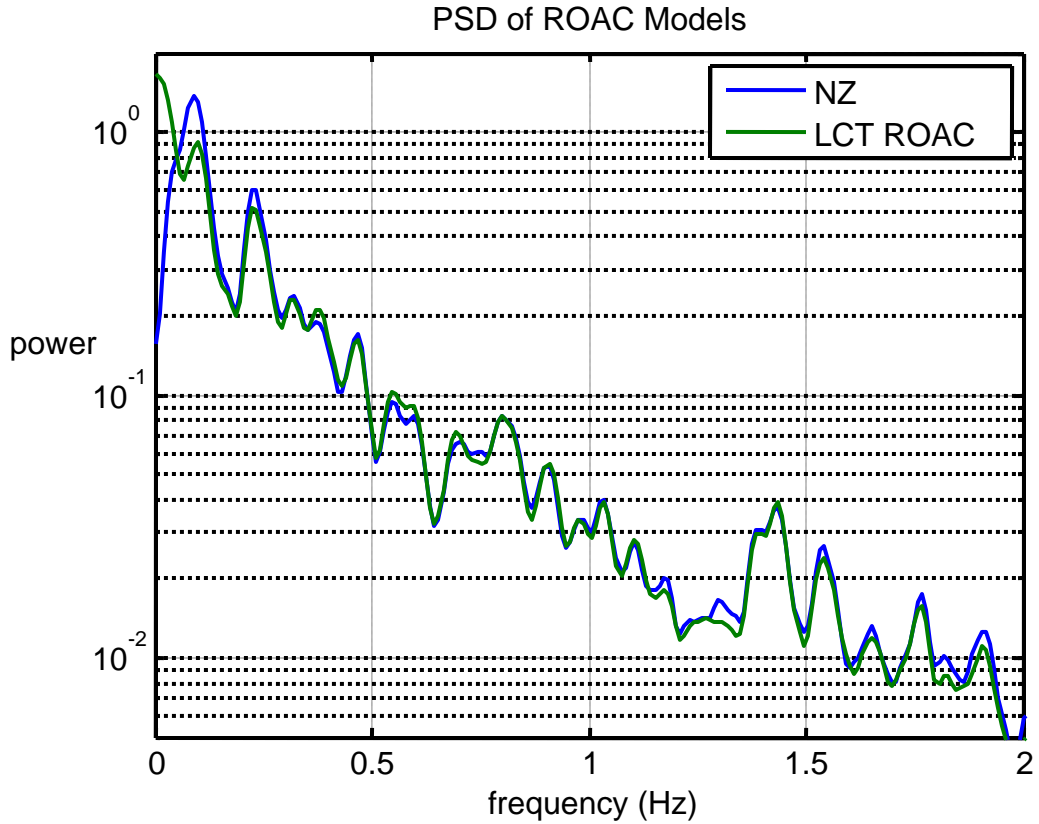


Figure 4.6.1 – PSD of Large Civil Transport ROAC and GHSCT Aircraft Acceleration (NZ)

In order to capture the aircraft response to turbulence, the GHSCT was flown at 30,000 ft ASL with altitude hold on, through severe turbulence (level 6). Since these runs were done at 80 Hz, 3 minute runs produced datasets of sufficient size to develop the reduced order model. The response data used in the parameter identification algorithms is shown below in Figure 4.6.2.

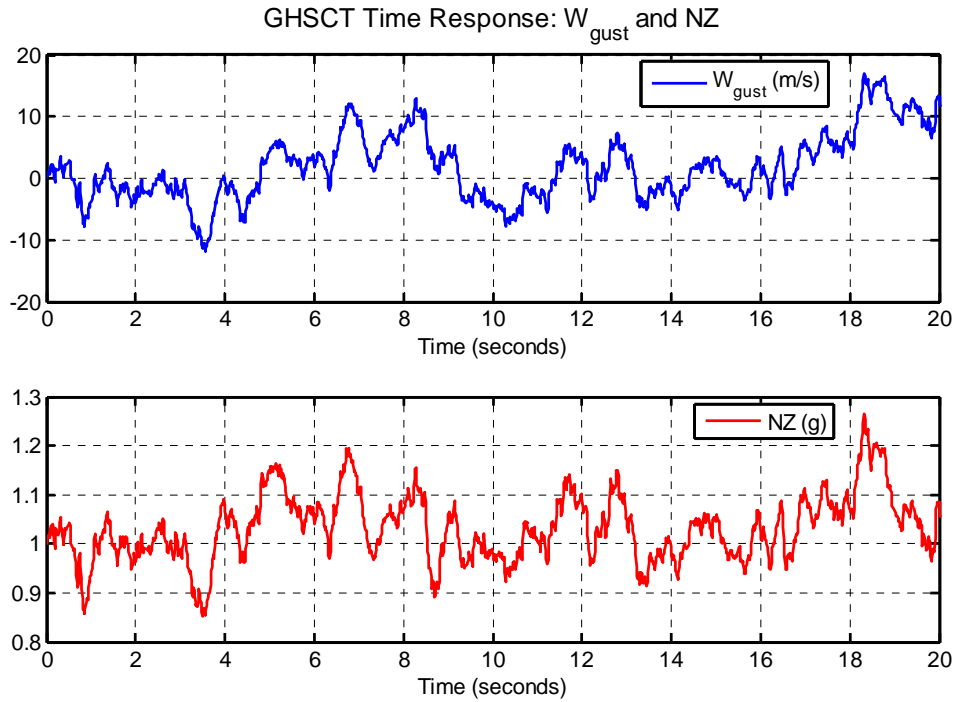


Figure 4.6.2 – Input and Output Data for GHSC T ROAC Development

The development of a ROAC for the GHSC T used the same parameter identification tools as with the Large Civil Transport. As with the Large Civil Transport, ARX and APID were employed. Fourth order transfer functions were used as the format for this model, the same as with the Large Civil Transport. The frequency response of each new model is shown in Figure 4.6.3. As with the Large Civil Transport model generated with ARX, there is considerable phase shift across all frequencies.

$$\frac{\ddot{Z}_{A_T}(s)}{G} = \frac{-0.4105s^3 + 26.93s^2 - 1213s - 8391}{s^4 + 22.31s^3 + 1.474 * 10^4 s^2 + 2.41 * 10^5 s + 3.425 * 10^4}$$

Eq. 4.6.1

$$\frac{\ddot{Z}_{AT}(s)}{G} = \frac{0.315s^3 + 12.25s^2 + 119.6s + 11.83}{s^4 + 57.8s^3 + 1121s^2 + 7473s + 3463}$$

Eq. 4.6.2

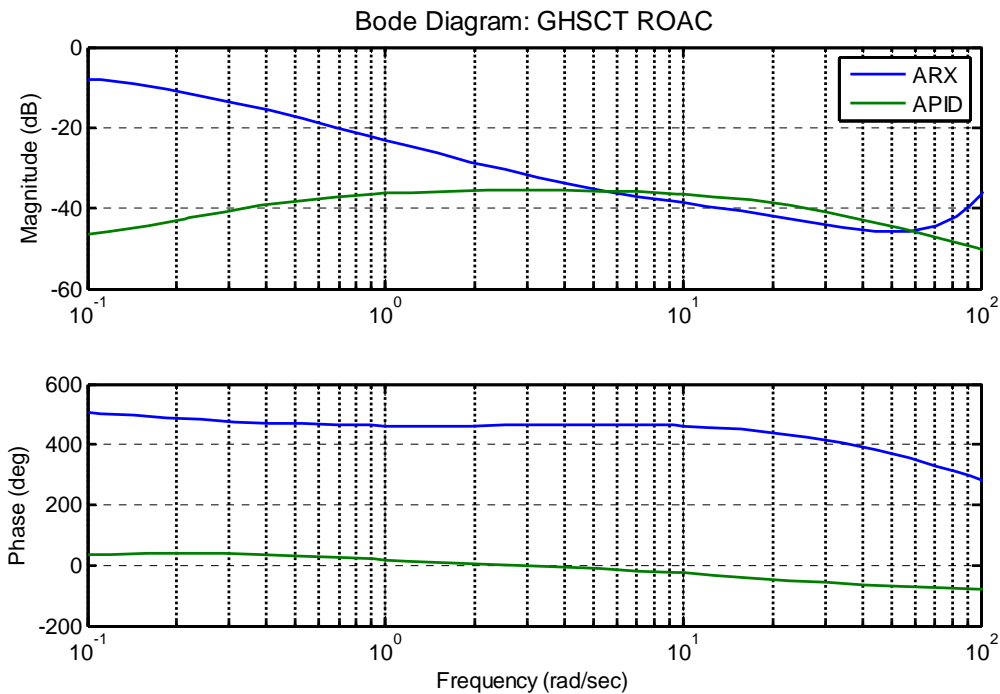


Figure 4.6.3 – Bode Diagram of GHSCT ROACs

The model developed using ARX was still not as accurate as APID. Figure 4.6.4 shows the most accurate APID model (Eq. 4.6.2) compared against the most accurate model generated with ARX (Eq. 4.6.1), the Large Civil Transport ROAC, and the GHSCT simulation output (NZ). The bottom plot of Figure 4.6.4 allows the reader to see the PSD of the most accurate ROAC (developed with APID) compared with NZ alone. There is minimal error at frequencies under 0.1 Hz, and at frequencies greater than this, the PSDs practically overlap. The time

response also shows much better performance characteristics than the model developed with ARX, in both the short period motion and high frequency characteristics of the signal (Figure 4.6.5).

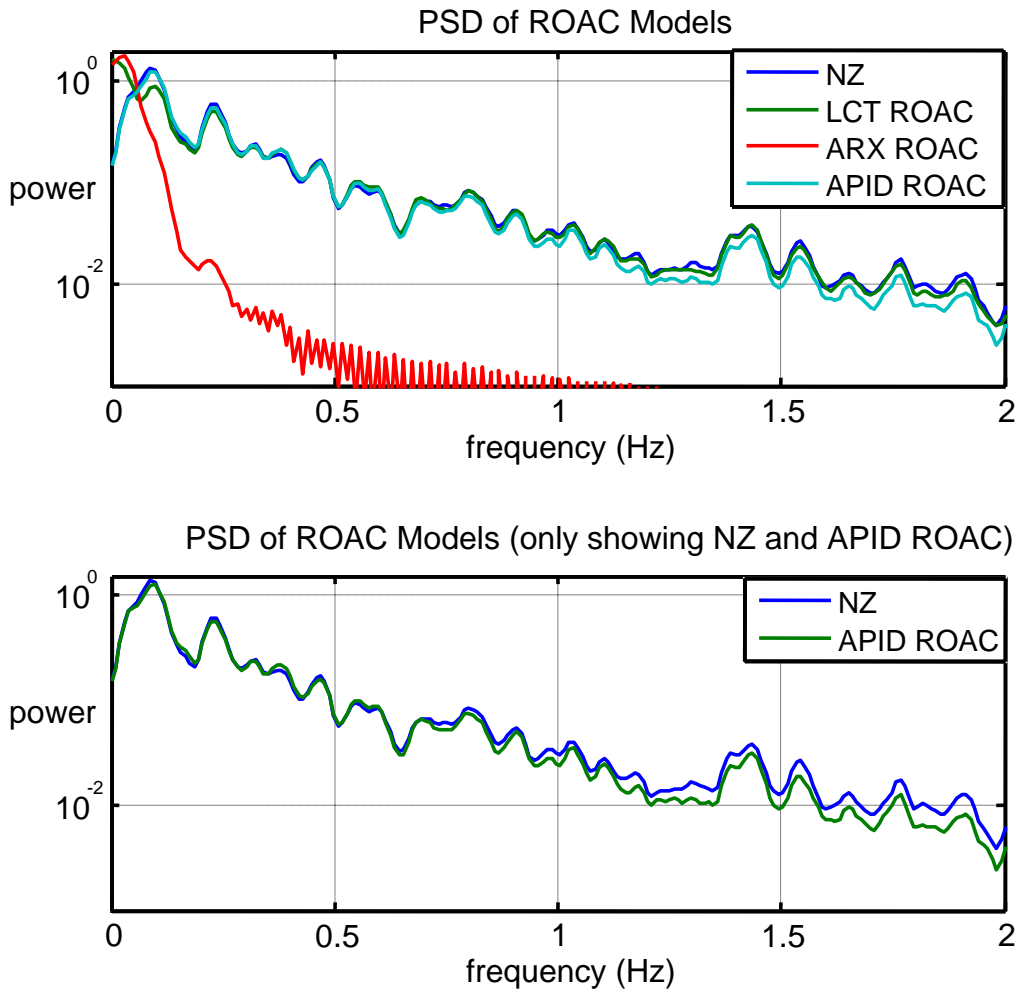


Figure 4.6.4 – PSD of GHSCT ROACs and Aircraft Acceleration (NZ)

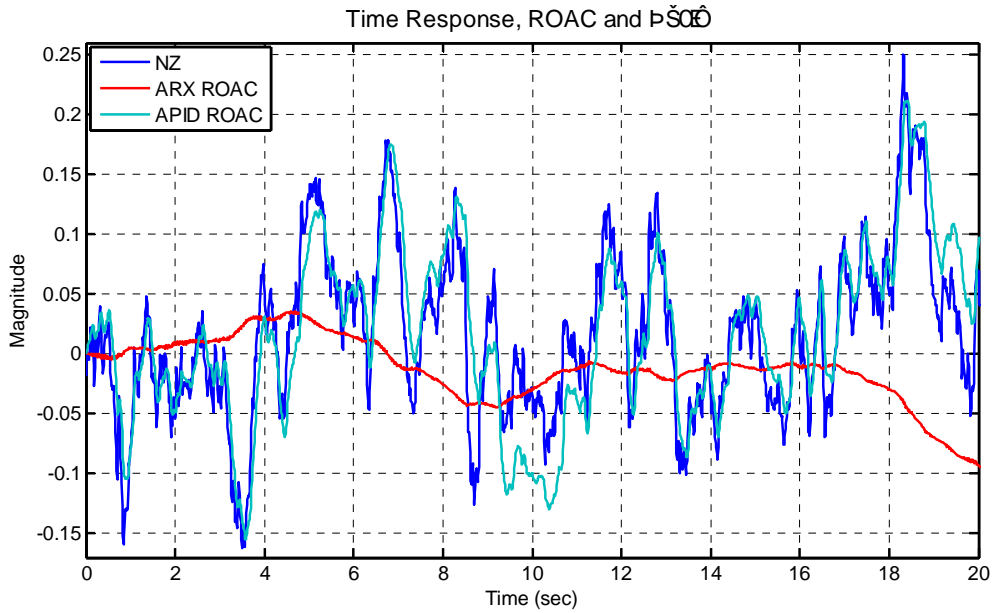


Figure 4.6.5 – Time Response of GHSC T ROACs and Aircraft Acceleration (NZ)

4.7 Turbulence Cueing Filter

The Reid Robinson algorithm employed a high-pass filter in the turbulence channel that was similar to the high-pass filter of the primary flight channel. In the implementation of the turbulence channel on the Nonlinear Algorithm, a low-pass filter was employed. This low pass filter was designed to attenuate the high frequency content generated by the ROAC, which was modeled as a high-pass filter.

A similar design was employed on Implementation 2 of the ATC. The Turbulence Cueing Filter, or TCF, was designed to attenuate high frequencies, out of the range of the aircraft response to turbulence. It is also designed to wash out the long period of the signal. Since the

primary cueing algorithm provides the pilot with long period motion due to turbulence, there is no reason to preserve this motion in the ATC.

A fourth order, band-pass filter design was chosen (Eq. 4.7.1). From 5 rad/s (0.79 Hz) to 25 rad/s (3.98 Hz), the gain of the filter remains near 0.0 dB (see Figure 4.7.1). Frequencies under 0.79 Hz and frequencies greater than 3.98 Hz are attenuated, and subjected to considerable phase shift.

$$\frac{Z_T(s)_{\text{filtered}}}{Z_T(s)} = \frac{s^2 + 0.5s}{2.04 * 10^{-4} s^4 + 0.020s^3 + 1.025s^2 + 1.255s + 0.25}$$

Eq. 4.7.1

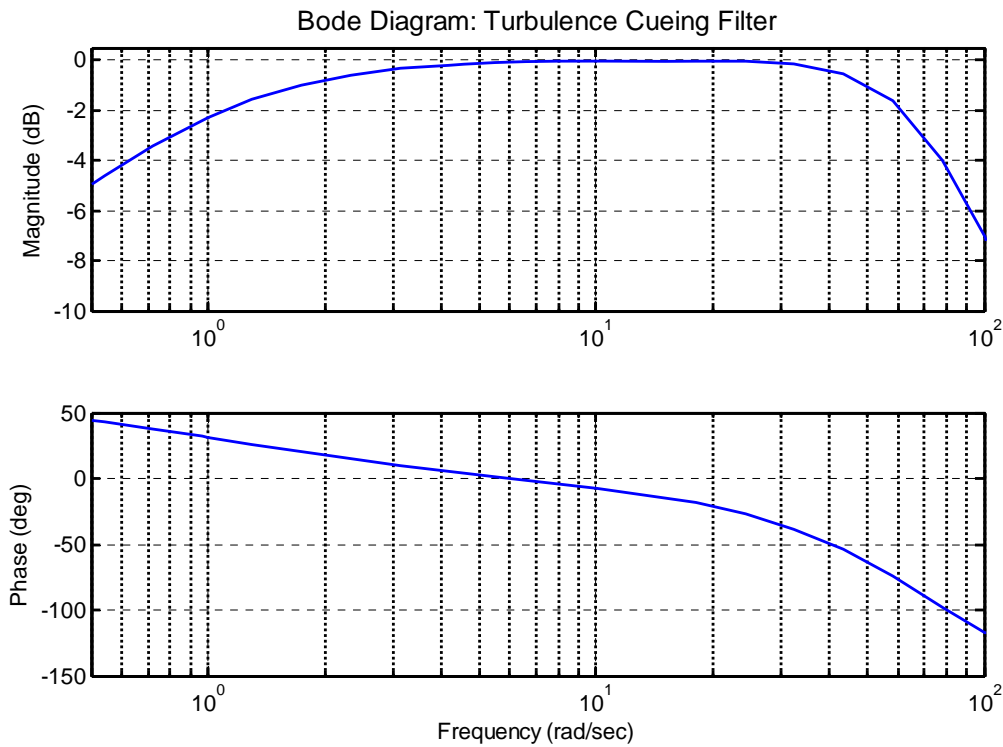


Figure 4.7.1 – Bode Diagram of Turbulence Cueing Filter

The step response of the filter shows the ability of this filter to wash out cues. The settling time is 11.2 seconds, however, 70% of the amplitude is washed out after 2 seconds.

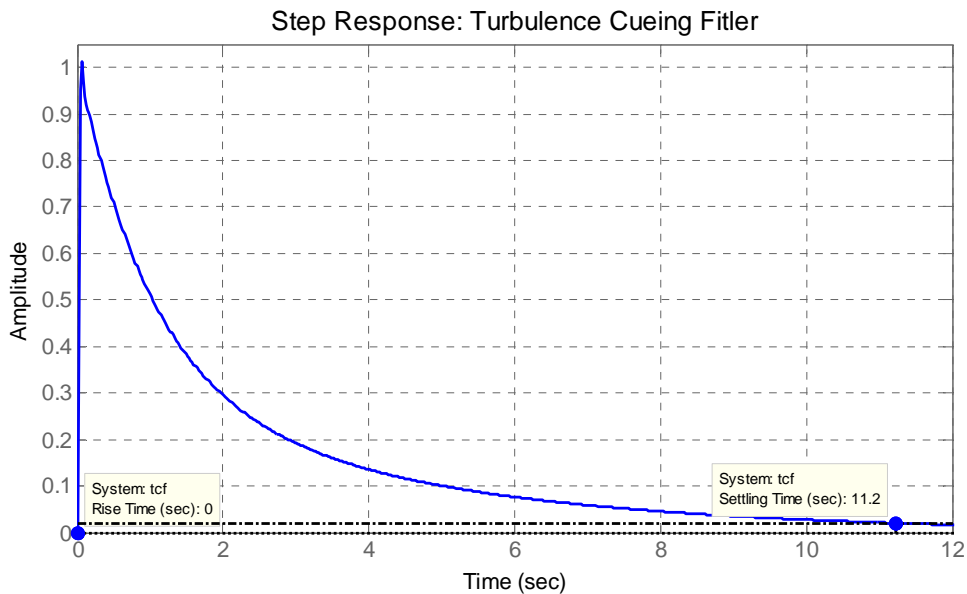


Figure 4.7.2 – Step Response of Turbulence Cueing Filter

Later testing with the real-time simulation revealed that the cueing filter in the turbulence channel caused the turbulence cue to lose some sharpness. The pilot noted that with the cueing filter activated, there was enough of a difference to slightly reduce the intensity rating. Some of the longer period turbulence cues appeared to be washed out before the motion was completed. The algorithms were tuned with the filter on, but the real-time experiments were all conducted without the TCF.

4.8 Integration with Aeroelastic Model

The GHSCT aircraft is integrated with the Dynamic Aeroservoelastic Model (DASE model) and the NASA Adaptive cueing algorithm. As mentioned in Chapter 3, the DASE model augments the output of the primary motion cueing algorithm, in a similar fashion to the ATC.

Figure 4.8.1 shows the block diagram of the integration of the two augmented channels.

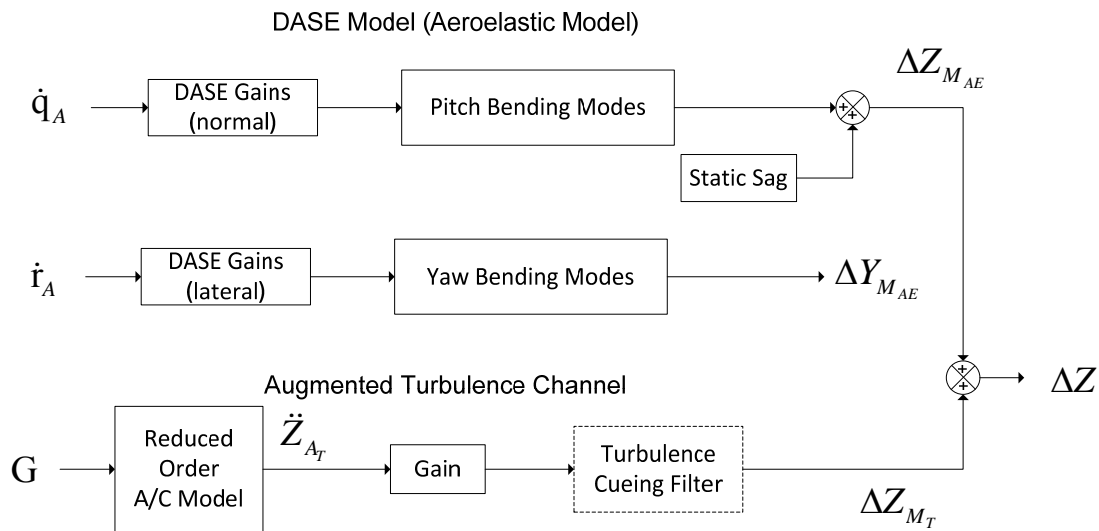


Figure 4.8.1 – Integration of DASE Model and Augmented Turbulence Channel

The inputs to the DASE Model (\dot{q}_A and \dot{r}_A) are directly from the aircraft model state vector. The aeroelastic model uses these angular accelerations along with a series of filters to calculate bending displacements in the vertical and lateral axis ($\Delta Z_{M_{AE}}$ and $\Delta Y_{M_{AE}}$, respectively); see Chapter 3 for more detail on this model. Now that the ATC and DASE models

are integrated, there are two augmentation cues in the vertical channel, one from the turbulence channel (ΔZ_{M_T}) and one from the aeroelastic model ($\Delta Z_{M_{AE}}$).

These augment the cueing algorithm in DOF space, the resulting augmentation cue in the vertical channel is ΔZ . This is summed with the output of the primary motion cue, \vec{X}_M , not shown in this figure.

The combined output of ΔZ and \vec{X}_M is then sent to the motion base, presenting the pilot with augmented cues representing both atmospheric turbulence and aeroelastic bending. See Appendix B for detail on the Fortran code used to execute the turbulence channel and integrate the two augmented channels.

4.9 Testing: Offline Simulation of Algorithms

Before implementing the Augmented Turbulence Channel on the real-time simulation, there must be some offline testing. These tests are designed to examine the effect of the augmented cue on the primary motion cue. The NASA Adaptive and SUNY Nonlinear algorithms, like most cueing algorithms, attenuate the amplitude and frequency content of atmospheric turbulence cues. Testing will show whether or not the frequency content of the primary motion cue has improved with the augmented algorithm.

When running the GHSCCT, the cueing algorithm must also contain the output from the flexible aircraft model. The offline testing will verify the implementation of the ATC and the integration with the DASE model.

The offline testing is broken down into two sections in this chapter: the Large Civil Transport and GHSCT implementations (sections 4.9.1 and 4.9.2, respectively). This was done because each aircraft is currently implemented with a different motion cueing algorithm and required a separate set of offline runs. Additionally, the integration of the ATC and DASE model requires a separate set of analysis, which only relates to the GHSCT.

4.9.1 Large Civil Transport: Offline Testing

In the case with the Large Civil Transport, the offline testing was conducted on the SUNY Nonlinear Motion Cueing Algorithm. This algorithm is set to run in batch mode using a Fortran compiler. The algorithm running on the flight simulator reads aircraft state data from the Large Civil Transport in real-time. Using this information, the motion cues are calculated by the cueing algorithm, also in real-time. The offline cueing algorithm is executed using an input file that contains the output of the nonlinear Large Civil Transport model.

To generate the cueing algorithm input file, the Large Civil Transport is executed offline. This model allows the user to define pilot input and atmospheric disturbances, among other things. The model itself cycles at 60 Hz, generating data comprising of every piece of information with regard to the aircraft state. Figure 4.9.1 shows the Large Civil Transport (NLAC) GUI that is executed to generate the aircraft state information.

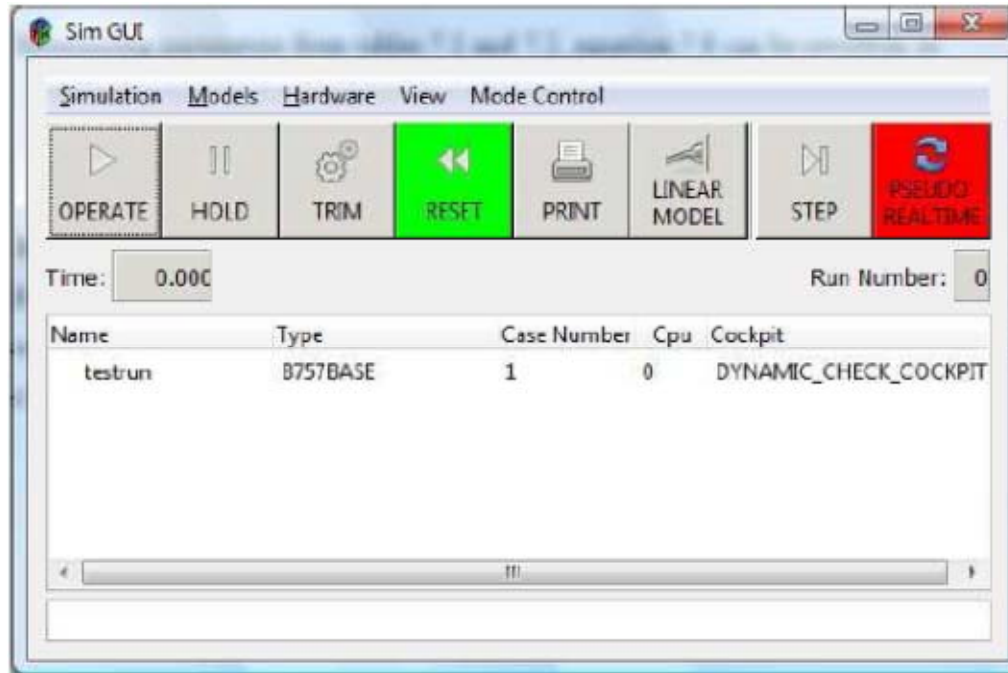


Figure 4.9.1 – Large Civil Transport Model GUI (courtesy of NASA LaRC)

The offline cueing algorithm treats the run in the same fashion as the real-time algorithm. The output of the cueing algorithm is the motion base state, in degree-of-freedom space and actuator leg space. To verify the implementation of the turbulence channel, the DOF output is evaluated with and without the ATC. When the ATC is activated, there should be a substantial increase in the high frequency motion of the final cue.

The two implementations are shown below in Figures 4.9.2 and 4.9.3. Here, the output of the NLAC (\vec{X}_A) represents the aircraft response to both atmospheric turbulence and pilot input. The NLAC that is executed in the turbulence channel produces the aircraft response to

turbulence alone (\ddot{Z}_{A_T}). In implementation 1, this output is scaled, producing the turbulence augmentation cue (ΔZ_{M_T}). Implementation 2 calculates ΔZ_{M_T} by filtering \ddot{Z}_{A_T} .

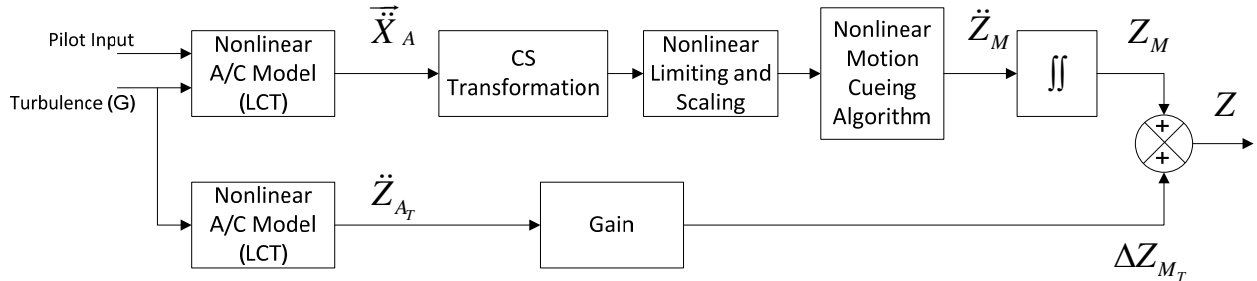


Figure 4.9.2 – Large Civil Transport Implementation 1 of Augmented Turbulence Channel

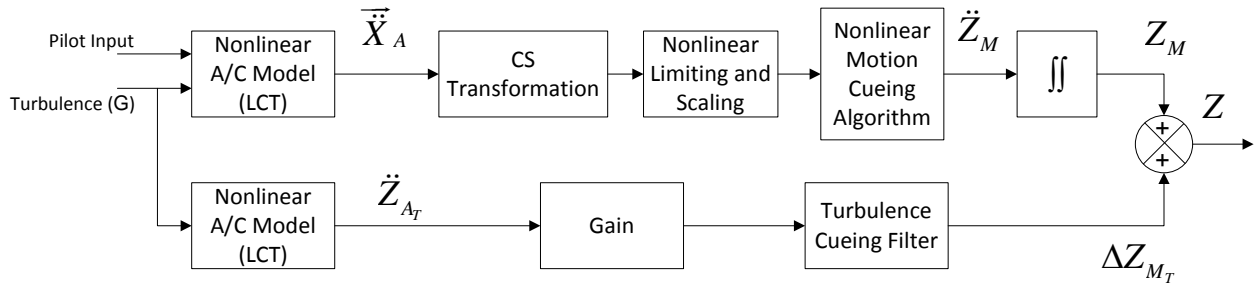


Figure 4.9.3 – Large Civil Transport Implementation 2 of Augmented Turbulence Channel

The cueing algorithm was executed using aircraft state data from level flight through level 5 turbulence. The first plot (Figure 4.9.4) shows the motion cue generated by the primary

motion cueing channel. This was executed running the modified cueing algorithm and turning the ATC off with a gain of 0.0 in the ATC.

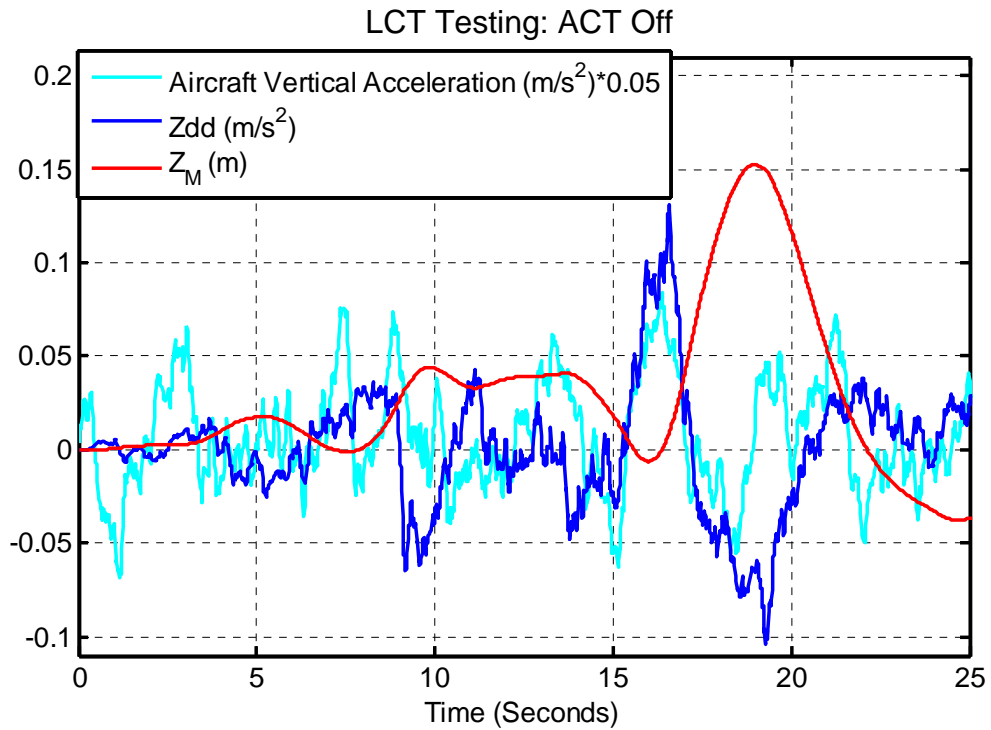


Figure 4.9.4 – Large Civil Transport Testing, Time Response, ACT Off, Vertical Channel Only

The aircraft vertical acceleration shown in this figure is the vertical component of $\ddot{\vec{X}}_A$. The high frequency accelerations of this output are due to turbulence. The next piece of data (Zdd) is the output of the cueing algorithm, prior to the integrations (also defined as \ddot{Z}_M). Once integrated, the high frequency motion that is apparent in the aircraft vertical acceleration and \ddot{Z}_M appear to have no impact on the primary motion cue (Z_M). This is the type of issue that is

usually faced when trying to simulate atmospheric turbulence, and the main motivation for this study.

The output of implementation 1 of the ATC is shown in Figure 4.9.5. The same data was used to execute the cueing algorithm; the only difference here is the addition of the turbulence channel. It is clear from this plot that Z contains high frequency motion and some greater peak amplitude. The gain used in the turbulence channel is 1.5. Accordingly, there seems to be some large amplitude excursions due to the turbulence. Tuning the algorithm using the simulator motivated a large reduction in the gain; the cues were amplifying the perceived turbulence level substantially, even under light turbulence.

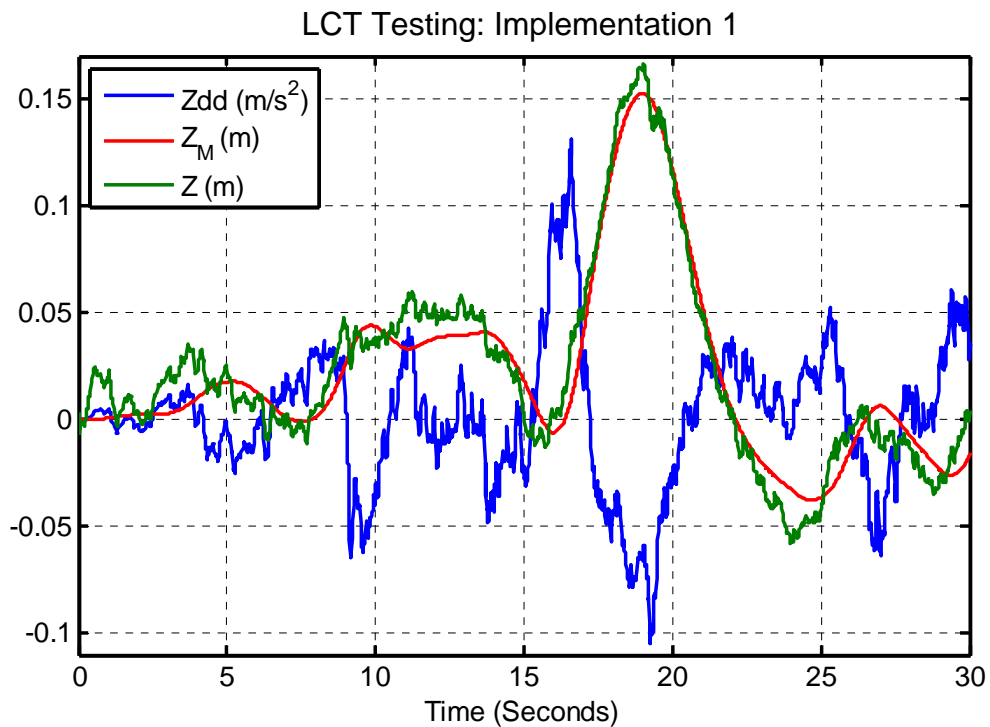


Figure 4.9.5 – Large Civil Transport Testing, Time Response, Implementation 1 of ATC, Vertical Channel Only

The time response of Implementation 2 is shown in Figure 4.9.6. There is not a substantial difference between the turbulence cues of these two implementations. The peak amplitude of Z is reduced slightly. It also appears that Z oscillates about Z_M rather than slightly above it. In Implementation 1, the augmented cue is usually greater than the output of the primary flight channel (Z_M). This does not happen with Implementation 2 because the Turbulence Cueing Filter washes out the long period motion. The only portion of the turbulence cue left in ΔZ_{M_T} is the high frequency component.

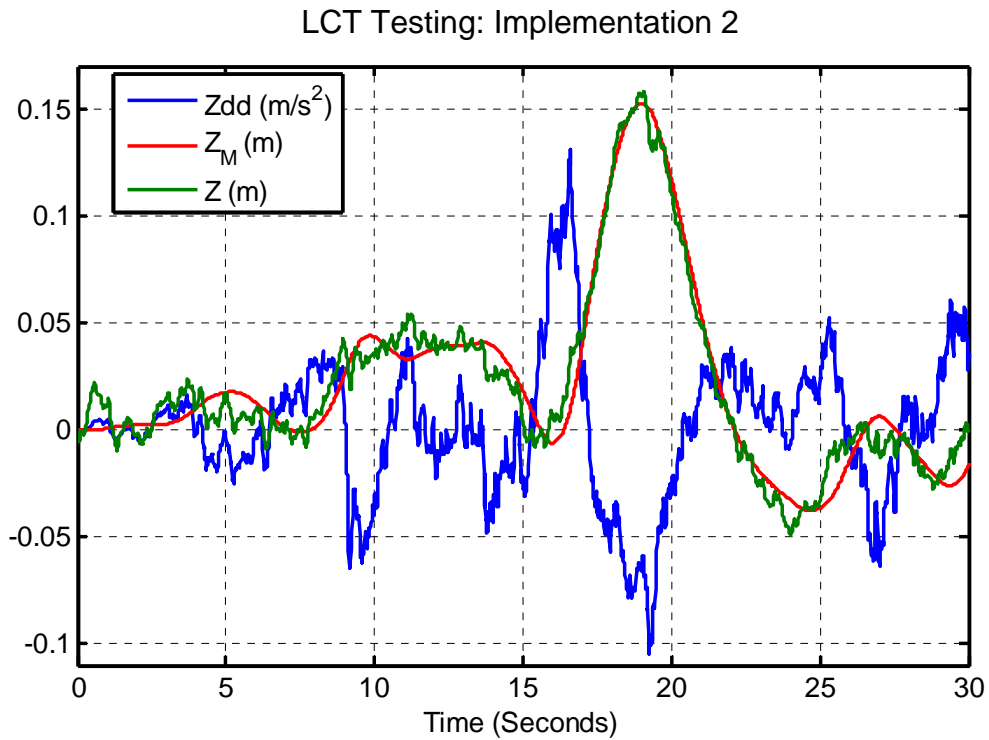


Figure 4.9.6 – Large Civil Transport Testing, Time Response, Implementation 2 of ATC, Vertical Channel Only

In order to analyze the effects of the TCF more closely, Figure 4.9.7 shows zoomed portions of the time response of Implementation 1 and 2. In this plot, it is more noticeable that Z Implementation 1 (without the added filter) adds some long period amplitude to the primary motion cue. The peak magnitude of Z is greater without the filter.

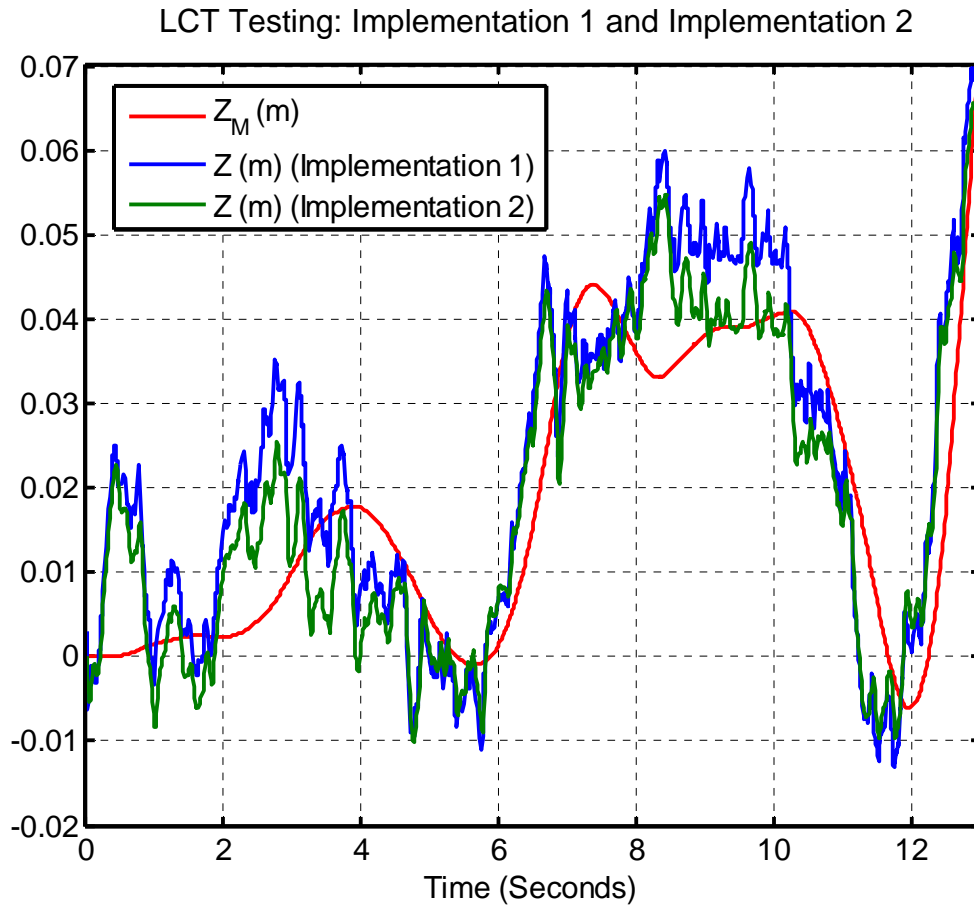


Figure 4.9.7 – Large Civil Transport Testing, Time Response, Comparison of Implementations 1 and 2

With the results of the offline testing, it was determined that the next step was to test the algorithm in real-time. The additional code that was added to the motion cueing algorithm is in

Appendix B. Both implementations were executed on the flight simulators at NASA LaRC. Chapter 5 details the real-time tuning of the algorithm and the piloted experiments.

4.9.2 Generic High-Speed Civil Transport: Offline Testing

To test the implementation on the GHSCCT, the ATC was implemented with the NASA Adaptive Motion Cueing Algorithm. Figure 4.9.8 shows Implementation 1 of the Augmented Turbulence Channel and DASE Model. Just as the Large Civil Transport testing, only the vertical channel is analyzed in this set of tests. The vertical output of the primary cueing channel (Z_M) is summed with the augmentation cues produced by the DASE Model ($\Delta Z_{M_{AE}}$) and the ATC (ΔZ_{M_T}). Each of these cues represents a position increment designed to provide motion at the pilot station that represents atmospheric turbulence and fuselage bending. Implementation 2 adds the Turbulence Cueing Filter to the algorithm (Figure 4.9.9).

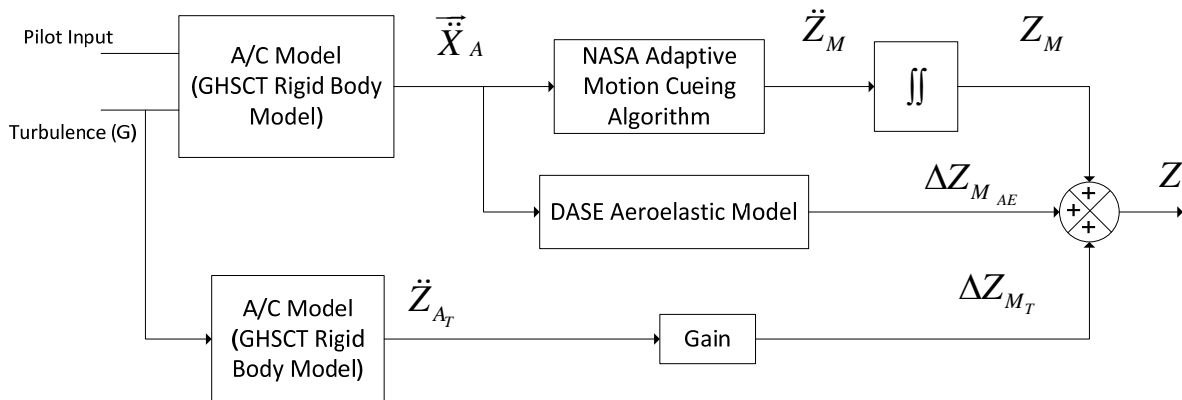


Figure 4.9.8 – GHSCCT Implementation 1 of Augmented Turbulence Channel and DASE Aeroelastic Model

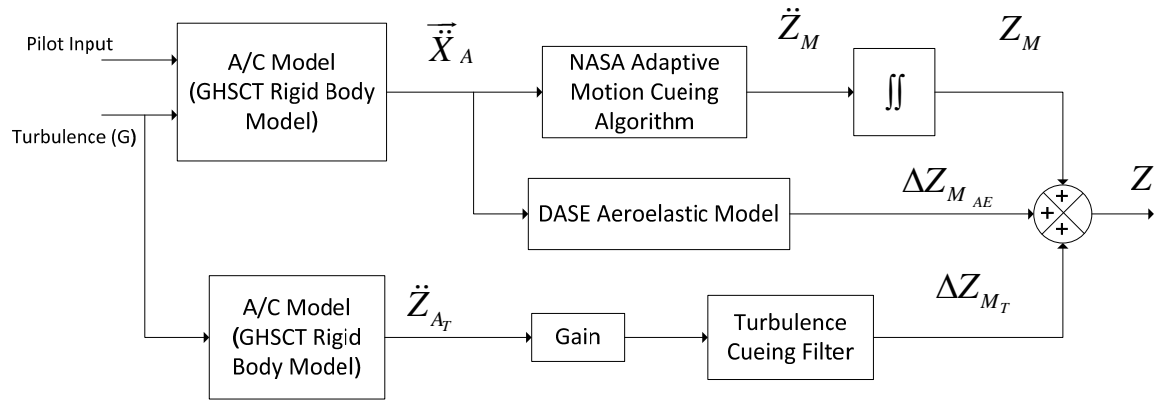


Figure 4.9.9 – GHSCT Implementation 2 of Augmented Turbulence Channel and DASE Aeroelastic Model

Aircraft state data were collected from running the rigid body model in real time. In order to obtain data that included fuselage bending, the GHSCT was flown with a pilot at the controls. The rigid body model could have been executed offline, along with the DASE Model, but this would not have generated appropriate aeroelastic bending cues without pilot input.

The aeroelastic cues are dependent on the size of the angular accelerations (\dot{q}_A and \dot{r}_A). The turbulence model that is implemented on the GHSCT does not produce rotational turbulence gust disturbances. A pure translational turbulence model does not produce much rotation of the aircraft, and therefore pilot input is needed to excite large bending modes.

To gather the data for this model, the GHSCT was flown through turbulence level 6. There was no pilot input during the first portion of the run; for this time, the only external disturbance was the turbulence wind gust. As the run progressed, the pilot began making inputs to compensate for the divergence from altitude. As expected, these inputs induced larger angular accelerations which excited the aeroelastic model. The same DASE Model parameters were

used on the real-time experiments. Parameters for the aeroelastic model are shown in Appendix B.

The Fortran code from the NASA Adaptive algorithm was modified to include a new subroutine that executes the augmented turbulence channel during each iteration. With this new piece of code, the algorithm can be executed offline with the turbulence channel. The aeroelastic output is calculated when running the GHSCCT rigid body model and simply summed with the primary cue along with the output of the ATC.

For the purpose of comparing Z_M and Z , the static sag offset was removed from the aeroelastic cue. The static sag is a constant that is summed with the vertical channel output of the DASE Model, more information on this term is provided in Chapter 3. Removing the term allowed the DASE Model output to oscillate about zero, rather than at an offset of 0.19 m.

The original implementation of the GHSCCT using the NASA adaptive algorithm is plotted in Figure 4.9.10. This time response is from the portion of the run without pilot input. The cueing algorithm attenuates the high frequency motion in the same manner as the Large Civil Transport run shown earlier in the chapter. The aircraft responds to the turbulence gust input (see Aircraft Vertical Velocity, from \overline{X}_A). The cue prior to integration (Z_{dd}) also contains this high frequency motion. Just as the other cueing algorithm, once Z_M is calculated, the turbulence is attenuated.

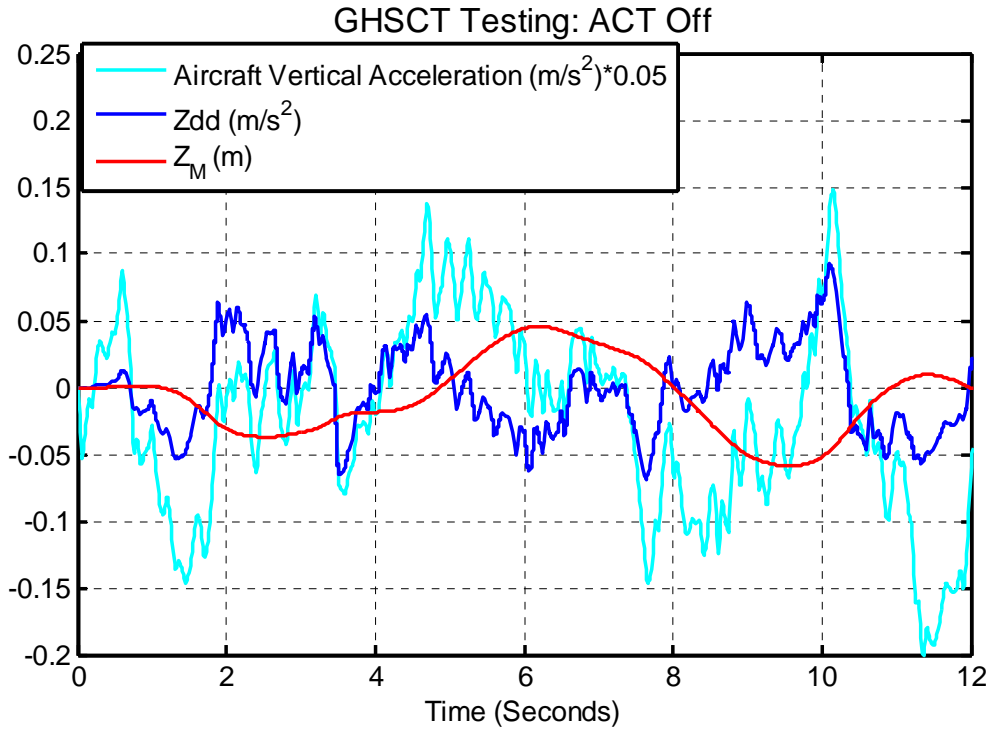


Figure 4.9.10 – GHSCT Testing, Time Response, ATC Off, Vertical Channel Only

Adding the ATC to the algorithm had the same effect as with the Large Civil Transport implementations. Implementation 1 and 2 were executed with a gain of 1.5 in the turbulence channel. The time response of each implementation was analyzed to ensure the cue was produced properly. Plots are shown in Figures 4.9.11 and 4.9.12.

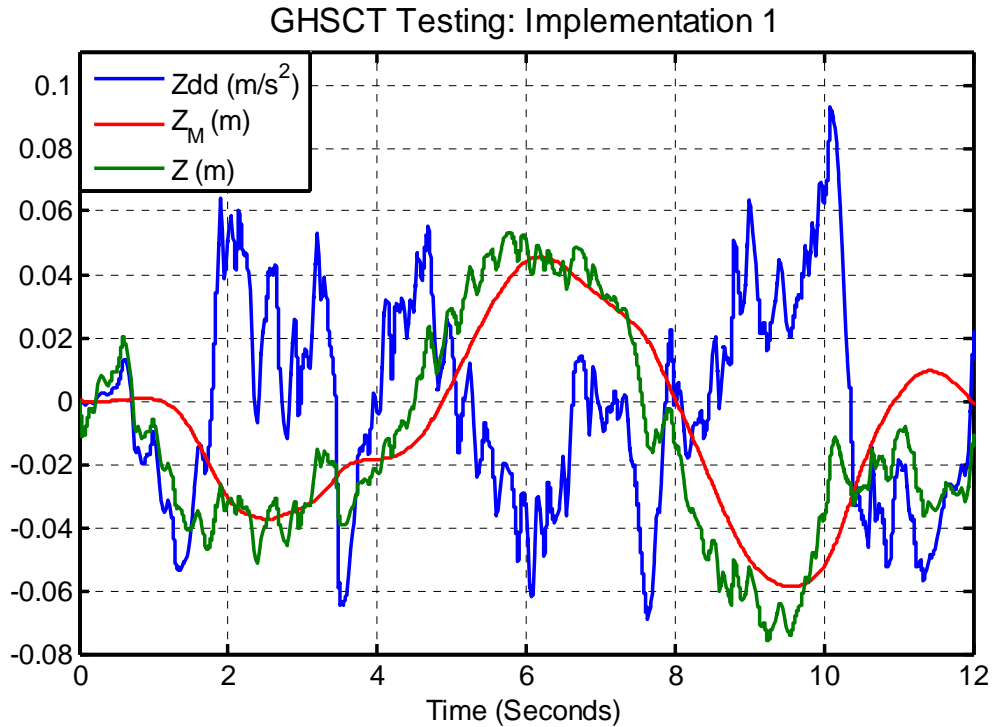


Figure 4.9.11 – GHSCT Testing, Time Response, Implementation 1 of ATC, Vertical Channel Only

The output of the ATC adds considerable high frequency motion to Z . In Implementation 1, the peak amplitude of Z is increased more. Applying the cueing filter to the turbulence channel manages to reduce the peak amplitude of Z (Figure 4.9.12). One of the other advantages of Implementation 2 is the ability to use a higher gain term without excessively amplifying the cue. This can be done because any amount of long period motion will be washed out from that signal by the filter; the only portion that is intensified by the gain is the short period oscillation.

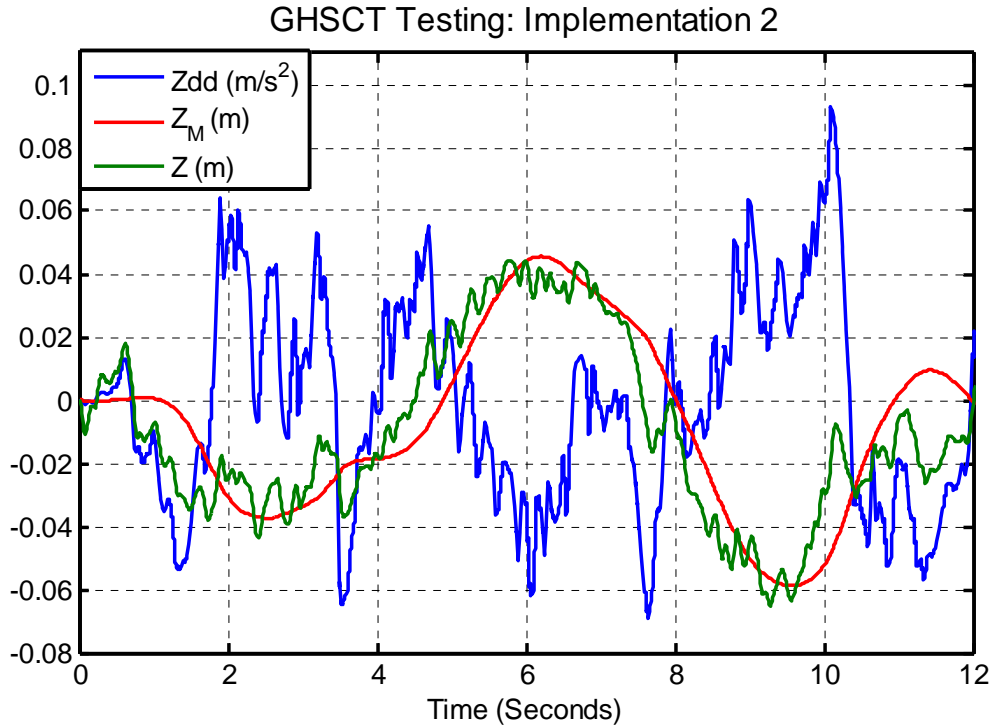


Figure 4.9.12 – GHSCT Testing, Time Response, Implementation 2 of ATC, Vertical Channel Only

The integration of the two augmented channels also needed to be tested. During this run, the pilot input began at 8.5 seconds. Figure 4.9.13 shows the effect of adding just the DASE Model to the algorithm. The resulting cue (Z) does not contain any high frequency content because the turbulence channel is off. According to the plot, there is no cue from the aeroelastic model until the pilot begins to make a small input. The resulting motion from the DASE Model ($\Delta Z_{M_{AE}}$) is shown in the in the second plot along with the scaled pitch stick input (force). The pilot control input also increases the amplitude of the simulator excursion considerably.

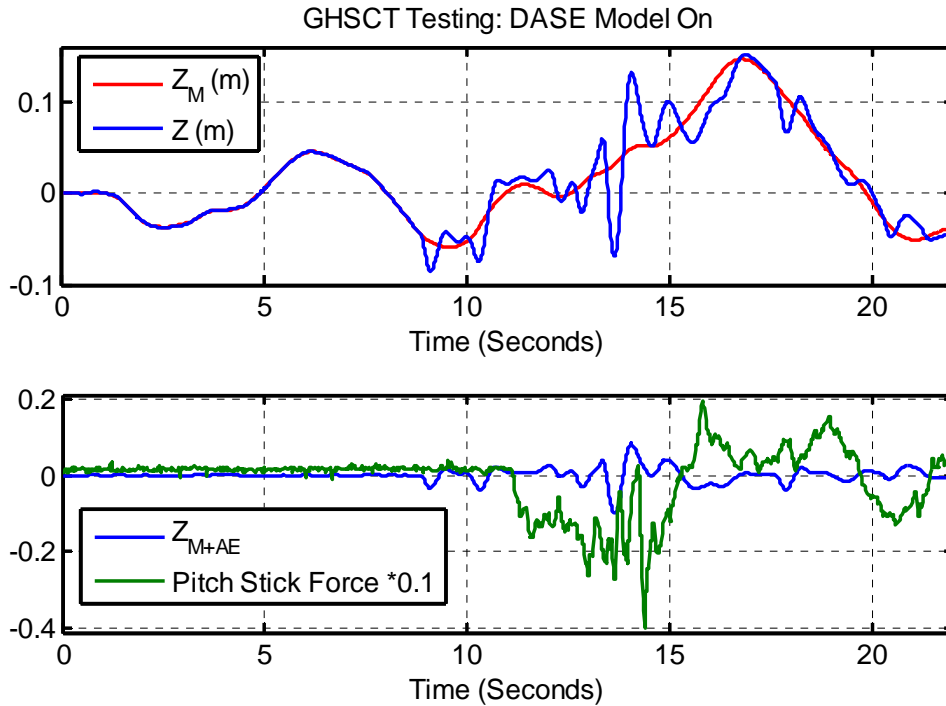


Figure 4.9.13 – GHSCT Testing, Time Response, ATC Off, DASE Model On

The next configuration includes the ATC and DASE Model. Figure 4.9.14 is the same as the above figure, however, Z includes the addition of the turbulence channel. This is Implementation 1 with the DASE Model active; the TCF was not used. Once the pilot begins to make inputs, the output of the DASE Model ($\Delta Z_{M_{AE}}$) reaches much higher amplitude than the turbulence channel (ΔZ_{M_T}). The turbulence cue present in Z is much less noticeable when combined with the aircraft flexibility.

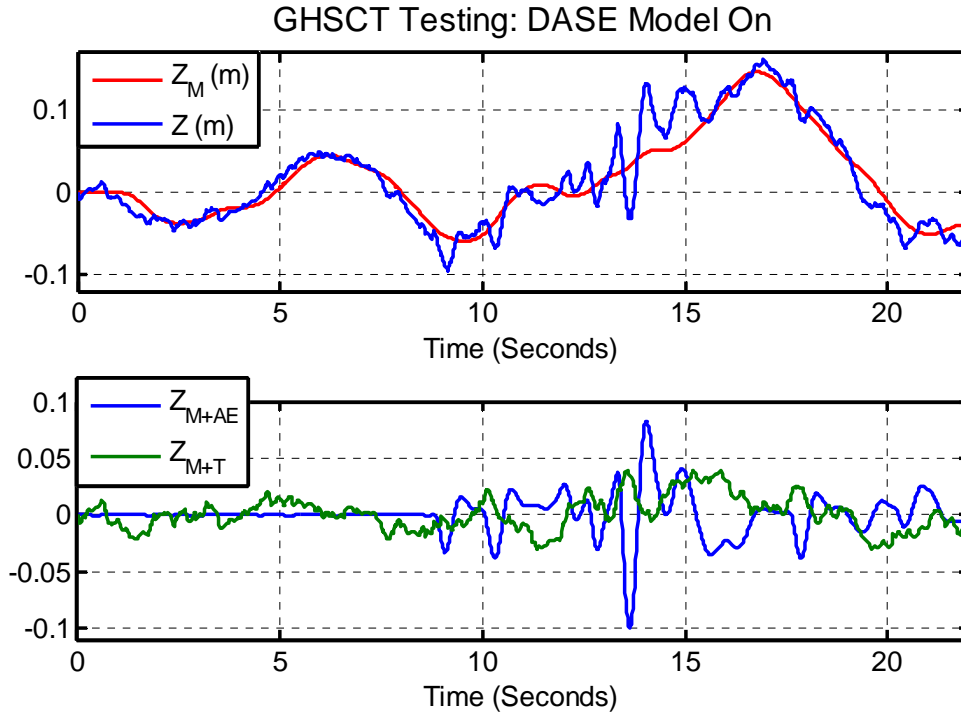


Figure 4.9.14 – GHST Testing, Time Response, ATC On, DASE Model On

Early in the run, the turbulence motion added by the ATC is very apparent in the cue. Once the flexibility model is excited by pilot input, the motion due to turbulence is not as visible. This offline testing simulates the ATC to allow visualization of the full algorithm. Normally the pilot would be responding to the cue produced by the ATC, thus changing the dynamics of their input. Here, the ATC is added in just to analyze the change in vertical response.

Offline testing shows distinct motion cues from both the turbulence channel and aeroelastic model are now part of the cue that drives the motion base. This output will change the dynamics of the motion cueing algorithm and potentially improve the simulation. The real-

time simulation discussed in Chapter 5 takes into account the response of the pilot with the new augmented cues and looks to validate the algorithm.

Modifications were made to the NASA Adaptive Algorithm to include the turbulence channel. This version of the cueing algorithm already comprised the aeroelastic model. In order to do this, a subroutine needed to be added that calculates the output of the ROAC. This output was then scaled by a gain term. This gain term was added to the GUI of the simulation for modification between runs when tuning the algorithm. The output of the turbulence channel was combined with the DOF output of the primary flight channel. This is the same output that is augmented by the DASE Model output. Fortran subroutines that comprise the turbulence channel can be found in Appendix B. There, the added code to apply the output of the ATC is also shown.

5. Design of Experiments

5.1 Introduction

Experiments were designed to demonstrate the efficacy of the augmented cueing channel and the effect on pilot control, in order to gain insight into the response of the pilot to the newly developed turbulence channel and aeroelastic model. These experiments have been divided into two studies: the Large Civil Transport study and the Generic High-Speed Civil Transport study. Three experiments were conducted under each study. The Augmented Turbulence Channel was implemented on both aircraft; only the GHSCT is outfitted with the aeroelastic channel.

This chapter contains a detailed description of each study, including the method by which the pilot will subjectively evaluate the experiments. Chapter 6 contains the quantitative results and subjective data as well as analyses of these real-time experiments.

5.2 Background Information

The studies were conducted on two flight simulators, each at NASA Langley Research Center. The Visual Motion Simulator, or VMS, is a general-purpose flight simulator with a synergistic motion base. It has a 60 inch usable stroke and uses six hydraulic actuators to provide the pilot with full six degree-of-freedom motion (Telban et al. (a)). Figure 5.2.1 shows the VMS.



Figure 5.2.1 – Visual Motion Simulator (Courtesy of NASA LaRC)

The current setup comprises six heads-down CRT displays, providing the pilot with aircraft state, engine information, and navigation and map display. There are also numerous instruments and gauges on the instrument panel. Figure 5.2.2 shows the inside the cockpit view.



Figure 5.2.2 – Visual Motion Simulator Flight Deck (Courtesy of NASA LaRC)

The second flight simulator is part of the newly developed NASA Cockpit Motion Facility, or CMF. This facility has one motion system that has the ability to accept

interchangeable flight decks. There are four fixed-base sites that allow for no-motion experiments to be conducted. Figure 5.2.3 shows an artist's concept of the facility, with three fixed-base simulators and one flight deck mounted on the motion system.

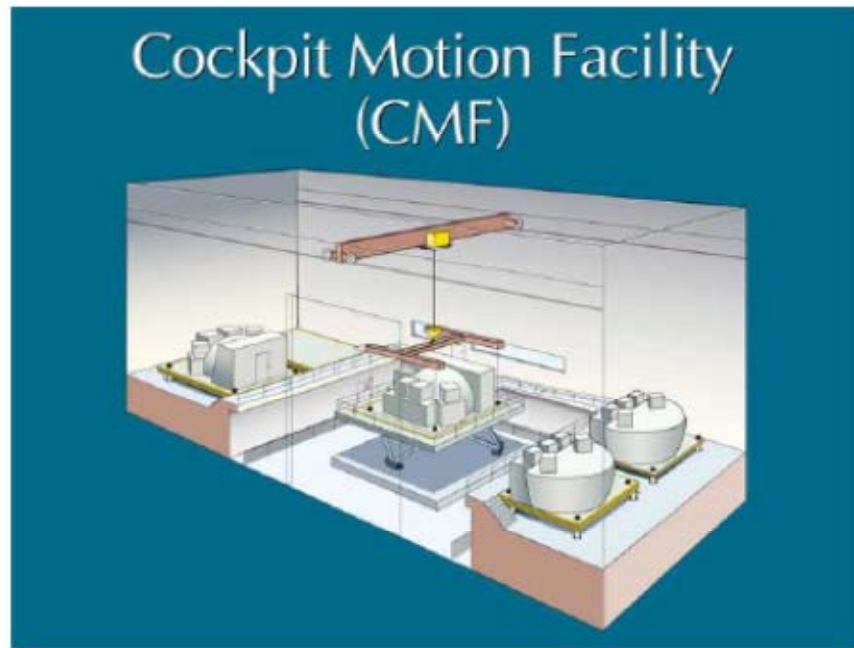


Figure 5.2.3 – Artist Rendition of Cockpit Motion Facility (Courtesy of NASA LaRC)

The motion system is a six degree-of-freedom, synergistic motion base with six 76 inch hydraulic actuators with 72 inch usable stroke. This state of the art motion system utilizes advanced control laws that allow for a bandwidth of up to 2.5 Hz. Future advancement of this control logic will allow for a bandwidth over 5 Hz. Each of the cockpits is equipped with an image generator and display hardware, flight input control loaders, and a full instrument panel. The flight deck that was used in this study was the Generic Flight Deck (GFD), shown in Figure 5.2.4. It uses four CRT/beam splitter/mirror collimated displays to provide the pilots with an out

the window view. The GFD instrument panel uses LCD panels and gauges to display sensor readings and other information.



Figure 5.2.4 – Generic Flight Deck on CMF motion system (Courtesy of NASA LaRC)

5.3 Tuning the Augmented Turbulence Channel (ATC)

The gain in the turbulence channel was tuned subjectively until the pilot was satisfied with the turbulence sensation. Each implementation of the ATC had to be tuned separately. The Large Civil Transport and GHSCT implementation required multiple tuning sessions, before the results were satisfactory. The VMS and CMF have very different control laws, and each motion base will filter the commanded motion slightly. Because of this, the algorithms had to be tuned

separately for each simulator as well. The GH SCT implementation was tuned on the CMF and VMS; the Large Civil Transport implementation was only tuned on the VMS.

The gain tuning sessions were conducted subjectively. The pilot was provided with the Turbulence Reporting Criteria Table, from the FAA Airman's Guide⁶. This guide, shown in Appendix C, details criteria for each specific intensity: Light, Moderate, Severe, and Extreme. The specific criteria are separated into two categories: Aircraft Reaction and Reaction Inside the Aircraft. As the aircraft is flown through the turbulence field, the pilot monitors the instruments and notes the sensation he feels. The pilot also indicates whether or not there was any portion of time in which he/she was not in positive control over the aircraft. With all this information, the pilot can accurately assess the turbulence level. The turbulence is then described as Occasional, Intermittent, or Continuous. Light and moderate chop are also designated in the guide as turbulence that causes rapid and rhythmic bumps, without appreciable changes in altitude.

According to the Airman's Guide, if the aircraft is under moderate or severe turbulence, the reaction inside the aircraft specifies that unsecured objects are dislodged or tossed about. It also states that occupants feel a certain amount of strain against their seatbelts. Due to the limitations of the simulator, enough motion could not be produced to actually displace unsecured objects. It was also difficult to produce any substantial strain against the seatbelts. It is possible that these criteria could be met using a simulator that can provide longer sustained acceleration, such as the Vertical Motion Simulator at NASA Ames.

The ability to continue food service and for people to walk is also assessed under the reaction inside the aircraft category. Under light turbulence, walking and food service should be possible. In moderate turbulence, walking and food service should be difficult and they should

be impossible in severe turbulence. These criteria were met with each turbulence level, when tuning the Large Civil Transport. Some of the reaction inside the aircraft criteria could not be met when tuning the GHST.

In order to support a rating of extreme turbulence, the aircraft reaction specification includes that the aircraft is violently tossed about and that control is practically impossible. It is also indicated that the turbulence may cause structural damage. To ensure the safety of the pilot and copilot, along with the simulator hardware, the algorithm was not tuned to meet the necessary measure for extreme turbulence.

The Dryden turbulence model is designed to provide the aircraft with severe turbulence at level 6. The gain tuning of the algorithm ensured the most realistic severe turbulence cue was provided to the pilot at this level and that each possible criterion in the FAA Airman's Guide was met. Since the ATC only supplements the vertical channel, the tuning was also intended to keep a balance of motion in each degree of freedom. It is not desirable for the vertical channel of turbulence to overshadow the other degrees-of-freedom. If the results of this experiment show that more balance between the heave and lateral channels is needed, the turbulence channel can be applied to other degrees-of-freedom.

It was noted that the only way to achieve each possible criterion for moderate and severe turbulence intensities, the rotational turbulence model (MIL-F-8785 B) had to be active. When just translational turbulence encounters the aircraft, it does not induce as much workload on the pilot; he/she compensates for little changes in attitude. It is also noted that even in a severe turbulence field, without rotational cues, the aircraft was always in positive control.

The rotational turbulence model also adds realism to the simulation since, in reality, atmospheric turbulence does not have an even distribution; this causes attitude changes to the aircraft. The GHSCT had not been outfitted with the rotational turbulence model; consequently, most of the turbulence reporting criteria were not met during the tuning of the ATC or the experiments.

Once the channel was tuned to ensure the turbulence met all possible criteria detailed in the FAA Airman's guide, the experiments could be conducted. The resulting gain for the Large Civil Transport implementation was tuned to 0.13. The GHSCT implementation gain was tuned to 0.015 on the VMS and 0.04 on the CMF. Tuning was done subjectively, also the two simulators are very different. The reason the gain was so much lower for the GHSCT implementation is because the turbulence gust input to the ATC is in ft/s. For the Large Civil Transport implementation, the gust input is in m/s. The pilot considered the visual cues, force feel, instruments and many other cues when determining an appropriate gain. The gain tuning test plans for each aircraft are shown in Appendix D.

5.4 Design of Experiments

The experiments are intended to test the effect of the ATC on the pilot and determine whether or not the ATC adds realism to the simulation. Since the turbulence and aeroelastic augmentation channels modify the dynamics of the simulation, the pilot should respond by changing his/her flying characteristics. It is hypothesized that increasing the motion to the pilot will result in an increase in their overall effort, thereby, increasing their workload. The

frequency of the pilot control will most likely shift as well, as they respond to higher frequency motion cues.

Workload is a human factors concept that is used to describe how difficult a system is to control. It is dependent on the amount of work the pilot does and the frequencies at which he/she operates. One of the goals of any simulation is to provide an environment where the pilot exerts the same workload as they do in an actual flight.

Three types of experiments were conducted during each study. The first task was to maintain straight and level flight at 30,000 feet above sea level for 2 minutes. The second was to perform a straight in approach and landing, starting on the glide slope. The third experiment was an offset approach and landing. For this experiment, the aircraft was trimmed on the localizer and glide slope of the runway. The pilot was then directed to switch to a parallel runway and complete the approach.

The Cooper-Harper Rating Scale was used to rate certain tasks in each experiment. Cooper-Harper Ratings (CHR) are a set of criteria used by test pilots and flight test engineers to evaluate the handling qualities of an aircraft. The scale ranges from 1 to 10; where 1 indicates the best handling characteristics and 10 indicates the worst.

Cooper-Harper Ratings were given during each of the experiments. For Experiment 1, the pilot provided a CHR on the task of maintaining level flight at the prescribed altitude. When conducting the two landing experiments (Experiments 2 and 3), the pilot provided a CHR on the task of maintaining the glide slope and a CHR on the touchdown. With regard to Experiments 2

and 3, it is noted that pilots would never be intentionally directed to land in severe turbulence. See Appendix E for the Cooper-Harper Rating Table.

Each experiment was conducted without turbulence and at different turbulence intensities. These included light, moderate, and severe; which correspond to Dryden levels 2, 4, and 6. Between runs, the structure of the algorithm was changed to represent three different configurations. Figure 5.4.1 shows the different configurations for running the experiments with the Large Civil Transport. Figure 5.4.2 shows each configuration of the GHSCT.

Configuration 1 used just the primary flight channel. This did not provide the pilot with any augmented cues. Configuration 2 applied the Augmented Turbulence Channel and Configuration 3 applied both the ATC and DASE model. Since the DASE model is only available on the GHSCT aircraft, Configuration 3 was not applied when running the Large Civil Transport.

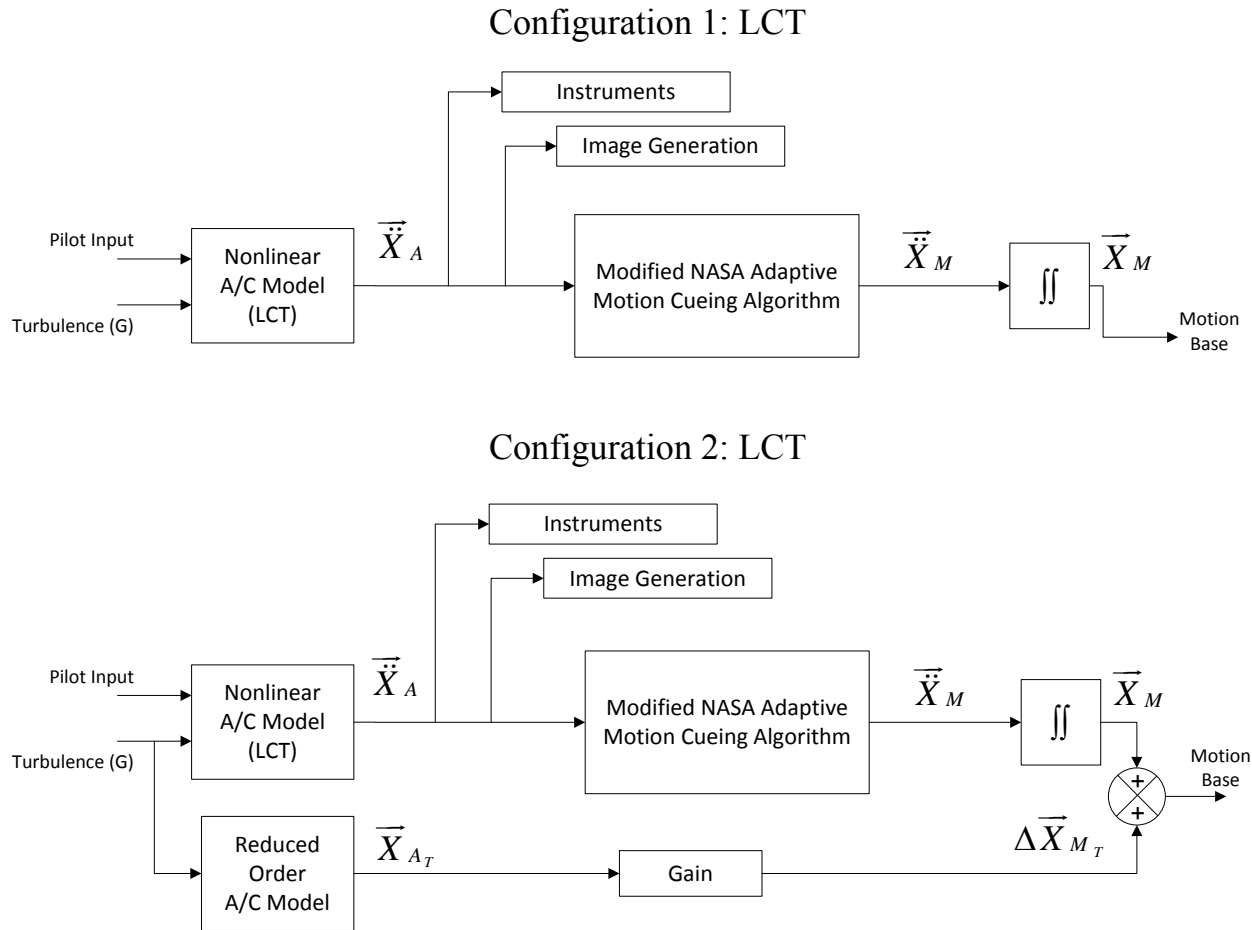
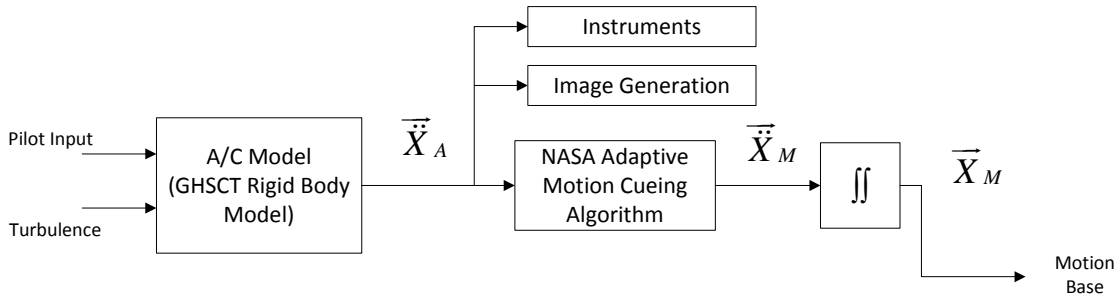
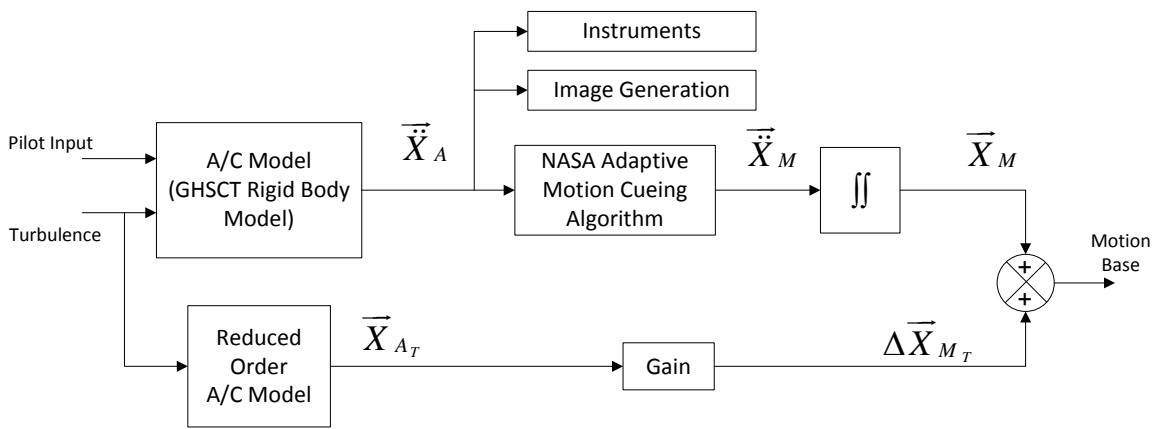


Figure 5.4.1 – Large Civil Transport Experiment Configuration Block Diagrams

Configuration 1: GHSCT



Configuration 2: GHSCT



Configuration 3: GHSCT

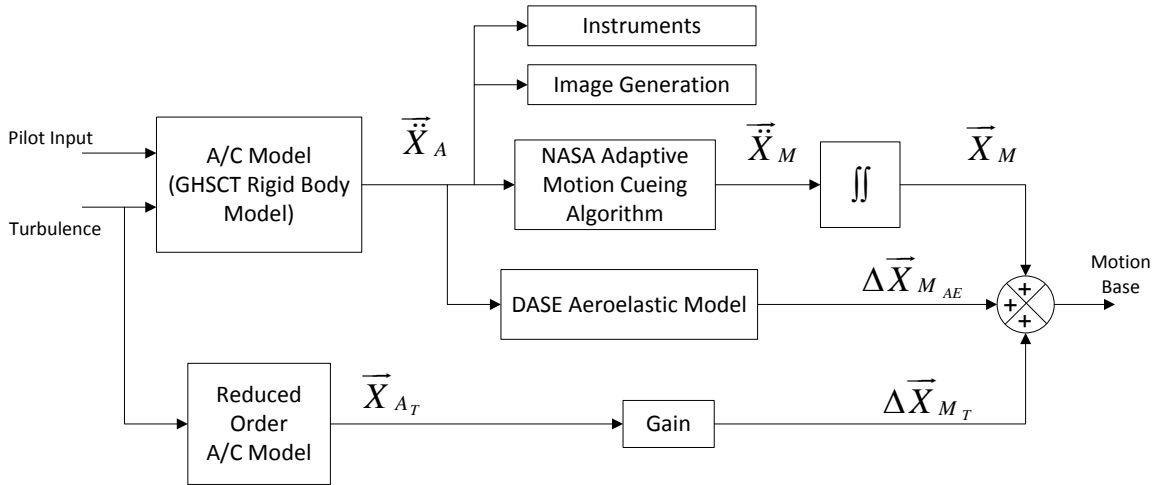


Figure 5.4.2 – GHSCT Experiment Configuration Block Diagrams

The runs were randomized based on both the turbulence level, and whether or not the ATC or DASE model was turned on. There were seven specific runs for each experiment with the Large Civil Transport, making a total of 21 runs. There were 10 runs for each experiment with the GHSCCT, which had a total of 30 runs. Table 5.4.1 shows the run order and conditions for the GHSCCT experiments. Appendix F details the run conditions and the randomized order that was followed along with the experimental protocol for each implementation.

| Run Conditions: Generic High Speed Transport | | | |
|---|-------------------------------|---------------|------------------|
| Run Order | Run Number - Data file number | Configuration | Turbulence level |
| Experiment 1: Maintain straight and level flight at 30000 feet ASL | | | |
| 1 | | 1 | OFF |
| 2 | | 2 | 6 |
| 3 | | 1 | 4 |
| 4 | | 3 | 2 |
| 5 | | 1 | 6 |
| 6 | | 1 | 2 |
| 7 | | 3 | 4 |
| 8 | | 2 | 4 |
| 9 | | 2 | 2 |
| 10 | | 3 | 6 |
| Experiment 2: Straight in approach and landing | | | |
| 1 | | 2 | 4 |
| 2 | | 1 | 2 |
| 3 | | 1 | 4 |
| 4 | | 1 | 6 |
| 5 | | 3 | 2 |
| 6 | | 3 | 6 |
| 7 | | 2 | 6 |
| 8 | | 3 | 4 |
| 9 | | 1 | OFF |
| 10 | | 2 | 2 |
| Experiment 3: Offset approach and landing | | | |
| 1 | | 1 | 6 |
| 2 | | 3 | 4 |
| 3 | | 2 | 4 |
| 4 | | 2 | 6 |
| 5 | | 1 | OFF |
| 6 | | 1 | 2 |
| 7 | | 2 | 2 |
| 8 | | 3 | 6 |
| 9 | | 1 | 4 |
| 10 | | 3 | 2 |

Table 5.4.1 – Run order and conditions for GHST experiments

Data were recorded during the runs, specifically; all pilot control inputs, along with the aircraft model state, and simulator sensor outputs. Both simulators have six platform accelerometers and a package of sensors at the centroid of the motion base. On the VMS, this centroid package contains three translational accelerometers (X, Y, Z) and three rotational accelerometers (ϕ, θ, ψ). The CMF has a similar package at the centroid; however there are three rotational rate sensors instead of three rotational accelerometers. The simulators also have sensors on the actuators. The VMS and CMF have position transducers; the CMF has accelerometers as well. Due to control feel system problems on the CMF simulator, the experiments for both the Large Civil Transport and the GHSCT were conducted on the VMS.

The experiments were conducted according to the randomized order shown in Appendix F. After each run, the pilot indicated the turbulence intensity sensation along with the turbulence reporting criteria from the FAA Airman's Guide that was fulfilled. Lastly, a Cooper-Harper Rating was provided for specific tasks. Chapter 6 contains the subjective analysis along with the quantitative results of each experiment, from both studies.

6. Results of Real-Time Experiments

6.1 Introduction

This chapter is separated into two main sections: the Large Civil Transport study and the GHSCT study. Each study is then broken down into the subjective analysis and quantitative results of the experiments. Each study is comprised of three different experiments. The experiments include an up and away case, where the pilot maintains altitude through atmospheric turbulence, a straight-in approach and landing, and an offset approach and landing.

As described in Chapter 5, the subjective analysis is performed on the information provided by the pilot after each run. The quantitative results are derived from data collected during each run.

Separate conclusions will be drawn from each set of experiments. The next two sections (6.2 and 6.3) provide analysis on the Large Civil Transport study. The GHSCT study is shown in sections 6.4 and 6.5. Each of these sections is broken down into subsections that describe the results of one experiment. This was done to allow separate conclusions to be drawn from each set of runs.

6.2 Large Civil Transport Study – Subjective Analysis

In order to assess the accuracy of the turbulence channel, a subjective evaluation of the turbulence field was conducted after each run. This included an intensity rating (Light, Moderate, or Severe) and reporting on all criteria from the FAA Airman's Guide. As mentioned in the Design of Experiments (section 5.4), Cooper Harper Ratings (CHR) were used to rate the

handling qualities of each run. The results of the Large Civil Transport implementation are provided in the following sections.

6.2.1 Large Civil Transport Experiment 1: Subjective Analysis

The Large Civil Transport subjective analysis on Experiment 1 provided insight into the effect of adding the turbulence channel. Even though the order of runs was randomized, the pilot was able to correctly identify the turbulence intensity for all runs. Table 6.2.1 shows the actual turbulence level and the perceived intensity by the pilot, for Experiment 1. It also details the CHR given by the pilot, on the specific task of maintaining altitude while flying through the turbulence field. Configuration 1 represents the simulation without the turbulence channel; configuration 2 employs the ATC.

| Experiment 1 – LCT | | | | CHR: Maintaining Altitude |
|---------------------------|-----------------------------|----------------------|-------------------------------|--|
| Run Number | Turbulence Level | Configuration | Reported Intensity | |
| 1 | 4 | 2 | Moderate, Continuous | 6 |
| 2 | 6 | 1 | Severe, Continuous | 8 |
| 3 | 2 | 1 | Light, Continuous | 3 |
| 4 | OFF | 1 | none | 1 |
| 5 | 2 | 2 | Light, Continuous | 3 |
| 6 | 4 | 1 | Moderate, Continuous | 5 |
| 7 | 6 | 2 | Severe, Continuous | 8 |

Table 6.2.1 – Large Civil Transport Experiment 1, Turbulence Intensity and CHR

For the case with no turbulence, the pilot gave a CHR of 1. This indicates that pilot compensation was not a factor in maintaining altitude during this run. For each of the light turbulence runs (3 and 5), the pilot rated the task as requiring minimal pilot compensation to achieve desired performance. At the moderate intensity, when adding the turbulence channel (configuration 2) the pilot reported an increase in the necessary compensation to perform the task, specifically from a CHR of 5 (Run 6) to a CHR of 6 (Run 1). Since the pilot was unaware of the specific conditions of each run, this indicates that the pilot perceived a difference when adding the channel at this turbulence level and that more compensation was required to complete the task. In the two cases with turbulence level 6, the pilot reported the intensity correctly (severe), however there was no change in the CHR.

The next table, Table 6.2.2, shows the pilot's reporting on the criteria from the FAA Airman's Guide. The Airman's guide has specific details with regard to the aircraft reaction at different turbulence levels. Once the intensity was estimated, the pilot then stated yes or no to the different reaction criteria. It was no surprise that the aircraft reaction criteria were met with and without the turbulence channel, as the ATC does not affect the instruments or dynamics of the aircraft model.

As mentioned earlier, the simulator was unable to cause object displacement or provide the pilot with much seatbelt strain. For this reason, these two "Reaction Inside Aircraft" criteria were not met in any runs. For assessing food service and walking, the pilot could respond with possible, difficult, or impossible. For Run 1, even though the turbulence intensity was moderate, it was determined that food service and walking were not possible. In this case, the ATC was

turned on. This increase to impossible under moderate turbulence also supports the increased CHR given for this run.

| Experiment 1 – LCT | | | | | | | |
|---------------------------|-----------------------------------|----------|----------|-----------------|---------------------------------|---------------------|------------------------|
| | Aircraft Reaction Criteria | | | | Reaction Inside Aircraft | | |
| Run Number | Altitude | Attitude | Airspeed | Controllability | Seatbelt Strain | Object Displacement | Food Service & Walking |
| 1 | yes | yes | yes | yes | no | no | impossible |
| 2 | yes | yes | yes | yes | no | no | impossible |
| 3 | yes | yes | yes | yes | no | no | possible |
| 4 | n/a | n/a | n/a | n/a | n/a | n/a | possible |
| 5 | yes | yes | yes | yes | no | no | possible |
| 6 | yes | yes | yes | yes | no | no | difficult |
| 7 | yes | yes | yes | yes | no | no | impossible |

Table 6.2.2 – Large Civil Transport Experiment 1, FAA Turbulence Reporting Criteria

6.2.2 Large Civil Transport Experiment 2: Subjective Analysis

The subjective results of Experiment 2 are shown in Table 6.2.3. The pilot’s task for this experiment was to maintain the glide slope and perform a touchdown. During each run, the pilot aimed for the same landing zone. For this experiment, a CHR was given for two tasks: maintaining the glide slope, and performing the touchdown. During the severe turbulence runs, the motion base was prone to tracking errors. From looking at the CHR, the workload of the

pilot control input is substantially greater when performing a landing under these extreme conditions, when compared to maintaining altitude (Experiment 1).

Each turbulence intensity was identified correctly by the pilot, just as in Experiment 1. In the case with no turbulence (Run 12), the pilot rated the task of maintaining the glide slope with a CHR of 2 and the landing task with a CHR of 3. During Run 8 (light turbulence, No ATC), the pilot increased his CHR to 4 and 6, for the glide slope and landing rating, respectively. For Run 13, the light turbulence run with the ATC on, the CHRs were both reduced to 3.

A possible explanation for this decrease in the necessary pilot compensation is that Run 8 was the first run of the set of straight-in approach and landing experiments. The pilot was more familiarized with the task by the later runs, and this could have contributed to the two decreased CHRs of Run 13. Another hypothesis for the decrease in the CHR is that the motion cues provided the pilot with better correlation with the visual and instrument cues. With the ATC on, the aircraft was easier to control.

| Experiment 2 – LCT | | | | CHR: Maintaining Glideslope | CHR: Performing Landing |
|--------------------|---------------------|---------------|-------------------------|-----------------------------------|-------------------------------|
| Run Number | Turbulence Level | Configuration | Reported Intensity | | |
| 8 | 2 | 1 | Light, Continuous | 4 | 6 |
| 9 | 4 | 1 | Moderate, Continuous | 7 | 7 |
| 10 | 6 | 1 | Severe, Continuous | 9 | 9 |
| 11 | 4 | 2 | Moderate, Continuous | 7 | 6 |
| 12 | OFF | 1 | none | 2 | 3 |
| 13 | 2 | 2 | Light, Continuous | 3 | 3 |
| 14 | 6 | 2 | Severe, Continuous | 9 | 9 |

Table 6.2.3 – Large Civil Transport Experiment 2, Turbulence Intensity and CHR

The aircraft reaction and reaction inside the aircraft were both indicative of the correct perceived turbulence level. Table 6.2.4 shows the criteria which were met for each specific run. As with Experiment 1, object displacement did not occur and seat belt strain was never great enough to meet the criteria. Walking was consistently rated as possible in light turbulence, difficult in moderate turbulence, and impossible in severe turbulence.

Pilot comments indicated increased difficulties with controllability, when performing the more control intensive task of landing the aircraft. In each of the severe cases, the pilot would remain out of positive control periodically during the runs. This happened more frequently than when conducting Experiment 1, and justified an increase of both CHRs to 9 (Runs 10 and 14).

For Runs 9 and 11 (moderate turbulence), it appears that adding the ATC decreased the amount of compensation required to perform the landing task. The landing task in general induces a much greater workload from the pilot; here, the addition of the cue from the ATC resulted in a decrease in the CHR from 7 to 6 between those two runs.

| Experiment 2 – LCT | | | | | | | |
|---------------------------|-----------------------------------|----------|----------|-----------------|---------------------------------|---------------------|------------------------|
| | Aircraft Reaction Criteria | | | | Reaction Inside Aircraft | | |
| Run Number | Altitude | Attitude | Airspeed | Controllability | Seatbelt Strain | Object Displacement | Food Service & Walking |
| 8 | yes | yes | yes | yes | no | no | possible |
| 9 | yes | yes | yes | yes | no | no | difficult |
| 10 | yes | yes | yes | yes | no | no | impossible |
| 11 | yes | yes | yes | yes | no | no | difficult |
| 12 | n/a | n/a | n/a | n/a | n/a | n/a | n/a |
| 13 | yes | yes | yes | yes | no | no | possible |
| 14 | yes | yes | yes | yes | no | no | impossible |

Table 6.2.4 – Large Civil Transport Experiment 2, FAA Turbulence Reporting Criteria

6.2.3 Large Civil Transport Experiment 3: Subjective Analysis

Experiment 3 required the most workload of all the experiments. This task, in itself, is a difficult maneuver; performing it under any level of atmospheric turbulence only increases the difficulty. The pilot always began the maneuver of switching runways at the same time during each run. This kept the task as consistent as possible. Table 6.2.5 shows the reported intensities for each run and the CHR.

When completing the task without any turbulence (Run 19), the pilot reported a CHR of 3 for both maintaining the glide slope and touchdown performance. There is an increase in one point for the CHR of the glide slope, compared to the on approach landing run (Experiment 2) without turbulence. When conducting the offset approach, the pilot has to align the aircraft on the glide slope of the parallel runway during the maneuver.

| Experiment 3 – LCT | | | | CHR: Maintaining Glideslope | CHR: Performing Landing |
|--------------------|---------------------|---------------|-------------------------|-----------------------------------|-------------------------------|
| Run Number | Turbulence Level | Configuration | Reported Intensity | | |
| 15 | 6 | 1 | Severe, Continuous | 9 | 9 |
| 16 | 4 | 1 | Moderate, Continuous | 7 | 7 |
| 17 | 2 | 1 | Light, Continuous | 3 | 4 |
| 18 | 4 | 2 | Moderate, Continuous | 6 | 7 |
| 19 | OFF | 1 | none | 3 | 3 |
| 20 | 2 | 2 | Light, Continuous | 3 | 4 |
| 21 | 6 | 2 | Severe, Continuous | 9 | 9 |

Table 6.2.5 – Large Civil Transport Experiment 3, Turbulence Intensity and CHR

In this experiment, all possible aircraft reaction and reaction inside aircraft criteria were met for each run. As with the other experiments, and the tuning sessions, seatbelt strain and object displacement criteria were not met. For the light turbulence runs (17 and 20), the pilot reported the same level of compensation, with and without the ATC. At this low level, the added motion from the ATC doesn't appear to increase the pilot workload.

The ATC has a different effect in level 4 turbulence. It appears that performing this experiment with the ATC on is slightly easier, specifically maintaining the glide slope. Run 16, ACT off, have a CHR of 7 for both ratings. Run 18 have a CHR of 6 and 7, for the glide slope and touchdown, respectively. This was also noticed in experiment 2 at level 4 turbulence (Figure 6.2.3). The CHR of the touchdown decreased from 7 to 6 with the addition of the ATC.

Similarly to the Experiment 2 runs, the severe turbulence runs (15 and 21) acquired ratings of 9 for each task. A CHR of 9 indicates that the strongest level of pilot compensation was necessary to complete the run. Even though this task is much more difficult, a CHR of 9 is justified because a CHR of 10 would indicate that control was lost during the entire run. Momentary lapse in control is a byproduct of severe turbulence, and does not necessarily warrant a CHR of 10 on the handling qualities of that run since the task was completed.

Some of the severe turbulence runs were repeated because of motion base failures. These motion base failures were because of tracking errors, or the excursion limits of the motion base forced the shutdown. After one or two repeat attempts at this turbulence level, the runs were all completed.

The reaction criteria for Experiment 3 are shown below in Table 6.2.6. When compared with the other experiments, the fluctuations in altitude, attitude, airspeed, and controllability were larger in all cases. The pilot control input is greater throughout these runs, and is definitely contributing to the increase in the amplitude of these measurements. This change in the pilot's dynamics is explained in more detail in the quantitative results, section 6.3.

| Experiment 3 – LCT | | | | | | | |
|---------------------------|-----------------------------------|----------|----------|-----------------|---------------------------------|---------------------|------------------------|
| | Aircraft Reaction Criteria | | | | Reaction Inside Aircraft | | |
| Run Number | Altitude | Attitude | Airspeed | Controllability | Seatbelt Strain | Object Displacement | Food Service & Walking |
| 15 | yes | yes | yes | yes | no | no | impossible |
| 16 | yes | yes | yes | yes | no | no | difficult |
| 17 | yes | yes | yes | yes | no | no | possible |
| 18 | yes | yes | yes | yes | no | no | difficult |
| 19 | n/a | n/a | n/a | n/a | n/a | n/a | n/a |
| 20 | yes | yes | yes | yes | no | no | possible |
| 21 | yes | yes | yes | yes | no | no | impossible |

Table 6.2.6 – Large Civil Transport Experiment 3, FAA Turbulence Reporting Criteria

With regard to experiments 2 and 3, the task of landing the aircraft detracts from the pilot's ability to perceive the turbulence level and gauge the control compensation necessary to land the aircraft. In both moderate turbulence cases, the pilot reported a decrease in the

necessary compensation to maintain the glide slope when the turbulence channel was added. This can also be due to an improvement in the pilot's understanding of the situation with the additional cue.

6.3 Large Civil Transport Study – Quantitative Results

The high volume of data being recorded during the experiments should allow formulation of conclusions with regard to the effect of the Augmented Turbulence Channel. The ATC adds a substantial amount of high frequency motion to the motion base, and the pilot should react to this. The majority of the results are shown in the frequency domain. Data from both pilot control input and aircraft reaction are analyzed in the following sections. Each section contains the results of one experiment.

6.3.1 Large Civil Transport: Experiment 1 – Quantitative Results

The task for Experiment 1 was to maintain straight and level flight through various turbulence levels. This was the least control intensive task, and resulted in the most conclusive data on the effects of the ATC. In order to maintain altitude, the pilot will take note of the baseline altitude, and then focus on the vertical velocity of the aircraft. If the aircraft begins to diverge from the set altitude, the pilot performs a control input intended to cancel out any growing vertical rates. Shortly after, the vertical speed will indicate that aircraft is returning to the task defined altitude. Once the aircraft has returned to the prescribed altitude, the pilot will compensate if drifting occurs again.

At mid and high levels of turbulence, this is an extremely intricate task. Large vertical wind gusts cause a great deal of fluctuation in altitude and vertical velocity. It requires the pilot to constantly focus on various instruments, and remain active in the control loop for the duration of the run.

When conducting frequency analysis, it is desirable to have datasets that are as stationary as possible. Since the pilot was constantly monitoring vertical velocity, stationarity was evaluated by inspecting the mean square of the aircraft vertical velocity throughout the run. The runs from Experiment 1 averaged around 6200 data points; they were cut into 128 point segments, producing about 50 windows of data. The mean square was calculated for each window. With this information, the portion of the signal with the most stationarity can be identified.

Figure 6.3.1 is a plot of the normalized mean square from Runs 1-7 (Experiment 1). The plot was normalized by dividing each separate signal by its maximum value. As the aircraft travels through different turbulence levels, the vertical velocity begins to grow. Consequently, the mean square of the vertical velocity is also amplified. Normalizing the data allows each run to be plotted together, and shows the sections of the runs that have the least variation.

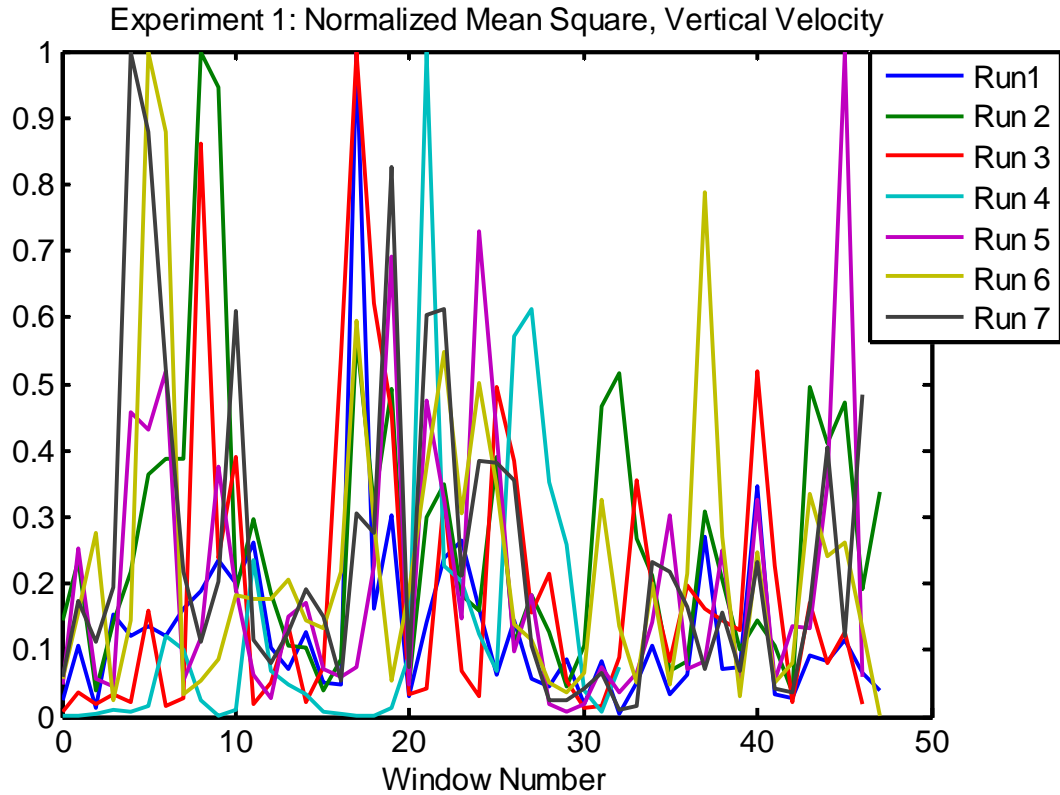


Figure 6.3.1 – Large Civil Transport Experiment 1, Normalized Mean Square of Vertical Velocity

The beginning of each signal was trimmed by 25 windows, removing 3200 data points. The end of each run was also trimmed so each signal was 19 windows long, or 2432 data points. Removing this portion of data isolated run information where frequency analysis could be performed effectively. Frequency analysis was conducted on the data between windows 26 and 45.

Except for a few outlying points in runs 2, 3, and 6, the mean square fluctuates far less than it did during other portions of the runs. The reduction of the irregularity of the mean square can be attributed to the pilot’s ability to better understand the task towards the end of the run.

Since the turbulence is continuous, the pilot control response is what changed as the runs progressed. Even though this analysis does not prove stationarity, it ensures the most credible frequency analysis.

Another assumption is that the selected portion of data is long enough to be ergodic. The simulation was run at 50 Hz, the portion of data that was analyzed includes about one minute of data per run. Accurate frequency analysis can be conducted on these data sets. Averaging and windowing were also performed to allow for smooth plots.

The first set of analysis is on the pilot control input. This was done on the pitch stick input, in the frequency domain. Pitch stick was chosen because the task of maintaining altitude requires compensation primarily in the pitch attitude of the aircraft. The next set of plots show the Power Spectrum Density (PSD) of the pilot input for specific runs conducted during

Experiment 1. In this case, the units of power are $\frac{(\% \text{ of stick deflection})^2}{\text{Hz}}$.

Figure 6.3.2 shows the light turbulence runs with the turbulence channel off (Run 3) and on (Run 5). The top plot shows the PSD of the pitch stick input, the bottom plot contains the same data, except it is normalized. Without the ATC, the peak power is 0.05 and at about 0.1 Hz. Turning on the ATC causes the amplitude of this peak to drop to 0.03. There is also an increase in the power of most frequencies above 0.5 Hz. Inspecting the normalized PSD plot shows that there is almost no shift in frequency domain of the peak power.

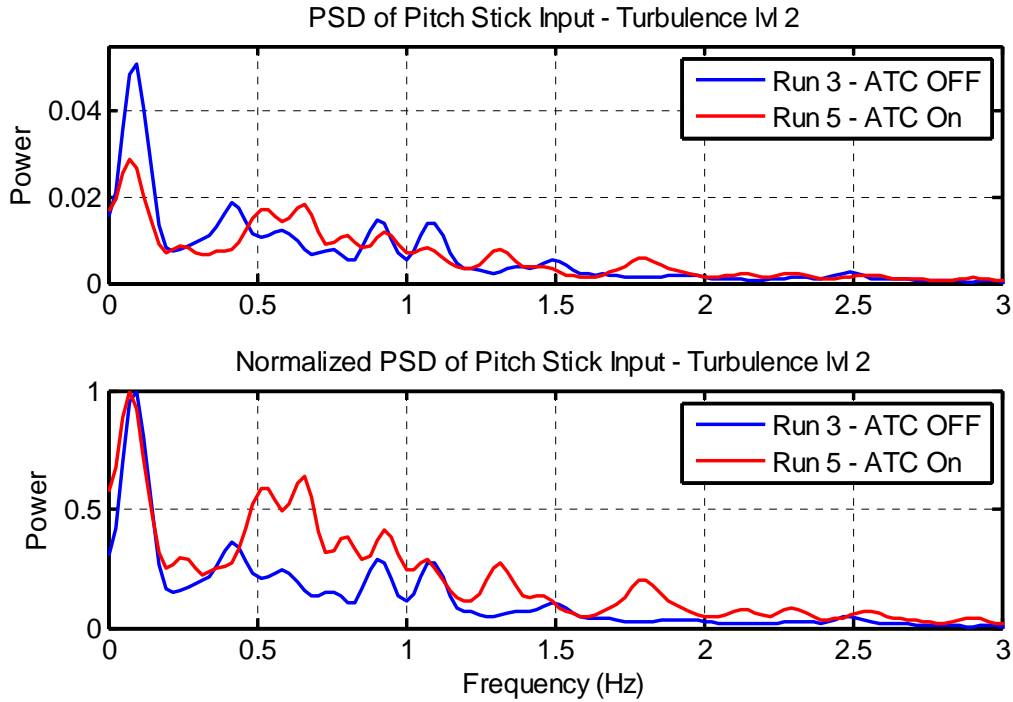


Figure 6.3.2 – Large Civil Transport Experiment 1, Light Turbulence, PSD of Pitch Stick Input and Normalized PSD of Pitch Stick Input

The moderate turbulence runs were plotted next, in Figure 6.3.3. Looking at this turbulence level, there is definitely a change in the characteristics of the pilot when adding the ATC. The power increases across almost all frequencies. The peak power is located at 0.48 Hz, the same frequency for both runs. The maximum power of the pilot input, with the turbulence channel on, is more than 4 times greater than with the ATC off. It appears the pilot is responding in most of the same frequencies, but increasing his amplitude as a response to the added motion cue.

The peak power of these runs is about 0.3, a substantial increase over the light turbulence cases (Figure 6.3.2). The peak frequency of the pilot has also shifted from 0.1 Hz to almost 0.5 Hz.

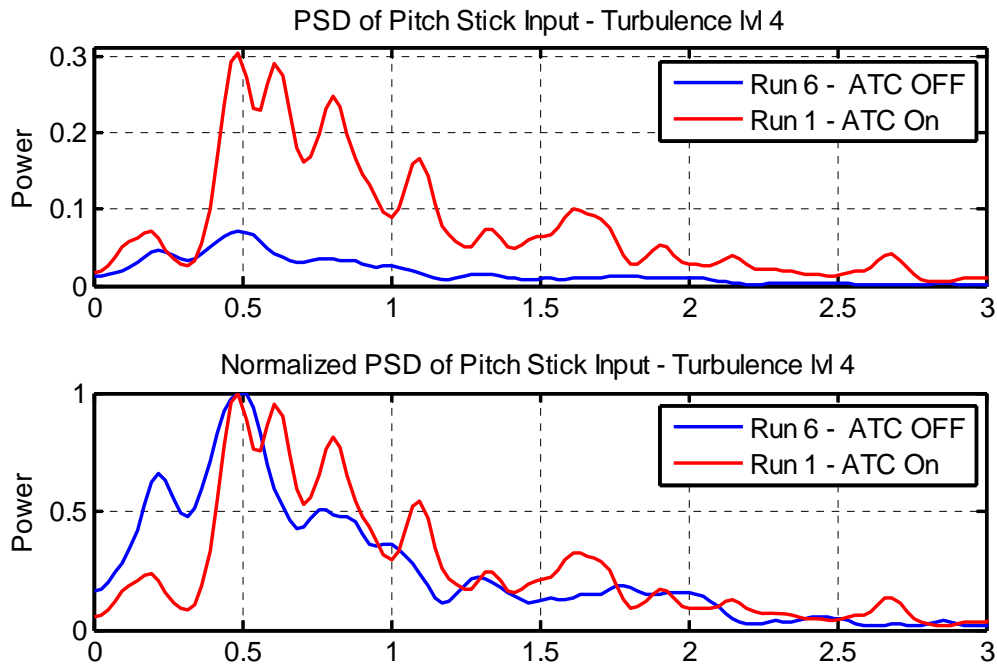


Figure 6.3.3 – Large Civil Transport Experiment 1, Moderate Turbulence, PSD of Pitch Stick Input and Normalized PSD of Pitch Stick Input

The response of the pilot under severe turbulence had the most apparent change when adding the ATC. Figure 6.3.4 shows the PSD of the pitch stick input as well as the normalized PSD. Here, there was a substantial decrease in the power of the pilot input, across all frequencies. The peak power without the ATC (Run 2) is 1.3, and drops to 0.1 when the ATC is turned on (Run 7). Adding the ATC also causes the peak power of the pilot to shift from 0.7 Hz to 0.4 Hz.

Inspecting the runs with the ATC off, going from moderate to severe turbulence increased the peak power from 0.3 to 1.3. In the frequency domain, this peak shifted from about

0.5 Hz to 1.3 Hz. Severe turbulence causes the pilot to respond at higher frequencies along with additional amplitude, when compared to both moderate and light turbulence.

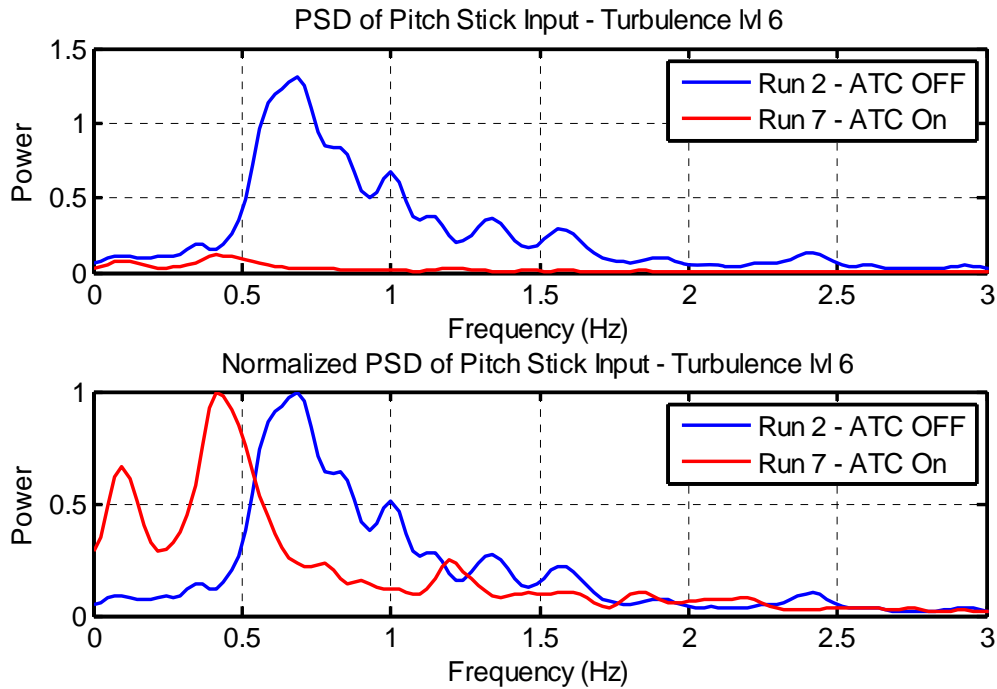


Figure 6.3.4 – Large Civil Transport Experiment 1, Severe Turbulence, PSD of Pitch Stick Input and Normalized PSD of Pitch Stick Input

Another useful piece of information is contained in the mean square of each run. The mean square is calculated by integrating the magnitude of the PSD across the frequency spectrum. Table 6.3.1 shows the mean square and details the conditions for each run. In this table, the run numbers are organized by turbulence level. This is done to allow for comparison between the different mean squares when the augmented channel is turned on. Turning on the ATC at level two turbulence (Runs 3 and 5) reduces the mean square slightly. This slight change

can be attributed to the fact that at such a low turbulence level, the necessary pilot input to perform the task is quite small.

| Experiment 1 – LCT | | | |
|---------------------------|-------------------------|----------------------|--------------------|
| Run Number | Turbulence Level | Configuration | Mean Square |
| 3 | 2 | (1) ACT Off | 0.02 |
| 5 | 2 | (2) ACT On | 0.019 |
| 6 | 4 | (1) ACT Off | 0.054 |
| 1 | 4 | (2) ACT On | 0.243 |
| 2 | 6 | (1) ACT Off | 0.817 |
| 7 | 6 | (2) ACT On | 0.069 |

Table 6.3.1 – Mean Square of Pitch Stick Input, Large Civil Transport Experiment 1

Under level 4 turbulence (Runs 6 and 1); turning the ATC on increases the mean square by a factor of 4.5. This substantial increase was expected; inspecting the PSD of the pilot input at turbulence level 4 (Figure 6.3.3) shows a major increase in power between the two runs.

In the level 6 turbulence runs, the trend shown in the mean square of the level 4 runs is reversed. Between runs 2 and 7, the mean square is reduced by a factor of 9 when adding the ATC. This ambiguity can be explained by the pilot’s decrease in power across all frequencies. Referring back to Figure 6.3.3, the entire Run 7 PSD curve remains at a much lower amplitude than the Run 2 plot, which has the ATC off.

Not many conclusions can be drawn by inspecting the pilot input alone. In order to analyze whether or not the pilot has a better understanding of the situation when adding the ATC, aircraft response data must also be inspected.

As specified earlier in this section, the pitch stick input is a direct response to the vertical velocity of the aircraft along with the motion the pilot senses in the vertical channel. If the pilot is in fact responding to the vertical velocity of the aircraft then there should be some correlation between the two. This type of analysis can be done a number of ways. Some methods include analyzing the remnant between the two signals, the cross-correlation function, and the coherence function.

The coherence function is a normalized, frequency domain plot that demonstrates correlation between two signals at each frequency. A coherence of 1.0 indicates that the two signals are highly correlated. It is hypothesized that the addition of the augmented turbulence channel will provide the pilot with missing turbulence cues and enhance the correlation between his control input and the response of the aircraft.

The literature indicates that the coherence function is used to validate sets of data and that if the data have a coherence less than 0.6, the data are not correlated enough to be evaluated. It is noted that in the cases with Experiments 2 and 3, there is difficulty reaching a coherence function of this magnitude. The task requires the pilot to focus on more than just atmospheric turbulence, causing his control input to be less correlated to the response of the aircraft vertical velocity.

The next set of plots displays the coherence function between the pilot control input (pitch stick) and aircraft vertical velocity. As with the PSD plots, the coherence functions are plotted against each other based on turbulence level. This is done to analyze whether adding the ATC improves the coherence function, or reduces it.

Figure 6.3.5 shows the two coherence functions from the light turbulence runs along with the PSD of the pitch stick control input. Turning the ATC on yields a much higher peak coherence, an increase from 0.64 to 0.79. The frequency range with the most correlation is between 0.5 Hz and 3 Hz. This frequency range also shows a difference in the pilot dynamics; with the ATC on, there is more power in the areas with increased coherence.

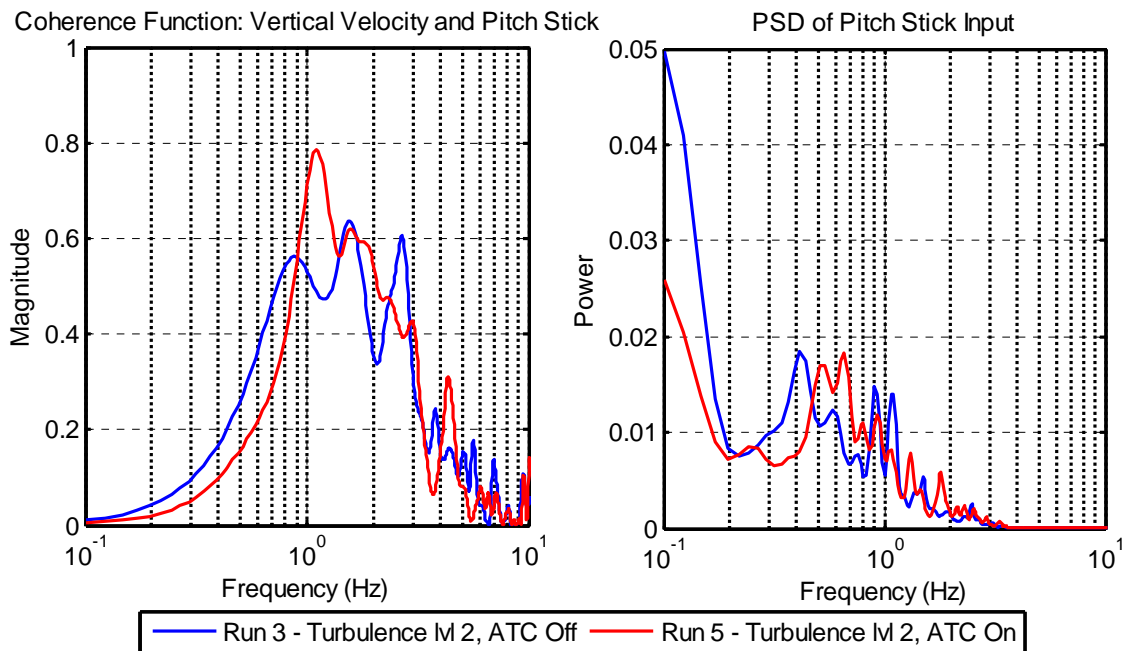


Figure 6.3.5 – Coherence Function of Vertical Velocity and Pitch Stick Input; PSD of Pitch Stick Input, Large Civil Transport Experiment 1, Level 2 Turbulence

The coherence function is distorted in the higher frequency range, over 5 Hz. Even with additional averaging and windowing, this distortion could not be removed from these plots. If a higher sampling rate were achieved by the hardware, this noise could be reduced with more post processing. Additionally, this portion of the plot does not provide useful information as the pilot's operating frequency peaks near 3 Hz, and the noise doesn't become overpowering until 5 Hz.

Adding the ATC to the moderate turbulence runs also results in an increase of the peak coherence (Figure 6.3.6). This increase was from 0.85 to 0.86, much less noticeable than the increase seen in the light turbulence runs. One major result of adding the ATC at this level is the increase in coherence over almost the entire frequency range. The pilot is much more correlated with the aircraft vertical velocity, especially in the high frequencies (1.0 – 3.0 Hz). The max coherence of almost 0.9 indicates a highly correlated signal. As with the other coherence function plot, there is quite a bit of distortion after about 5 Hz.

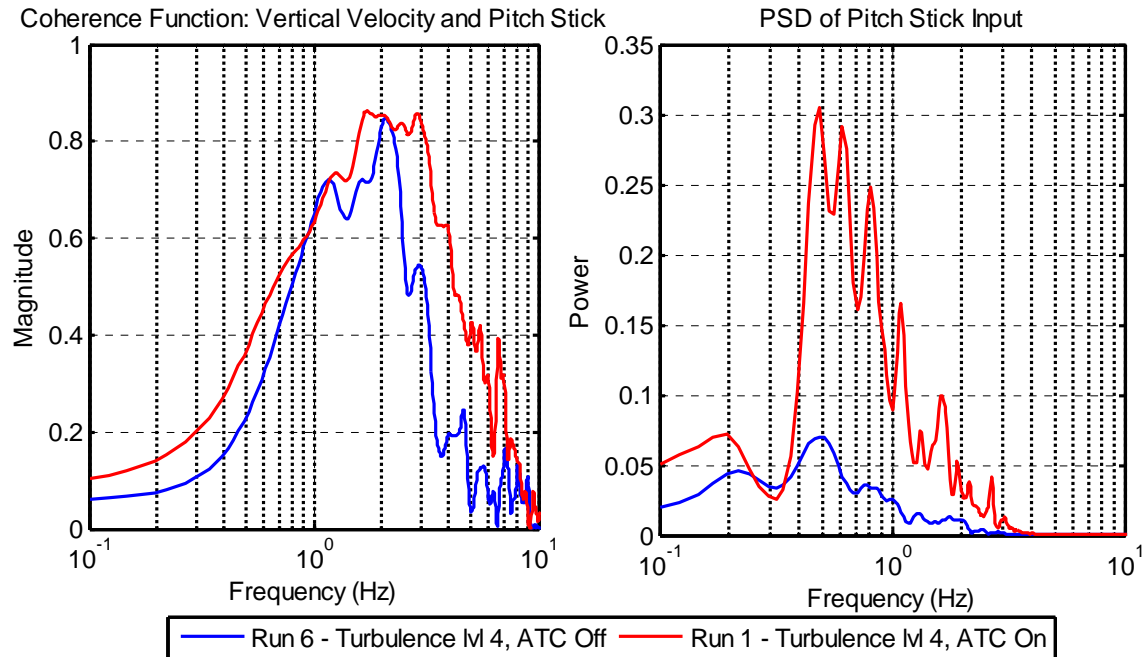


Figure 6.3.6 – Coherence Function of Vertical Velocity and Pitch Stick Input; PSD of Pitch Stick Input, Large Civil Transport Experiment 1, Level 4 Turbulence

Under moderate turbulence, the dynamics of the pilot change substantially throughout the entire frequency range. With the ATC on, the pilot exerts more power in higher frequencies. This added power also improves the coherence at these frequencies. The only difference between these two runs is the augmented channel; therefore, this additional power is a result of the additional motion cue the pilot is receiving.

The cue provides the pilot with more information on the turbulence field, and his reaction is more correlated with the vertical velocity, which is what the pilot is compensating for during the run. At this turbulence level, the cues from the ATC induce a more correlated reaction by the pilot.

The power of the pilot input was severely attenuated after adding the ATC and running with level 6 turbulence. Not only was the peak power of the pilot input much lower; it shifted to a lower frequency. Inspecting the coherence function across the same frequency range provides some insight into the effect of this change in pilot dynamics (Figure 6.3.7).

In the case with the ATC off, the pilot is quite correlated with the vertical velocity of the aircraft. The maximum coherence is 0.87 with the ATC off; it drops to 0.76 with the ATC on. The other insightful characteristic of the coherence functions is the drop in magnitude across the entire operating range of the pilot after adding the ATC. The coherence drops to 0.3 at .9 Hz, where it once was 0.7 without the ATC.

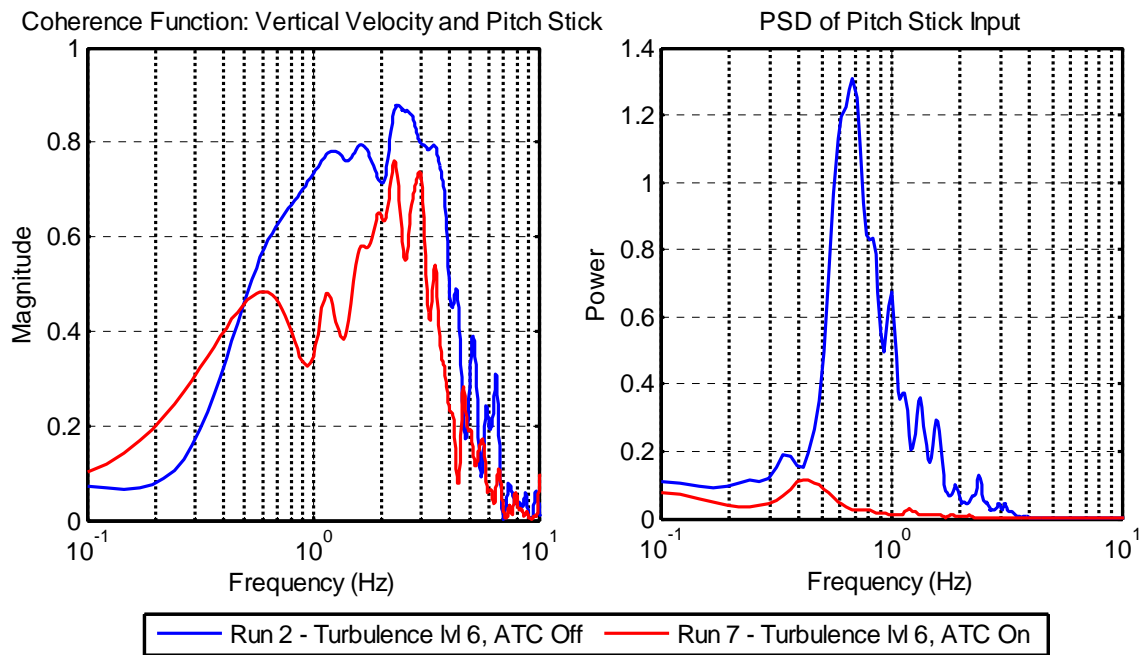


Figure 6.3.7 – Coherence Function of Vertical Velocity and Pitch Stick Input; PSD of Pitch Stick Input, Large Civil Transport Experiment 1, Level 6 Turbulence

It can be seen in the PSD plot that the pilot reduces the power and frequency of his pitch stick input when the ATC is added. It is hypothesized that the lack of pilot input across this frequency range is because he simply cannot keep up with the added cue. It is possible the ATC is producing large amplitude motion cues that the pilot is unable to compensate. Without the ATC, the cue is strong enough to induce a reaction, but not overpowering the pilot. Once the motion is so large that it cannot be responded to, the pilot remains less active in the control loop. Chapter 6 provides possible solutions to rectify this ambiguity between the different turbulence levels.

6.3.2 Large Civil Transport: Experiment 2 – Quantitative Results

In Experiments 2 and 3, the pilot's focus is not solely on compensating for disturbances due to atmospheric turbulence. In Experiment 2, the pilot has to maintain the glide slope as he descends towards the runway. The initial portion of this task is similar to maintaining altitude in Experiment 1.

At the start of the run, the pilot takes note of the altitude, sink rate, and DME (Distance Measuring Equipment). The glide slope is then monitored; as glide slope error starts to build, pitch attitude is adjusted to change the vertical velocity of the aircraft. This will arrest the rate of departure from the glide slope and bring the error down to zero. As the aircraft approaches the runway, the corrections become smaller and more precise. At about 200 feet, the tracking task becomes purely visual; the pilot focuses on the landing site and ensures a proper touchdown. Glide slope error is ignored by the pilot for this portion of the run.

The task during the early portion of each run is the least control intensive. This is the portion of the dataset that will be analyzed. It is quite difficult to support a substantial amount of stationarity in these signals; however, the beginning of each run has the least fluctuation in the mean square of the vertical velocity. Figure 6.3.8 shows the normalized mean square for each 128 point window, from the Experiment 2 Runs.

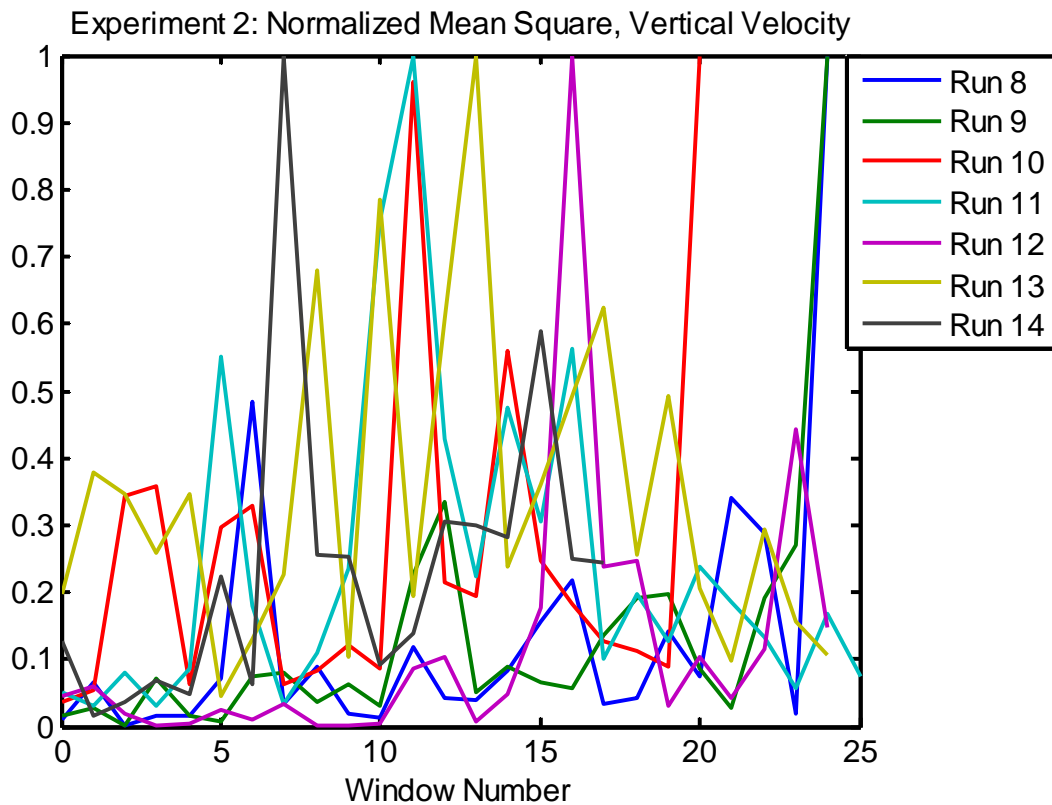


Figure 6.3.8 – Large Civil Transport Experiment 2, Normalized Mean Square of Vertical Velocity

There is quite a bit of fluctuation of the mean square, but according to this plot, the mean square is most stable until about 9 windows of data. Run 14 has some outlying points, but the rest remain the most stable during this time period. These runs are quite a bit shorter than the

Experiment 1 runs; lasting about one minute. When cut at 9 windows, the runs are trimmed to a length of 23 seconds. The following analysis comes from that portion of data.

The first set of analysis inspects the mean square of the pilot input. There is a definite trend in this data; the addition of the turbulence channel at different levels always brings about an increase in the mean square (Table 6.3.2). With light turbulence, the mean square went from 0.191 to 0.319 (Runs 8 and 13). For moderate turbulence, the mean square increased from 0.437 to 0.467 (Runs 9 and 11). The largest increase was observed when adding the ATC to the level 6 turbulence run. The mean square increased from 1.039 to 1.69 (Runs 10 and 14). Run 14 also had the largest mean square of all the runs. This indicates that the pilot consistently works harder with the additional turbulence cue.

Conditions for Run 12 allowed the pilot to land the aircraft without any turbulence turned on. The mean square of the pitch stick input was 0.014; a fraction of the mean square when flying through any turbulence intensity.

| Experiment 2 – LCT | | | |
|---------------------------|-------------------------|----------------------|--------------------|
| Run Number | Turbulence Level | Configuration | Mean Square |
| 8 | 2 | (1) ACT Off | 0.191 |
| 13 | 2 | (2) ACT On | 0.319 |
| 9 | 4 | (1) ACT Off | 0.437 |
| 11 | 4 | (2) ACT On | 0.467 |
| 10 | 6 | (1) ACT Off | 1.039 |
| 14 | 6 | (2) ACT On | 1.69 |
| 12 | OFF | n/a | 0.014 |

Table 6.3.2 – Mean Square of Pitch Stick Input, Large Civil Transport Experiment 2

The next set of analysis is designed to inspect the correlation between the pilot input and the aircraft dynamics. Since the pilot is responding mainly to vertical velocity when performing this task just as with Experiment 1, the correlation between these two parameters was evaluated by inspecting the coherence function. This next set of plots shows the coherence of the two signals and details the PSD of the pilot input. Figure 6.3.9 is from Run 12, where the pilot lands the aircraft without any turbulence.

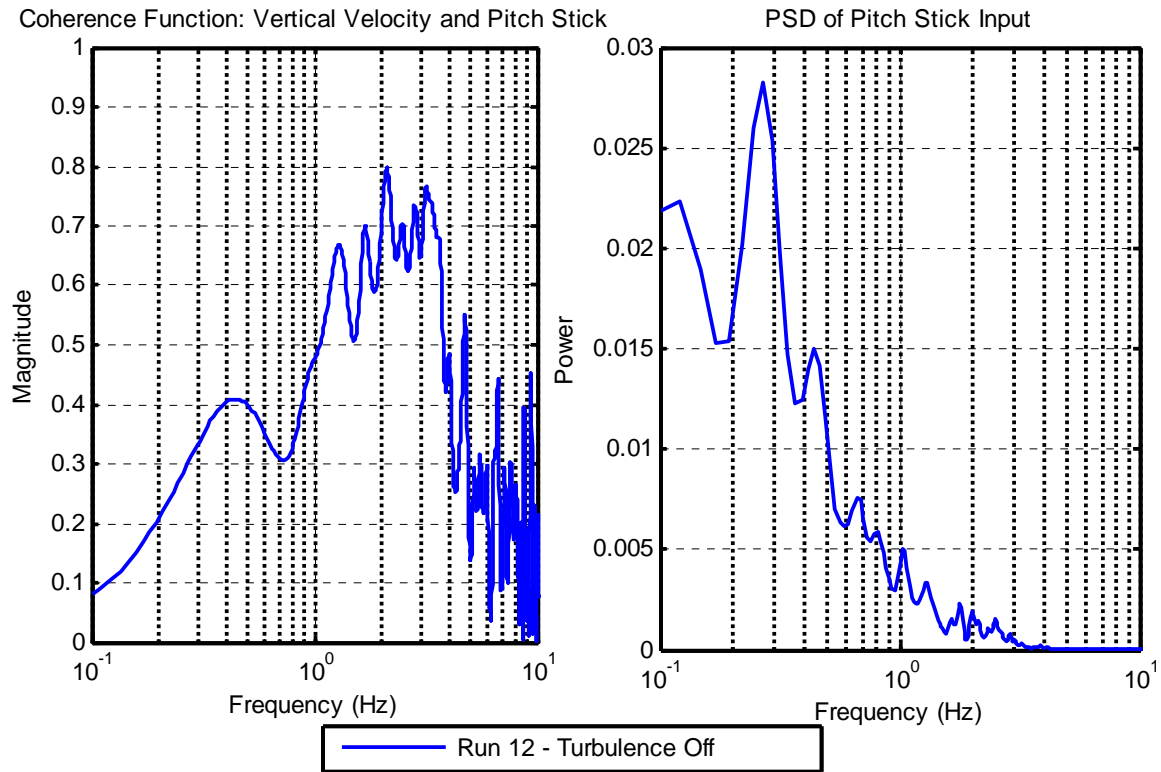


Figure 6.3.9 – Coherence Function of Vertical Velocity and Pitch Stick Input; PSD of Pitch Stick Input, Large Civil Transport Experiment 2, Turbulence Off

Out of all the runs for Experiment 2, this produced the highest coherence, with a peak amplitude of 0.8 at 2 Hz. This frequency is in the upper range of the spectrum of pilot control input. The control input power at this portion is quite low, close to 0.002. The majority of the coherence function indicates a strong correlation between the pilot and the aircraft. Without any atmospheric turbulence, the pilot can devote all control inputs to countering the deviation from the glide slope, by monitoring the vertical velocity of the aircraft.

At level 2 turbulence, the addition of the ATC causes the pilot to increase his power over almost all frequencies. The pilot's maximum power increases from 0.4 to 0.7, and shifts to a

higher frequency. Figure 6.3.10 shows the PSD of the pilot control input and the coherence function between the vertical velocity of the aircraft and the pitch stick input. The coherence function at this turbulence level shows a major improvement in the maximum coherence, from 0.44 to 0.79. It is also noted that the PSD of the pilot input is much greater than the light turbulence runs from Experiment 1.

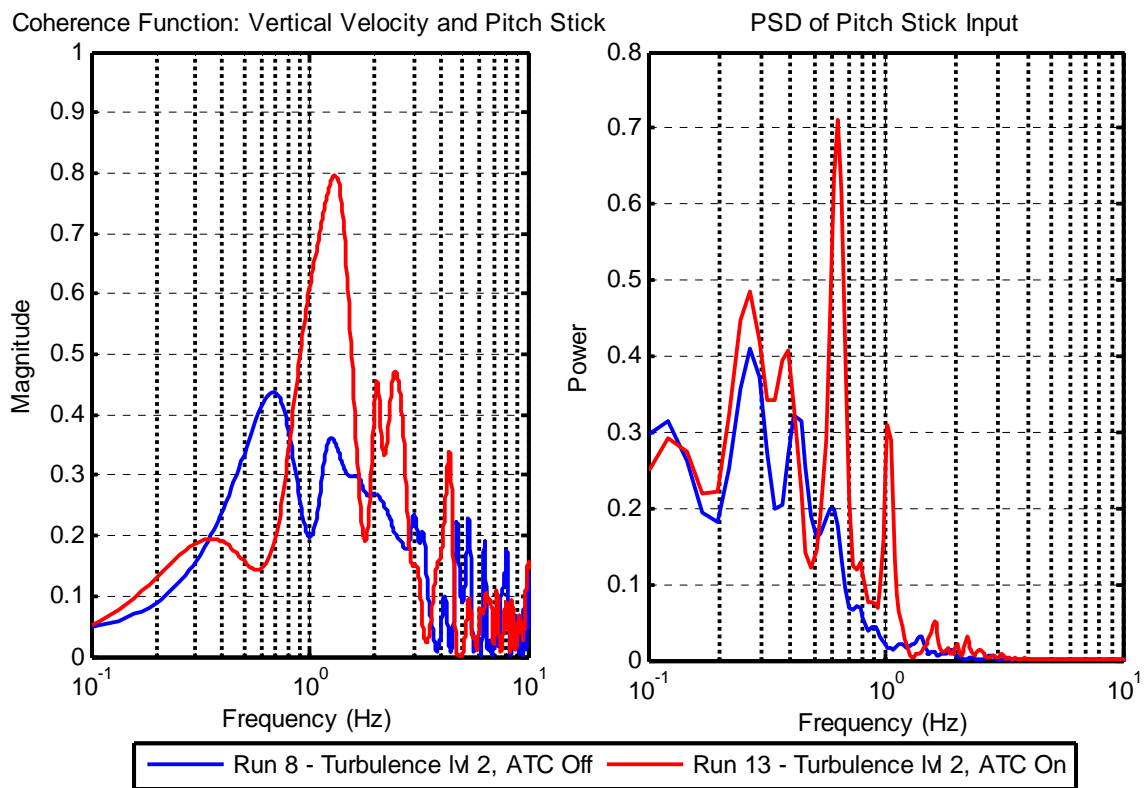


Figure 6.3.10 – Coherence Function of Vertical Velocity and Pitch Stick Input; PSD of Pitch Stick Input, Large Civil Transport Experiment 2, Turbulence Level 2

Both light turbulence runs are correlated with the vertical velocity of the aircraft. The run with the ATC on (Run 13) maintains a stronger coherence over most of the spectrum. The

higher power in the pilot control input around 0.7 Hz appears to add to the pilot's correlation with the vertical velocity of the aircraft. The coherence at lower frequencies, under 0.5 Hz, is deteriorated by the addition of the augmented channel. Just as the coherence plots from the analysis of Experiment 1, the signal is too noisy to be analyzed at frequencies over 5 Hz.

Figure 6.3.11 shows the coherence function and PSD of the moderate turbulence runs. The peak power of the pilot input shifted from 0.37 Hz to 0.63 Hz when the ATC was turned on. The maximum power of the signal decreased when the channel was added.

The coherence function acquires some noticeable changes when running with the ATC. There is improvement in the peak coherence, especially between 0.5 and 2.5 Hz. During this portion, the Run 11 coherence remains greater than the coherence of Run 9.

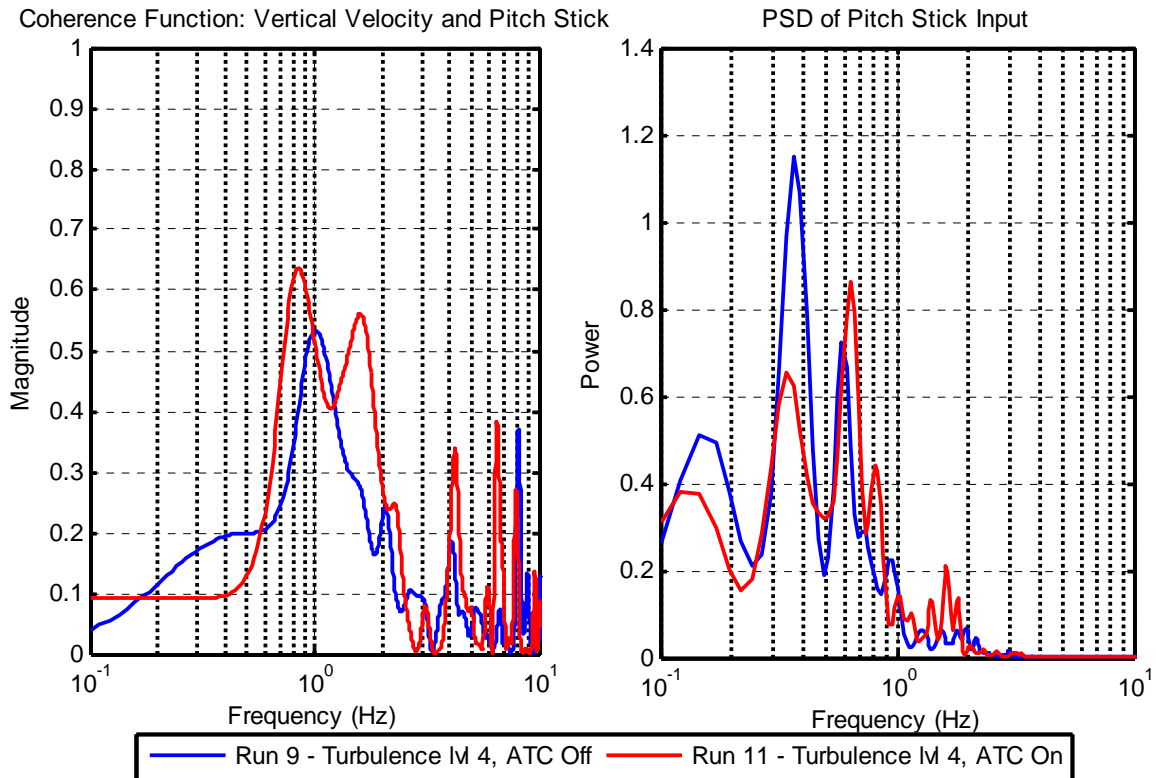


Figure 6.3.11 – Coherence Function of Vertical Velocity and Pitch Stick Input; PSD of Pitch Stick Input, Large Civil Transport Experiment 2, Turbulence Level 4

The pilot’s operating frequencies appear to shift to the right, in doing this; the pilot amplifies his coherence with the vertical velocity of the aircraft. This indicates that the change in dynamics of the pilot, brought about by the augmented turbulence cues, is improving the pilot’s correlation with the motion of the aircraft.

Results of the severe turbulence runs are also similar to the data from Experiment 1. In this case, the pilot increases the power of his control input in the low frequency range. The peak power grows from 2.5 to 3.2, and shifts from 0.5 to 0.4 Hz. (Figure 6.3.12).

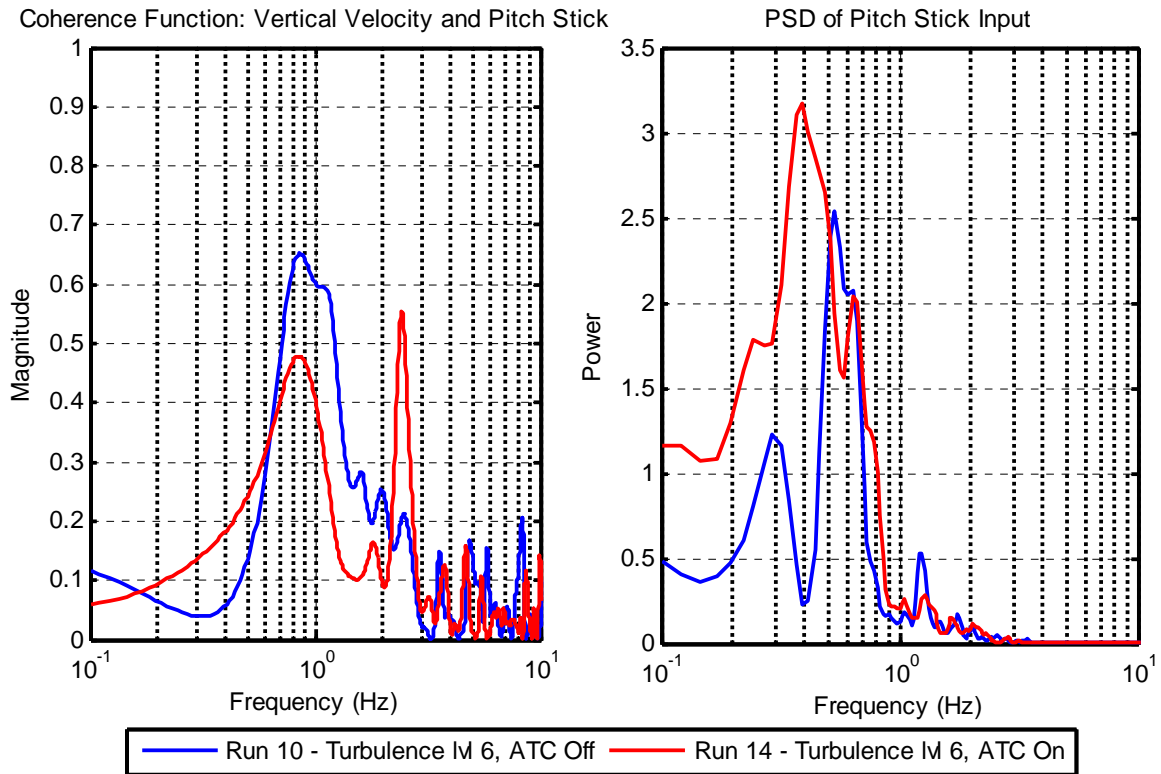


Figure 6.3.12 – Coherence Function of Vertical Velocity and Pitch Stick Input; PSD of Pitch Stick Input, Large Civil Transport Experiment 2, Turbulence Level 6

For the most part, the coherence function indicates that the addition of the ATC reduces the pilot's correlation with the aircraft vertical velocity. The only portion where the pilot is better correlated is in low frequencies, under 0.5 Hz, and the peak coherence of Run 14, which is at 2.4 Hz. The rest of the frequency range shows a lack of correlation between the two signals.

At level 6 turbulence it appears the pilot stops responding to the high frequency cue. His peak power always shifts to the lower frequencies when adding the ATC. At all other turbulence levels, the pilot increases his power at higher frequencies when the ATC is added.

Further conclusions were drawn by comparing the results of Experiments 1 and 2. The data indicates that the pilot is always more correlated with the vertical velocity of the aircraft when simply maintaining altitude. It appears that the added difficulty of maintaining the glide slope while on approach reduces the coherence function under all turbulence intensities.

The coherence function is usually improved when adding the ATC in both light and moderate turbulence. The improvement of the coherence is much more apparent in the moderate turbulence cases. When flying through severe turbulence, the pitch stick control is more correlated with the aircraft vertical velocity without the augmented channel.

6.3.3 Large Civil Transport: Experiment 3 – Quantitative Results

Producing Quantitative results from a very control intensive task is somewhat problematic. In order to justify frequency analysis, the simulation must not be dependent on time. When performing an offset approach, the entire experiment forces a wide range of maneuvers from the pilot. Results of frequency analysis can be useful to calculate the work the pilot is inputting to the system.

The mean square of each run is shown in Table 6.3.3. The overall mean square is much greater than what was seen in Experiments 1 and 2. The pilot exercises more work in each of these runs. One interesting piece of information is the decrease in the mean square at level six turbulence, when the ATC is added. This was also noted in Experiment 1. As mentioned before, the evidence suggests that the pilot is simply not responding to the high frequency motion. It is

possible that the pilot is unable to respond because the increase in magnitude is too large and in the higher frequency content.

| Experiment 3 – LCT | | | |
|---------------------------|-------------------------|----------------------|--------------------|
| Run Number | Turbulence Level | Configuration | Mean Square |
| 17 | 2 | (1) ACT Off | 0.478 |
| 20 | 2 | (2) ACT On | 1.08 |
| 16 | 4 | (1) ACT Off | 1.487 |
| 18 | 4 | (2) ACT On | 2.478 |
| 15 | 6 | (1) ACT Off | 2.635 |
| 21 | 6 | (2) ACT On | 1.921 |
| 19 | OFF | n/a | 0.403 |

Table 6.3.3 – Mean Square of Pitch Stick Input, Large Civil Transport Experiment 3

6.4 Generic High-Speed Civil Transport Study – Subjective Analysis

6.4.1 GHST Experiment 1: Subjective Analysis

The generic aircraft model used in this study is still under development, and the current dynamics resulted in difficulties assessing the turbulence level and completing the experiments. Flying the GHST in its current form was a difficult task in itself; the aircraft handling qualities

require the pilot to constantly perform control adjustments to keep the aircraft on task. The pilot found it very difficult to identify turbulence intensities, even when just maintaining altitude.

The actual motion of this aircraft when under the influence of turbulence is severely lacking as it is only outfitted with a translational turbulence model. Rotational turbulence cues produce a more realistic feel, and also require the pilot to compensate for abrupt changes in attitude.

The first set of results is from Experiment 1. As with the experiments conducted on the Large Civil Transport, the pilot is to maintain straight and level flight at a set altitude. He then gives a CHR rating on the compensation required to perform this task. Configurations 1 and 2 are the same as the Large Civil Transport experiments. Configuration 3 indicates that both the ATC and aeroelastic channel are turned on. Table 6.4.1 shows the Dryden turbulence level, configuration, reported turbulence intensity, and the CHR for maintaining altitude.

| Experiment 1 – GHSCT | | | | CHR: Maintaining Altitude |
|---|---------------------|---------------|---------------------------------|---------------------------------|
| Run Number | Turbulence Level | Configuration | Reported Intensity | |
| 1 | OFF | 1 | none | 2 |
| 2* | 6 | 2 | Light, Continuous | 3 |
| 3* | 4 | 1 | Light, Continuous | 3 |
| 4 | 2 | 3 | Light, Continuous | 3 |
| 5* | 6 | 1 | Light, Continuous | 4 |
| 6 | 2 | 1 | Light, Continuous | 3 |
| 7* | 4 | 3 | Light, Continuous (high end) | 4 |
| 8* | 4 | 2 | Light, Continuous (low end) | 2 |
| 9 | 2 | 2 | Light, Continuous | 2 |
| 10* | 6 | 3 | Moderate, Continuous | 5 |
| * Indicates incorrect intensity rating for that run | | | | |

Table 6.4.1 – GHSCT Experiment 1, Turbulence Intensity and CHR

These subjective ratings indicate that the pilot had a very difficult time identifying the turbulence level. During the up and away flight, the intensity never actually reached severe. Cooper Harper Ratings also show that the pilot never needed to exert much compensation when completing this task. The run numbers where the turbulence level was misidentified are marked with an asterisk (*).

The aeroelastic channel appears to consistently increase the effects of the turbulence intensity. At level 4 turbulence, with the DASE channel turned off, the intensity was reported as light turbulence (Runs 3 and 8). Adding the DASE channel caused this to increase to the high end of light turbulence (Run 7). The CHR also increased to 4 with the aeroelastic effects on. As described in Chapter 4, the aeroelastic channel is excited very little by turbulence. Most of the bending is due to pilot control input. When running with Configuration 3, the pilot feels the cues added by the turbulence channel and the flexible response of the aircraft as the pilot makes control inputs.

Since some turbulence intensities were reported incorrectly, the aircraft reaction criteria that were met are related to the perceived erroneous intensity. For example, if the pilot identified a level 4 turbulence run as light turbulence, then the aircraft reaction criteria would have been indicative of the light turbulence that was perceived. If level 4 turbulence was observed correctly, the aircraft response criteria would represent moderate turbulence. Table 6.4.2 shows the reaction criteria from the FAA Airman's guide which were satisfied for Experiment 1.

| Experiment 1 – GHST | | | | | | |
|---|--------------|----------------------------|----------|----------|-----------------|--------------------------|
| | | Aircraft Reaction Criteria | | | | Reaction Inside Aircraft |
| Run Number | Base Failure | Altitude | Attitude | Airspeed | Controllability | Food Service & Walking |
| 1 | no | n/a | n/a | n/a | n/a | possible |
| 2* | no | yes | yes | yes | yes | possible |
| 3* | no | yes | yes | yes | yes | possible |
| 4 | no | yes | yes | yes | yes | possible |
| 5* | no | yes | yes | yes | yes | possible |
| 6 | no | yes | yes | yes | yes | possible |
| 7* | no | yes | yes | yes | yes | possible |
| 8* | no | yes | yes | yes | yes | possible |
| 9 | no | yes | yes | yes | yes | possible |
| 10* | no | yes | yes | yes | yes | difficult |
| * Indicates incorrect intensity rating for that run | | | | | | |

Table 6.4.2 – GHST Experiment 1, FAA Turbulence Reporting Criteria

The reaction inside the aircraft criteria for seatbelt strain and object displacement were removed from the tables because these conditions were never met. The pilot still determined whether walking and food service was possible, difficult, or impossible. For the Experiment 1 runs, walking was always possible, except at level 6 turbulence with the ATC and DASE model both turned on (Run 10). In this run, the highest CHR for this experiment was given, and

walking and food service were recorded as difficult. Typically, level 6 turbulence should produce a more extreme reaction by the aircraft and the motion base, making the aircraft difficult to control and impossible to walk in.

6.4.2 GHSCT Experiment 2: Subjective Analysis

Experiment 2 was a more control intensive task than Experiment 1. Since the pilot is much more active in the control loop, it is more difficult to identify the turbulence intensity. The Dryden turbulence model was turned off during Run 19, however the pilot identified light, intermittent, turbulence for that run. A possible explanation for this is that abrupt changes in vertical velocity can be due to the dynamics of the aircraft response to pilot input. It is likely that the aircraft response is erratic enough that it shares some characteristics with the aircraft response to turbulence. Table 6.4.3 shows the CHR for each Experiment 2 run and the perceived turbulence intensity.

| Experiment 2 – GHST | | | | CHR: Maintaining Glide Slope | CHR: Performing Landing |
|---|---------------------|---------------|-------------------------|------------------------------------|-------------------------------|
| Run Number | Turbulence Level | Configuration | Reported Intensity | | |
| 11* | 4 | 2 | Light, Continuous | 4 | 6 |
| 12 | 2 | 1 | Light, Continuous | 3 | 4 |
| 13* | 4 | 1 | Light, Continuous | 4 | 5 |
| 14* | 6 | 1 | Moderate, Continuous | 6 | 7 |
| 15* | 2 | 3 | Moderate, Continuous | 5 | 6 |
| 16 | 6 | 3 | Severe, Continuous | n/a | n/a |
| 17 | 6 | 2 | Severe, Continuous | 8 | 9 |
| 18* | 4 | 3 | Severe, Continuous | 7 | 8 |
| 19* | OFF | 1 | Light, Intermittent | 3 | 3 |
| 20 | 2 | 2 | Light, Continuous | 3 | 4 |
| * Indicates incorrect intensity rating for that run | | | | | |

Table 6.4.3 – GHST Experiment 1, Turbulence Intensity and CHR

There is a substantial increase in the CHR of the different runs now that the task has become more difficult. The pilot still had trouble identifying turbulence levels, but severe turbulence was achieved at level six, with the ATC on (Run 17). This run also received the highest CHR; 8 for maintaining the glide slope and 9 for the landing.

There is a consistent trend in these results; the addition of the flexibility channel causes the turbulence intensity to be assessed one level higher than the configuration without the

augmentation. Level 2 turbulence is reported as light turbulence with configuration 1 (Run 11). Adding the aeroelastic channel causes the rating to go up to moderate (Run 15). The moderate turbulence runs feel like light turbulence (Runs 11 and 13) until the DASE model is activated (Run 18). This particular run was identified as severe.

Running turbulence level 6 without any augmented cues, the pilot sensed moderate turbulence (Run 14). Adding the ATC increased the accuracy of his judgment, as he identified Run 17 as severe. With the flexible model and ATC activated, this level was also correctly identified (Run 16). Run 16 could not be fully evaluated as the motion induced by this configuration caused the base to receive a tracking error early in the run. Repeat attempts had the same problem and criteria with regard to aircraft reaction could not be evaluated, nor could CHR be assigned to the different tasks. It was noted that food service and walking would be impossible in these conditions (Table 6.4.4).

| Experiment 2 – GHST | | | | | | |
|---|---------------------|-----------------------------------|----------|-------------|-----------------|---------------------------------|
| | | Aircraft Reaction Criteria | | | | Reaction Inside Aircraft |
| Run Number | Base Failure | Altitude | Attitude | Airspeed | Controllability | Food Service & Walking |
| 11* | no | yes | yes | yes | yes | possible |
| 12 | no | yes | yes | yes | yes | possible |
| 13* | no | yes | yes | yes | no (Moderate) | possible |
| 14* | no | yes | yes | no (Severe) | yes | difficult |
| 15* | no | yes | yes | yes | yes | difficult |
| 16 | yes | n/a | n/a | n/a | n/a | impossible |
| 17 | yes | yes | yes | yes | yes | difficult |
| 18* | yes** | yes | yes | yes | yes | impossible |
| 19* | no | yes | yes | yes | yes | possible |
| 20 | no | yes | yes | yes | yes | possible |
| * Indicates incorrect intensity rating for that run | | | | | | |
| ** Notes that base failed at or near the touchdown location | | | | | | |

Table 6.4.4 – GHST Experiment 2, FAA Turbulence Reporting Criteria

Turbulence levels for Runs 13 and 14 were not identified correctly, but some of the aircraft reaction criteria did point to the proper turbulence intensity. During Run 13, the pilot noticed that there were periods of time where the aircraft was difficult to control. This is specified in the FAA Airman’s guide under moderate turbulence, and that is why the controllability rating for Run 13 was not fulfilled.

Run 14 showed high amplitude fluctuations in indicated airspeed. This is detailed as a response to severe turbulence. It is also noted that the only time it was impossible to walk in the aircraft was with the flexibility model turned on, in level 4 or 6 turbulence (Runs 16 and 18).

Since motion base failures were quite common during the runs, a column was added to identify these occurrences. In these situations, data was saved from the run; however, the run was not completed. If the motion base failed but the data included the touchdown of the aircraft, or was very close to a touchdown, it is indicated by a double asterisk (**). Multiple attempts for these runs were made; however, it was just not possible to complete some of the runs without producing a tracking error or overdriving the motion system.

6.4.3 GHSCT Experiment 3: Subjective Analysis

The analysis of Experiment 3 resulted in conclusions similar to Experiment 2. The run without turbulence (Run 25) was identified as light, continuous turbulence. A similar result was seen in Experiment 2, Run 19, and can be attributed to the aircraft dynamics. Table 6.4.5 shows the results of each run and the CHR.

| Experiment 3 – GHSCT | | | | CHR: Maintaining Glide Slope | CHR: Performing Landing |
|---|-----------------------------|----------------------|-------------------------------|---|--|
| Run Number | Turbulence Level | Configuration | Reported Intensity | | |
| 21 | 6 | 1 | Severe, Continuous | 9 | 9 |
| 22* | 4 | 3 | Severe, Continuous | 8 | 8 |
| 23 | 4 | 2 | Moderate, Continuous | 6 | 6 |
| 24 | 6 | 2 | Severe, Continuous | 8 | 9 |
| 25* | OFF | 1 | Light, Continuous | 3 | 3 |
| 26 | 2 | 1 | Light, Continuous | 3 | 4 |
| 27 | 2 | 2 | Light, Continuous | 4 | 5 |
| 28 | 6 | 3 | Severe, Continuous | n/a | n/a |
| 29 | 4 | 1 | Moderate, Continuous | 6 | 7 |
| 30 | 2 | 3 | Light, Continuous | 5 | 5 |
| * Indicates incorrect intensity rating for that run | | | | | |

Table 6.4.5 – GHSCT Experiment 3, Turbulence Intensity and CHR

Identification of the perceived turbulence level was much more accurate in Experiment 3. Experiments 1 and 2 had many incorrectly identified runs; there were only two in Experiment 3. The aeroelastic effects caused Run 22 to be reported as severe turbulence even though it was only turbulence level 4. Since this is an offset approach, the pilot has to switch to a parallel runway and attempt to maintain the glide slope of the new runway once he is aligned with it.

Motion due to the flexibility of the aircraft becomes quite powerful when the pilot is required to input this much control, this is why the perceived turbulence intensity increased.

According to the Cooper Harper Ratings, this set of runs had a significant increase in the compensation required to maintain the glide slope and successfully land the aircraft. Even the level 4 turbulence case received a CHR of 8 (Run 22); an increase of one point in the glide slope rating from Run 18, Experiment 2. Only one run was incomplete (Run 28) and did not receive any CHR. The glide slope could not be maintained for a long enough time period to be rated, and the touchdown was never completed.

The task of repositioning the aircraft on approach with the parallel runway led to more unavoidable motion base failures. Luckily, most of these occurred when the aircraft was at or in close proximity to the touchdown point (indicated by **). This allowed the pilot to rate the glide slope task, and in some cases, the touchdown as well. The aircraft reaction and reaction inside aircraft criteria are detailed in Table 6.4.6.

| Experiment 3 – GHST | | | | | | |
|---|---------------------|-----------------------------------|----------|----------|-----------------|---------------------------------|
| | | Aircraft Reaction Criteria | | | | Reaction Inside Aircraft |
| Run Number | Base Failure | Altitude | Attitude | Airspeed | Controllability | Food Service & Walking |
| 21 | yes** | yes | yes | yes | yes | impossible |
| 22* | yes** | yes | yes | yes | yes | impossible |
| 23 | yes** | yes | yes | yes | yes | difficult |
| 24 | no | yes | yes | yes | yes | difficult |
| 25* | no | yes | yes | yes | yes | possible |
| 26 | no | yes | yes | yes | yes | possible |
| 27 | no | yes | yes | yes | yes | possible |
| 28 | yes | yes | yes | yes | yes | impossible |
| 29 | no | yes | yes | yes | yes | difficult |
| 30 | no | yes | yes | yes | yes | difficult |
| * Indicates incorrect intensity rating for that run | | | | | | |
| ** Notes that base failed at or near the touchdown location | | | | | | |

Table 6.4.6 – GHST Experiment 3, FAA Turbulence Reporting Criteria

For all experiments, the reaction criteria correspond to the pilot’s reported turbulence intensity. Under reported moderate turbulence, it is indicated that walking and food service is difficult (Runs 23 and 29). In light turbulence, food service and walking are possible (Runs 26 and 27). The resulting motion from the flexibility model always increased the difficulty to walk and serve food (see Runs 22, 30).

As with Experiment 2, the addition of the ATC (Configuration 2) had mixed results. In the light turbulence case, it increased the compensation necessary to perform the task (Run 27). In Run 23 (moderate turbulence), simply adding the ATC reduced the CHR of performing the touchdown. In Run 24 (severe turbulence), turning on the ATC caused the pilot to sense that less control input is required to maintain the glide slope.

Adding both the ATC and DASE model (Configuration 3) always resulted in an increased CHR for at least one of the ratings. This is attributed to the fact that the flexibility model heightens the response of the aircraft to pilot input. The motion cues from this flexibility are easily felt by the pilot and may have overpowered the added motion of the ATC in some runs.

Some of the ambiguities from all three GHSCT experiments can be attributed to the pilot's unfamiliarity with aircraft. For a study such as this one, the aircraft must not play a factor in the identification of the turbulence level. Runs 26 and 36 were not conducted with an atmospheric turbulence model or a flexible aircraft model, however, the pilot perceived the dynamics of the simulation to include continuous light turbulence or intermittent light turbulence.

The addition of the ATC seemed to have little effect on the pilot evaluation, and in some cases, allowed the pilot to adequately perform the task with reduced compensation. The turbulence channel has the potential to improve this simulation. Perhaps when the GHSCT rigid body model is complete, more conclusive results can be obtained from a similar set of experiments. With a more refined aircraft model, the pilot can better understand the GHSCT

dynamics. This will allow him to accurately assess the turbulence intensity and the new augmentation cues.

6.5 Generic High-Speed Civil Transport Study – Quantitative Results

6.5.1 GHSCCT: Experiments 1, 2 and 3: Quantitative Results

Quantitative results of the experiments conducted on the GHSCCT were not conclusive. The goal of the experiments was to gain insight into the effect of the ATC on the way the pilot controlled the aircraft. In order to perform this analysis, the pilot must have sufficient familiarity with the aircraft dynamics, and must also have the ability to perform the specific maneuvers.

It was mentioned in the subjective analysis that a considerable number of runs suffered from repeated motion base failures. The added motion from the DASE model tends to drive the base at high amplitudes. Performing a landing will also make use of more of the available actuator length. This also causes problems with the excursion limits.

The complexity of the experiments is also increased because of the addition of the aeroelastic cues. With both augmented channels, the pilot is receiving a tremendous amount of information as he tries to maintain altitude or land the aircraft.

One main difficulty with the subjective analysis is that the pilot was unable to accurately determine the turbulence intensity that the aircraft was subjected to. Without properly sensing the aircraft dynamics, analysis of the pilot control input is not applicable. In order to conduct quantitative analysis, the perception of the conditions which the aircraft is under must be accurate.

Without subjective analysis to support this data, the results are inconclusive. The mean square fluctuates far too much during these experiments to support stationarity and frequency analysis. The integration of the two augmented channels was successful; however, results on the accuracy of the additional motion cues are mostly indeterminate. Recommendations to improve and continue this study are provided in Chapter 7.

7. Conclusions and Future Recommendations

7.1 Summary and Conclusions

The goal of this project was to improve the simulation of disturbances above the frequency range of most pilot control input. Typically these motion cues are a response to atmospheric turbulence or aeroelastic bending of the aircraft. These two concepts were analyzed in this report with the intent of creating a more realistic flight simulation experience.

Using a standard motion cueing algorithm, simulation of the motion environment associated with atmospheric turbulence has been less than satisfactory; this results in attenuated and misrepresented cues being sent to the pilot. The primary goal of this research was to present to pilots a higher fidelity motion environment. There have been previous advancements in this area, Reid (1990) and Telban et al. (a). Analysis of their algorithms led to a revised turbulence channel implementation. This augmentation channel was designed to supplement the missing high frequency motion cues in the vertical degree of freedom.

The design of the Augmented Turbulence Channel (ATC) was based on the Telban et al. (a) implementation of the SUNY Nonlinear Algorithm. This algorithm had a tendency to cause the simulator to diverge during long runs. It was concluded that double integrating the signal produced by the turbulence channel was the cause of the divergence, and also contributed to the attenuation of the frequency content of the signal.

Further inspection of the original design revealed flaws which led to more changes in the architecture. The reduced order aircraft model was redesigned to better represent the dynamics of a specific aircraft. The original ROAC was modeled as a high-pass filter. In the original implementation, the output of the turbulence channel was sent through low bandwidth filters that

were not designed for signals with this frequency content. A high bandwidth cueing filter was designed to filter the output of the ATC.

Reduced order models were determined using parameter identification software. APID, which was developed at the Man-Machine Systems Research Lab, SUNY Binghamton, determines a linear model and verifies it based on PSD. For a single input, single output system, the PSD of the model is compared with the PSD of the data provided to the algorithm. This data represents the input and output to the system; in this case the input is the vertical turbulence gust vector and output is the vertical acceleration of the aircraft. This was chosen to identify the model because the frequency content of the ROAC is important, and must reflect the response of the NLAC model.

The ATC was implemented on two different simulated aircraft; the Large Civil Transport and the Generic High-Speed Civil Transport. A separate study was conducted on each aircraft. The GHSCT is also outfitted with an aeroelastic model. This model generates motion cues representing the bending of the fuselage in the vertical and lateral direction. The flexibility model was integrated with the turbulence channel to provide the pilot with both cues during the experiments.

Verification of the turbulence simulation was conducted subjectively and quantitatively. To evaluate the aircraft response to atmospheric turbulence, the FAA Airman's Guide to Reporting Turbulence was employed by the pilot. This guide has specific criteria for the aircraft response to turbulence and the reaction inside the aircraft. After each run, the pilot determined which criteria were met. Next, the results of the runs with and without the augmented turbulence channel were compared.

Before experiments could be conducted, the algorithm had to be tuned. The LCT implementation was tuned on the VMS; the GHSCT implementation was tuned on both the VMS and CMF, each at NASA Langley Research Center. The algorithms were tuned subjectively using the FAA Airman's Guide. The LCT implementation managed to meet almost all criteria at the different turbulence levels (light, moderate and severe). The Airman's Guide indicates that there will be a certain amount of seatbelt strain under moderate and severe turbulence. It also indicates that loose objects will be dislodged. Due to the motion limitations of the flight simulators, these criteria could not be met. With the LCT there were no issues meeting the altitude, attitude, airspeed, controllability, walking and food service criteria.

When tuning the GHSCT implementation, it was difficult to meet certain criteria in the Airman's Guide. The GHSCT is only outfitted with a translational turbulence model; unlike the LCT which supplements rotational turbulence motion in the primary cueing channel. This rotational response of the aircraft was necessary to meet the criteria for controllability and attitude fluctuations. When flying through severe turbulence, without the rotational turbulence model, changes in attitude were minimal. The guide also states that in severe turbulence, the aircraft may be momentarily out of positive control; this criterion was never met on the GHSCT. The reduced ability to walk and serve food was met with moderate turbulence, and rated impossible under severe turbulence.

Both studies included three types of experiments, each flown through different levels of turbulence. The first was to maintain straight and level flight, the second was to maintain the glide slope and perform a landing. The third experiment was an offset approach; the aircraft was trimmed on the glide slope and localizer of a runway and directed to land on a parallel runway.

Pilots would not normally be directed to perform landings in high intensity turbulence; however, training for this event will help prepare them if a situation such as this is unavoidable.

The LCT study and GHSCT study were both conducted on the VMS. After each run, the turbulence intensity was rated, and the pilot indicated which criteria were met from the FAA Airman's Guide.

The order of the experiments was randomized based on the turbulence level and configuration of the algorithm. In the experiments conducted with the LCT, there were two configurations: one with the ATC, one without. During these experiments the pilot was able to accurately identify the turbulence level for each run. Typically, there was a noticeable difference in the runs with and without the ATC.

The pilot rated his ability to maintain the glide slope using the Cooper Harper Rating scale. The touchdown task was also given a CHR. This scale uses specific descriptions with regard to the amount of pilot compensation needed to adequately perform the task. In some cases, the added motion from the ATC increased the CHR.

Each task became increasingly difficult under high levels of turbulence. In some cases, the added motion of the turbulence channel caused the pilot to rate the task with a lower CHR. The motivation for this decrease in the amount of compensation to perform the task is not clear. It is possible that the pilot has a better understanding of the aircraft motion with the augmented channel. The pilot should only provide control input when it is necessary; it's possible that the added cue allows the pilot to reduce his input and still adequately perform the task.

In order to conduct the quantitative evaluation of the augmented channel, the pilot control input was analyzed along with the response of the aircraft. Vertical velocity was chosen for the evaluation because it is a very important piece of aircraft state information during the

performance of this task. When maintaining altitude, the pilot will assess his deviation from altitude by monitoring vertical velocity. If the altitude begins to deviate, control input is applied to cancel growing vertical rates. Control input is maintained until the vertical velocity indicates the aircraft is returning to the task defined altitude.

For the first experiment, the pilot was directed to maintain altitude at 30,000 feet ASL. According to the quantitative results of the LCT study, this is the task where the pilot was most correlated with the aircraft dynamics. The analysis was conducted in the frequency domain. Under light and moderate turbulence, the pitch stick input of the pilot was more correlated with the aircraft vertical velocity with the ATC on. Inspecting the PSD of the pilot input showed changes in the operating frequencies of the pilot. The additional coherence showed that the added cue from the ATC increased the pilot's ability to respond to the turbulence cue.

In the severe turbulence case, adding the ATC reduced the correlation between the pitch stick input and the aircraft vertical velocity. This indicated that the pilot had more difficulty controlling the aircraft. When flying through severe turbulence, adding the ATC caused the PSD of the pilot to decrease across all frequencies. The peak operating frequency also shifted to a lower frequency. It appeared as though the pilot simply could not keep up with the cue and since the aircraft response comprised turbulence response, the lacking control input of the pilot reduced the coherence.

The fact that the pilot was less correlated in severe turbulence does not mean that the ATC does not add realism. In a real flight through this turbulence intensity, it is possible that the pilot has the same reaction. The main goal of a simulation such as this one is to replicate the workload of an actual flight, and that can be verified through other means.

When performing a landing, the pilot compensated for deviation from the glide slope by countering changes in the vertical rate of the aircraft. The aircraft sink rate was monitored throughout the run; control input was used to cancel building vertical rates and bring the aircraft back to the glide slope. Since experiments 2 and 3 were landing tasks, the quantitative results of these experiments were also based on the pilot input and the aircraft vertical velocity.

In experiment 2 of the LCT study, the aircraft started lined up on the approach and required the pilot to maintain the glide slope and perform the landing. This task required more pilot control input than maintaining altitude, but was still a task based on vertical velocity. The pilot also monitored glide slope error, to aid in determining how much input was needed to minimize the error. This was also a lateral tracking task where the pilot was directed to aim for the center of the runway touchdown zone. Since the ATC only impacted the vertical channel, the pilot's correlation with the lateral channel was not analyzed. Near the end of the approach, the pilot completed the landing using mainly visual cues.

Similar conclusions were formed from both experiments 1 and 2. According to the coherence function, the pilot was more correlated with the response of the aircraft at light and moderate turbulence. In these cases, the pilot increased the power of his control input over almost all frequencies when the ATC is on. The peak power tended to shift to the right.

Under severe turbulence, the trend in the pilot control input dynamics was reversed. It appeared that the addition of the ATC caused the pilot control to shift to lower frequencies and drop in power. The result was less correlation between the pilot input and vertical velocity. It was possible that the pilot just simply could not keep up with the intensity of the cue. Rather than responding to the high frequency motion, the pilot only added control input in lower frequencies. Results of experiment 2 did not have as much coherence as the experiment 1

analysis. This was due to the fact that the pilot was performing a more advanced task, and more factors affected his pitch stick input.

Experiment 3 was the most control intensive task, and led to less conclusive quantitative results. It was difficult to perform frequency analysis on these runs because the task required various pilot control inputs. Since this was an offset approach, the pilot had to maneuver the aircraft to align it with the parallel runway. This entire run is conducted with turbulence and the control input during the run is not necessarily a response to changes in the aircraft vertical velocity. Because of this, inspecting the coherence function can only provide minimal insight into the effect of the ATC. Stationarity of the signal was also a factor, limiting the ability to conduct frequency analysis.

When adding the ATC, the work done by the pilot increased substantially during light and moderate turbulence. Just as in experiment 1, there was a decrease in the overall work done by the pilot when flying through severe turbulence.

The same three experiments were conducted during the GHSCT study. There were three configurations of the GHSCT; the first configuration had no ATC and no aeroelastic model. The second configuration employs the ATC. The third configuration uses both the ATC and aeroelastic model.

Like the LCT study, the run order was randomized based on the configuration of the algorithm and turbulence level. These experiments yielded inconclusive results, both subjectively and quantitatively. The subjective analysis of experiment 1 indicated that the pilot was unable to determine the turbulence intensity for most runs. In moderate and severe turbulence, the perceived intensity was always lower than the actual intensity. Also, criteria for severe turbulence were never met in this experiment.

During experiment 2, the pilot incorrectly identified the turbulence intensity for 6 out of 10 runs. Severe turbulence was achieved during this experiment; an improvement over the previous experiment. In most cases, the activation of the aeroelastic channel caused the pilot to perceive a higher turbulence intensity, even though the turbulence level was not changed. Level 4 turbulence (moderate) was identified as light turbulence without the ATC or DASE Model; however activating both of the augmentation channels caused the intensity to be reported as severe.

The DASE model response was almost entirely due to pilot control input. As the pilot maintained the glide slope and compensated for turbulence, control inputs excited the bending modes of the fuselage. The additional motion resulted in an increase in the perceived turbulence intensity.

Another source of ambiguity was from the results of the run without turbulence. During this run, the pilot reported light, intermittent turbulence. There was no flexibility model during this run. The sensation of turbulence indicated that the aircraft response to the pilot was erratic enough to feel like turbulence.

Experiment 3 required the most work by the pilot. This experiment also had the most issues with tracking errors and excursion limits of the simulator motion base. The task required a great deal of pilot input which drove the simulator towards its physical limits. In most cases, the motion base failures occurred late in the run, allowing the pilot to provide a CHR for both the glide slope and the landing.

Out of all three GHST experiments, turbulence intensity was reported with the most accuracy on this task. Only two runs were incorrectly identified. Similarly to experiment 2, the run with no turbulence was reported to be light, continuous turbulence. During this run, aircraft

dynamics were not being driven by external gust inputs, or aeroelastic effects. This indicates that a portion of the aircraft response to control inputs was not completely understood by the pilot.

Without the ability to support quantitative analysis with pilot perception, the analytical results were inconclusive. The frequency analysis was also hindered by the lack of stationarity in the signal. The pilot's response to the aircraft was more erratic and usable portions of data could not be isolated.

Aside from the inconsistencies with the results, the augmented channel was successfully implemented along with the aeroelastic channel on the GHSCT. Currently, it appears that the aircraft dynamics were affecting the pilot's ability to analyze the turbulence simulation. Further tuning and refining of the channel may lead to more conclusive results.

7.2 Future Recommendations

It would be beneficial to continue this study to further investigate some of the ambiguities in both the subjective and quantitative results. Based on the Cooper Harper Ratings, there were instances when the pilot's subjective analysis indicated that the addition of the ATC negatively affected the handling qualities of the simulation. There are other cases where the opposite occurred. A multi-pilot study can determine trends in the CHR and allow for more conclusive results.

Some ambiguities in the quantitative results of the LCT study indicate that there may be a need to further refine the augmented turbulence algorithm. During the severe turbulence runs, the power of the pilot control input decreased over all frequencies. This reduced the correlation between the pilot input and aircraft response. This decrease in correlation does not warrant

changes to the algorithm if it reflects the true reaction of the pilot in this turbulence intensity. One way to assess this is to compare actual flight data to the results of these experiments. If modifications are applicable, the algorithm will have to be tuned again, and reevaluated subjectively and quantitatively.

Currently it seems that the most attenuated degree of freedom is the vertical channel; however, the addition of another ATC in the lateral degree of freedom could benefit the simulation. Lateral cues produced from atmospheric turbulence can be modeled in the same fashion; using a reduced order aircraft model and adding a position augmentation cue to the lateral motion cue before driving the motion system. This channel could be developed and tested by having the pilot perform a task that requires more lateral response compensation. This added motion has the potential to allow the simulation to meet more criteria from the FAA turbulence reporting standard; such as seat belt strain or object displacement.

The GHSCT simulation would benefit from the addition of a rotational turbulence model. The Mil-F-8785B model has been implemented on the LCT and produces adequate rotational cues. These cues allow most of the FAA turbulence criteria to be met during the LCT simulation, something that was not the case in the GSCHT runs. If the additional cue is enough to meet more of the subjective turbulence criteria, then another GHSCT study should be conducted. The ATC has the potential to add realism to the GHSCT simulation and compliment the cues produced by the flexible aircraft dynamics.

Further verification of the turbulence channel is necessary to validate the augmented algorithm. In order to do this, results of a multi-pilot study must clearly indicate a more realistic simulation is provided to the pilot by the ATC. Pilots should fly different versions of the

algorithm and rate the realism provided by the simulation. Finally, pilot workload analysis should be compared to actual flight data.

Appendices

Appendix A: Turbulence Spectrums Defined:

1. Dryden Spectrum Translational Turbulence Model:

$$\phi_u(\omega) = \frac{L}{V} \frac{2\sigma^2}{\pi} \frac{1}{1 + \left(\frac{L\omega}{V}\right)^2} \quad \phi_v(\omega) = \frac{L}{V} \frac{\sigma^2}{\pi} \frac{1 + 3\left(\frac{L\omega}{V}\right)^2}{\left[1 + \left(\frac{L\omega}{V}\right)^2\right]^2} \quad \phi_w(\omega) = \frac{L}{V} \frac{\sigma^2}{\pi} \frac{1 + 3\left(\frac{L\omega}{V}\right)^2}{\left[1 + \left(\frac{L\omega}{V}\right)^2\right]^2}$$

$$\phi_{u_g}(\Omega) = \sigma_u^2 \frac{2L_u}{\pi} \frac{1}{1 + (L_u\Omega)^2} \quad \phi_{v_g}(\Omega) = \sigma_v^2 \frac{L_v}{\pi} \frac{1 + 3(L_v\Omega)^2}{\left[1 + (L_v\Omega)^2\right]^2} \quad \phi_{w_g}(\Omega) = \sigma_w^2 \frac{L_w}{\pi} \frac{1 + 3(L_w\Omega)^2}{\left[1 + (L_w\Omega)^2\right]^2}$$

Variables Defined:

ϕ_u Longitudinal Spectrum component of turbulence $\frac{m}{(\text{rad} \cdot \text{s}^2)}$

ϕ_v Lateral Spectrum component of turbulence $\frac{m}{(\text{rad} \cdot \text{s}^2)}$

ϕ_w Vertical Spectrum component of turbulence $\frac{m}{(\text{rad} \cdot \text{s}^2)}$

σ^2 Variance of turbulence $\frac{m^2}{\text{s}^2}$

Ω Wave Number $\frac{\text{rad}}{m}$

ω Frequency $\frac{\text{rad}}{s}$

V Mean velocity of the mean wind vector relative to the aerospace vehicle $\frac{m}{s}$

ϕ_{u_g} Longitudinal Spectrum component of gust $\frac{m}{(\text{rad} \cdot \text{s}^2)}$

ϕ_{v_g} Lateral Spectrum component of gust $\frac{m}{(\text{rad} \cdot \text{s}^2)}$

ϕ_{w_g} Vertical Spectrum component of gust $\frac{m}{(\text{rad} \cdot \text{s}^2)}$

σ_u^2 Variance of turbulence in longitudinal direction $\frac{m^2}{\text{s}^2}$

- σ_v^2 Variance of turbulence in the lateral direction $\frac{m^2}{s^2}$
 σ_w^2 Variance of turbulence in the vertical direction $\frac{m^2}{s^2}$
 L_u Length scale of turbulence in longitudinal direction m
 L_v Length scale of turbulence in lateral direction m
 L_w Length scale of turbulence in vertical direction m

2. MIL-F-8785B Rotational Turbulence Model

$$\phi_{p_g}(\Omega) = \frac{\sigma_w^2 \cdot 8 \left(\frac{\pi L_w}{4b} \right)^{1/3}}{L_w \left[1 + \left(\frac{4b}{\pi} \Omega \right)^2 \right]} \quad \phi_{q_g}(\Omega) = \frac{\Omega^2}{1 + \left(\frac{4b}{\pi} \Omega \right)^2} \cdot \phi_{w_g}(\Omega) \quad \phi_{r_g}(\Omega) = \frac{\Omega^2}{1 + \left(\frac{3b}{\pi} \Omega \right)^2} \cdot \phi_{v_g}(\Omega)$$

$$p_g = -\frac{\partial w_g}{\partial y} \quad q_g = +\frac{\partial w_g}{\partial x} \quad v_g = -\frac{\partial v_g}{\partial x}$$

Variables Defined:

- L_u Length scale of turbulence in longitudinal direction
 L_v Length scale of turbulence in lateral direction
 L_w Length scale of turbulence in vertical direction
 ϕ_{p_g} p-rotational Spectrum component of gust
 ϕ_{q_g} q-rotational Spectrum component of gust
 ϕ_{r_g} r-rotational Spectrum component of gust
 p_g p-rotational velocity component of gust
 q_g q-rotational velocity component of gust
 v_g Lateral turbulence velocity

b Wing Span

Appendix B: Fortran code for ATC; DASE model parameters

Fortran code for augmented turbulence channel implementation:

c Modified Turbulence Channel
c Comprising: Reduced Order Aircraft Model (ROAC)
c and Turbulence Cueing Filter

```
      SUBROUTINE TURB_CHANNEL                ! added by GAT

      INCLUDE "comint2.com"                 ! added by GAT
      INCLUDE "wcomgust.com"               ! added by GAT
      INCLUDE "optint3.com"                ! added by lck
```

c Define coefficients

```
      REAL HT1N4,HT1N3,HT1N2,HT1N1,HT1N0,HT1D3,HT1D2,HT1D1,HT1D0
      REAL WTN4,WTN3,WTN2,WTN1,WTN0,WTD3,WTD2,WTD1,WTD0
      REAL KT
```

```
      REAL DT                                ! added by GAT
      REAL BTW1
      REAL BT1,CT1,DT1,BT2,CT2,DT2          ! added by GAT
      REAL CTW1,DTW1,ETW1,BTW2,CTW2,DTW2,ETW2 ! added by GAT
```

c Turbulence Cueing Filter

```
      DATA HT1N3,HT1N2,HT1N1,HT1N0,
+ HT1D2,HT1D1,HT1D0/
```

```
+ 0.0000,49.35,24.67,0.000,
+ 50.59,61.94,12.34/
```

c Reduced Order Aircraft Model

```
      DATA WTN4,WTN3,WTN2,WTN1,WTN0,
+ WTD3,WTD2,WTD1,WTD0/
```

```
+ 0.0000,0.000,7,2.94,0.63,
+ 28.84,423.6,336.9,12.8/
```

```
      DT = H                                ! added by GAT
```

C
C
C

Compute Augmented Acceleration from W-Gust

```
      BTW1=DT*(-WTD3*YW1O+YW2O+(WTN3-WTD3*WTN4)*WGUSTO)
      CTW1=DT*(-WTD2*YW1O+YW3O+(WTN2-WTD2*WTN4)*WGUSTO)
      DTW1=DT*(-WTD1*YW1O+YW4O+(WTN1-WTD1*WTN4)*WGUSTO)
      ETW1=DT*(-WTD0*YW1O+(WTN0-WTD0*WTN4)*WGUSTO)

      BTW2=DT*(-WTD3*(YW1O+BTW1)+YW2O+CTW1+(WTN3-WTD3*WTN4)*WGUST)
      CTW2=DT*(-WTD2*(YW1O+BTW1)+YW3O+DTW1+(WTN2-WTD2*WTN4)*WGUST)
      DTW2=DT*(-WTD1*(YW1O+BTW1)+YW4O+ETW1+(WTN1-WTD1*WTN4)*WGUST)
      ETW2=DT*(-WTD0*(YW1O+BTW1)+(WTN0-WTD0*WTN4)*WGUST)
```

YYW1=YW1O+0.5*(BTW1+BTW2)
YW2=YW2O+0.5*(CTW1+CTW2)
YW3=YW3O+0.5*(DTW1+DTW2)
YW4=YW4O+0.5*(ETW1+ETW2)

ACZT=YYW1+WTN4*WGUST
ACZT=ACZT*9.81*KT

YW1O=YYW1
YW2O=YW2
YW3O=YW3
YW4O=YW4

WGUSTO=WGUST

C

C APPLY THE FILTER (Remove comments to run with filter)

C

c BT1=DT*(-HT1D2*Y1O+Y2O+(HT1N2-HT1D2*HT1N3)*ACZTO)

c CT1=DT*(-HT1D1*Y1O+Y3O+(HT1N1-HT1D1*HT1N3)*ACZTO)

c DT1=DT*(-HT1D0*Y1O+(HT1N0-HT1D0*HT1N3)*ACZTO)

c BT2=DT*(-HT1D2*(Y1O+BT1)+Y2O+CT1+(HT1N2-HT1D2*HT1N3)*ACZT)

c CT2=DT*(-HT1D1*(Y1O+BT1)+Y3O+DT1+(HT1N1-HT1D1*HT1N3)*ACZT)

c DT2=DT*(-HT1D0*(Y1O+BT1)+(HT1N0-HT1D0*HT1N3)*ACZT)

c YY1=Y1O+0.5*(BT1+BT2)

c Y2=Y2O+0.5*(CT1+CT2)

c Y3=Y3O+0.5*(DT1+DT2)

c ACZTF=YY1+HT1N3*ACZT

Y1O=YY1

Y2O=Y2

Y3O=Y3

ACZTO=ACZT

END

! added by GAT

DASE Model Parameters:

Note: all experiments used DASE Model 1

| DASE Model 1 | | | |
|--------------------------|---------------------------|---------|---------------|
| Bending Mode | Natural Frequency (rad/s) | Gain | Damping Ratio |
| 1st Pitch | 1.45 | -1.9074 | 0.03 |
| 1st Yaw | 1.61 | -1.9074 | 0.03 |
| 2nd Pitch | 2.33 | -0.2429 | 0.03 |
| 2nd Yaw | 2.47 | -0.2429 | 0.03 |
| 3rd Pitch | 3.13 | -0.0221 | 0.03 |
| 3rd Yaw | 3.27 | -0.0221 | 0.03 |
| DASE Model 2 | | | |
| Bending Mode: Number and | Natural Frequency | Gain | Damping Ratio |
| 1st Pitch | 2 | -2.537 | 0.03 |
| 1st Yaw | 2.22 | -0.763 | 0.03 |
| 2nd Pitch | 3.22 | -0.2429 | 0.03 |
| 2nd Yaw | 3.41 | -0.2429 | 0.03 |
| 3rd Pitch | 4.32 | -0.0221 | 0.03 |
| 3rd Yaw | 4.51 | -0.0221 | 0.03 |
| DASE Model 3 | | | |
| Bending Mode: Number and | Natural Frequency | Gain | Damping Ratio |
| 1st Pitch | 1.45 | -4.58 | 0.03 |
| 1st Yaw | 1.61 | -1.9074 | 0.03 |
| 2nd Pitch | 2.33 | -0.2429 | 0.03 |
| 2nd Yaw | 2.47 | -0.2429 | 0.03 |
| 3rd Pitch | 3.13 | -0.0221 | 0.03 |
| 3rd Yaw | 3.27 | -0.0221 | 0.03 |

Appendix C: FAA Airman’s Guide to Reporting Turbulence Intensity (TBL 7-9-1)

| Intensity | Aircraft Reaction | Reaction Inside Aircraft | Reporting Term-Definition |
|---|---|---|--|
| Light | <p>Turbulence that momentarily causes slight erratic changes in altitude and/or attitude (pitch, roll, yaw) Report as Light Turbulence;*</p> <p>or</p> <p>Turbulence that causes slight rapid and somewhat rythmic bumpiness without appreciable changes in altitude or attitude. Report as Light Chop.</p> | Occupants may feel a slight strain against seat belts or shoulder straps. Unsecured objects may be displaced slightly. Food service may be conducted and a little or no difficulty is encountered in walking. | <p>Occasional –Less than 1/3 of the time.</p> <p>Intermittent – 1/3 to 2/3</p> <p>Continuous – More than 2/3</p> |
| Moderate | <p>Turbulence that is similar to Light Turbulence but of greater intensity. Changes in altitude and/or attitude occur but the aircraft remains in positive control at all times. It usually causes variations in indicated airspeed. Report as Moderate Turbulence;*</p> <p>or</p> <p>Turbulence that is similar to Light Chop but of greater intensity. It causes rapid bumps or jolts without appreciable changes in aircraft altitude or attitude. Report as Moderate Chop.*</p> | Occupants feel definite strains against seat belts or shoulder straps. Unsecured objects are dislodged. Food service and walking are difficult. | |
| Severe | Turbulence that cause large, abrupt changes in altitude and/or attitude. It usually causes large variations in indicated airspeed. Aircraft may be momentarily out of control. Report as Severe Turbulence.* | Occupants are forced violently against seat belts or shoulder straps. Unsecured objects are tossed about. Food service and walking are impossible. | |
| Extreme | Turbulence in which the aircraft is violently tossed about and is practically impossible to control. It may cause structural damage. Report as Extreme Turbulence.* | | |
| * High level turbulence (normally above 15,000 feet) not associated with cumuliform cloudiness, including thunderstorms, should be reported as CAT (clear air turbulence) preceded by the appropriate intensity, or light or moderate chop. | | | |
| <p>NOTE:</p> <p>1. Pilots should report location(s), time (UTC), intensity, whether in or near clouds, altitude, type of aircraft and, when applicable, duration of turbulence</p> <p>2. Duration may be based on time between two locations or over a single location. All locations should be readily identifiable.</p> | | | |

Appendix D: Gain Tuning Test Plans

Test Plan for LCT:

Record video and audio (pilot comments) during runs

- Initial Flight Test (without motion)
 - Ensure motion system commands will not overdrive the system
- Initial Flight Test (with motion)
 - Ensure aircraft reacts properly to pilot input
 - Test data recording of A/C output
 - Test data recording of simulator sensors
- Turbulence Gain Tuning, Turbulence Cueing Filter OFF:
 - For all runs, trim to 30,000 ft., M=0.8
 - Initialize Gain at 0.05 (tuned gain from last visit)
 - Test flight without motion – look for bump when going to operate (VMS only) and ensure turbulence channel is not producing cues that will overdrive the motion base
 - Tuning Flights – Start with low turbulence level and adjust gain after all runs
 - Turbulence lvl 1
 - Note if gain needs to be adjusted (only adjust if cues are overdriving simulator)
 - Turbulence lvl 4
 - Note if gain needs to be adjusted
 - Turbulence lvl 6
 - Note if gain needs to be adjusted
 - Turbulence lvl 7
 - Note if gain needs to be adjusted
 - After running with turbulence level 7, adjust gain accordingly and test lower levels of turbulence until tuning is complete
- Turbulence Gain Tuning, Turbulence Cueing Filter ON:
 - For all runs, trim to 30,000 ft., M=0.8
 - Initialize Gain at 0.05
 - Test flight without motion – Ensure turbulence channel is not producing cues that will overdrive the motion base
 - Tuning Flights – Start with low turbulence level and adjust gain after all runs
 - Turbulence lvl 1
 - Note if gain needs to be adjusted (only adjust if cues are overdriving simulator)
 - Turbulence lvl 4
 - Note if gain needs to be adjusted
 - Turbulence lvl 6
 - Note if gain needs to be adjusted
 - Turbulence lvl 7
 - Note if gain needs to be adjusted

- After running with turbulence level 7, adjust gain accordingly and test lower levels of turbulence until tuning is complete

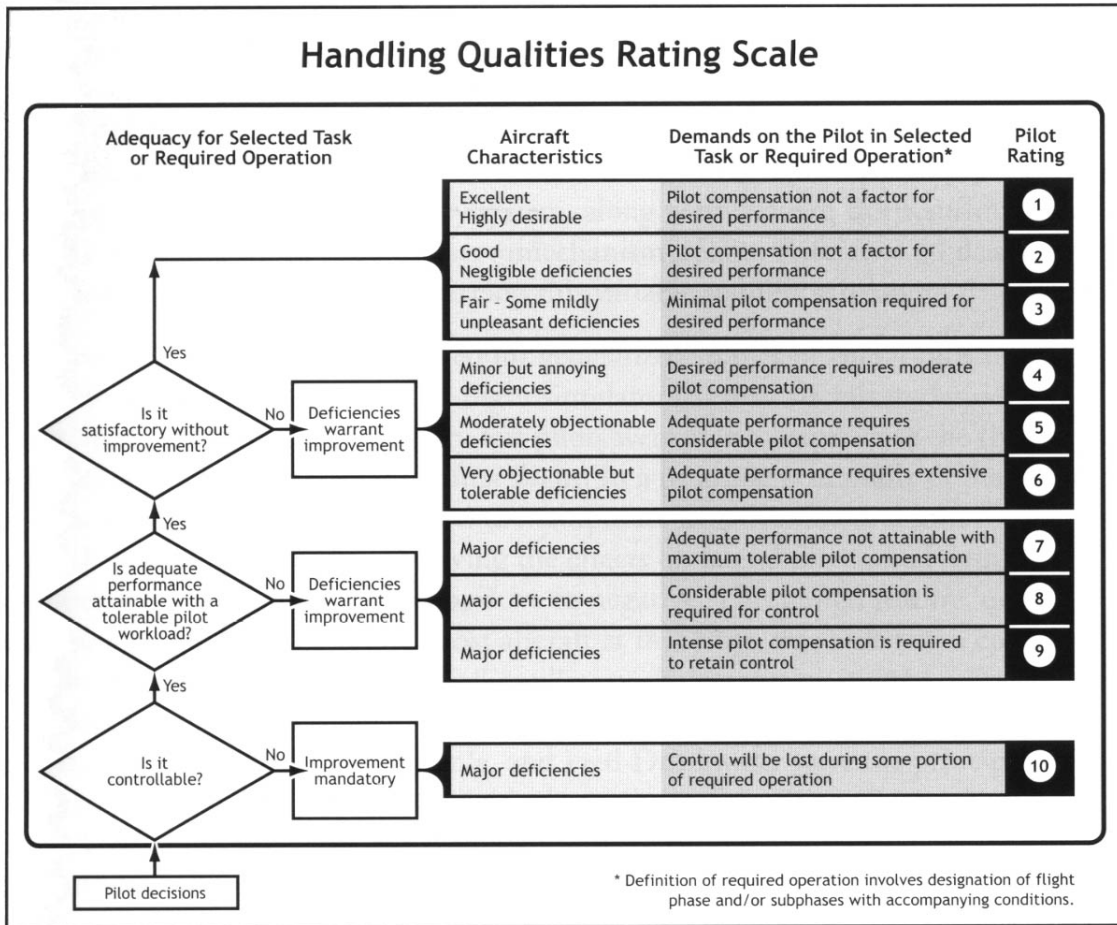
Test Plan for GHSCT:

Record video and audio (pilot comments) during runs

- Initial Flight Test (without motion)
 - Ensure motion system commands will not overdrive the system
- Initial Flight Test (with motion)
 - Ensure aircraft reacts properly to pilot input
 - Test data recording of A/C output
 - Test data recording of simulator sensors
- Turbulence Gain Tuning, Turbulence Cueing Filter OFF, Aeroelastic Model OFF:
 - For all runs, trim to 30,000 ft., M=0.8
 - Initialize Gain at 0.02 (tuned gain for original ROAC on GHSCT)
 - Test flight without motion – Ensure turbulence channel is not producing cues that will overdrive the motion base
 - Tuning Flights – Start with low turbulence level and adjust gain after all runs
 - Turbulence lvl 1
 - Note if gain needs to be adjusted (only adjust if cues are overdriving simulator)
 - Turbulence lvl 4
 - Note if gain needs to be adjusted
 - Turbulence lvl 6
 - Note if gain needs to be adjusted
 - Turbulence lvl 7
 - Note if gain needs to be adjusted
 - After running with turbulence level 7, adjust gain accordingly and test lower levels of turbulence until tuning is complete
- Repeat above tuning for each Aeroelastic Model
- Turbulence Gain Tuning, Turbulence Cueing Filter ON, Aeroelastic Model OFF:
 - For all runs, trim to 30,000 ft., M=0.8
 - Initialize Gain at 0.02
 - Test flight without motion – Ensure turbulence channel is not producing cues that will overdrive the motion base
 - Tuning Flights – Start with low turbulence level and adjust gain after all runs
 - Turbulence lvl 1
 - Note if gain needs to be adjusted (only adjust if cues are overdriving simulator)
 - Turbulence lvl 4
 - Note if gain needs to be adjusted

- Turbulence lvl 6
 - Note if gain needs to be adjusted
 - Turbulence lvl 7
 - Note if gain needs to be adjusted
 - After running with turbulence level 7, adjust gain accordingly and test lower levels of turbulence until tuning is complete
-
- Repeat above tuning for each available aeroelastic model

Appendix E: Cooper-Harper Rating Scale



Appendix F: Experiment Conditions and Run Order

Large Civil Transport Experiments: Run Order, Configuration, and Turbulence Level

Initial Test Plan for LCT:

Record video and audio (pilot comments) during runs

- Initial Flight Test (without motion)
 - Ensure motion system commands will not overdrive the system
- Initial Flight Test (with motion)
 - Ensure aircraft reacts properly to pilot input
 - Test data recording of A/C output
 - Test data recording of simulator sensors (all accelerometers)
- Begin Experiments

| Run Order | Run Number - Data file number | Configuration | Turbulence level |
|---|-------------------------------|---------------|------------------|
| Experiment 1: Maintain straight and level flight at 30000 feet ASL | | | |
| 1 | | 2 | 4 |
| 2 | | 1 | 6 |
| 3 | | 1 | 2 |
| 4 | | 1 | OFF |
| 5 | | 2 | 2 |
| 6 | | 1 | 4 |
| 7 | | 2 | 6 |
| Experiment 2: Straight in approach and landing | | | |
| 1 | | 1 | 2 |
| 2 | | 1 | 4 |
| 3 | | 1 | 6 |
| 4 | | 2 | 4 |
| 5 | | 1 | OFF |
| 6 | | 2 | 2 |
| 7 | | 2 | 6 |
| Experiment 3: Offset approach and landing | | | |
| 1 | | 1 | 6 |
| 2 | | 1 | 4 |
| 3 | | 1 | 2 |
| 4 | | 2 | 4 |
| 5 | | 1 | OFF |
| 6 | | 2 | 2 |
| 7 | | 2 | 6 |

Run order and conditions for LCT experiments

GHSCT Experiments: Run Order, Configuration, and Turbulence Level

Initial Test Plan for GHSCT:

Record video and audio (pilot comments) during runs

- Initial Flight Test (without motion)
 - Ensure motion system commands will not overdrive the system
- Initial Flight Test (with motion)

- Ensure aircraft reacts properly to pilot input
 - Test data recording of A/C output
 - Test data recording of simulator sensors (all accelerometers)
- Begin Experiments

| Run Order | Run Number - Data file number | Configuration | Turbulence level |
|---|-------------------------------|---------------|------------------|
| Experiment 1: Maintain straight and level flight at 30000 feet ASL | | | |
| 1 | | 1 | OFF |
| 2 | | 2 | 6 |
| 3 | | 1 | 4 |
| 4 | | 3 | 2 |
| 5 | | 1 | 6 |
| 6 | | 1 | 2 |
| 7 | | 3 | 4 |
| 8 | | 2 | 4 |
| 9 | | 2 | 2 |
| 10 | | 3 | 6 |
| Experiment 2: Straight in approach and landing | | | |
| 1 | | 2 | 4 |
| 2 | | 1 | 2 |
| 3 | | 1 | 4 |
| 4 | | 1 | 6 |
| 5 | | 3 | 2 |
| 6 | | 3 | 6 |
| 7 | | 2 | 6 |
| 8 | | 3 | 4 |
| 9 | | 1 | OFF |
| 10 | | 2 | 2 |
| Experiment 3: Offset approach and landing | | | |
| 1 | | 1 | 6 |
| 2 | | 3 | 4 |
| 3 | | 2 | 4 |
| 4 | | 2 | 6 |
| 5 | | 1 | OFF |
| 6 | | 1 | 2 |
| 7 | | 2 | 2 |
| 8 | | 3 | 6 |
| 9 | | 1 | 4 |
| 10 | | 3 | 2 |

Run order and conditions for GHSC experiments

References

1. Beal, T.R. (1993): Digital Simulation of Atmospheric Turbulence for Dryden and von Karman Models. *Journal of Guidance, Control, and Dynamics*, Vol. 16, no.1
2. Conrad, B.; Schmidt, S. F.' Douvillier, J. G. (1973): Washout Circuit Design for Multi-Degree-of-Freedom Moving Base Simulators. AIAA Visual and Motion Simulation Conference
3. Davis, Randall C., Keith Hoffler. (2009): Generic Dynamics Flexural Model for Slender Bodies Aircraft. AIAA Modeling and Simulation Technologies
4. Dinu, A.D., R.M. Botez, Iulian Cotoi. (2006): Chebyshev Polynomials for Unsteady Aerodynamic Calculations in Aeroservoelasticity. *Journal of Aircraft*, Vol. 43, no.1
5. Ercole Anthony V., Frank M. Cardullo, Kirill Zaychik, Lon Kelly, Jacob Houck. (2009): Motion Cueing Algorithm Modification for Improved Turbulence Simulation. AIAA Modeling and Simulation Technologies Conference.
6. Federal Aviation Administration Aeronautical Information Manual. February 11, 2010. http://www.faa.gov/air_traffic/publications/atpubs/aim/.
7. Flying Qualities of Piloted Aircraft. Department of Defense Handbook. MIL-STD-1797A
8. Garrod, Stuart T., L.D. Reid. (1994): Pilot Evaluations of Augmented Flight Simulator Motion. *Journal of Aircraft*, Vol. 31, no. 4, July-Aug. 1994.
9. Houbolt, J.C., Roy Steiner, K.G. Pratt. (1964) Dynamic Response of Airplanes to Atmospheric Turbulence including Flight Data on Input and Response. NASA TR R-199. Langley Research Center, Hampton, Va.
10. Jackson, E.B., D.L. Raney, D.E. Hahne, S.D. Derry, L.J. Glaab. (1999): Reference H Piloted Assessment (LaRC.1) Pilot Briefing Guide. NASA/TM-1999-209533
11. Parrish, R.V., J.E. Dieudonne, R.L. Bowles, D.J. Martin. (1973): Coordinated Adaptive Washout for Motion Simulators. AIAA Visual and Motion Simulation Conference (1973). No. 73-930
12. Raney, D.L., E.B. Jackson, C.S. Buttrill. (2002): Simulation Study of Impact of Aerolastic Characteristics on Flying Qualities of a High Speed Civil Transport. NASA/TP-2002-211943. Langley Research Center, Hampton, Va.
13. Reid, L.D., P.A. Robinson. (1990): Augmenting Flight Simulator Motion Response to Turbulence. *Journal of Aircraft*, Vol. 27, no. 4
14. Reid, L.D.,M.A. Nahon. (1985): Flight Simulation Motion-Base Drive Algorithms: Part 1- Developing and Testing the Equations. Utias Report No. 296.
15. Reid, L.D.,M.A. Nahon. (a) (1986): Flight Simulation Motion-Base Drive Algorithms: Part 2- Selecting the System Parameters. Utias Report No. 307.

16. Reid, L.D., M.A. Nahon. (b) (1986): Flight Simulation Motion-Base Drive Algorithms: Part 3- Pilot Evaluations. Utias Report No. 319.
17. Telban, R.J., Weimin Wu, F.M. Cardullo. (2000): Motion Cueing Algorithm Development: Initial Investigation and Redesign of the Algorithms. NASA/CR-2000-209863.
18. Telban, R.J., Frank M. Cardullo. (a) (2005): Motion Cueing Algorithm Development: New Motion Cueing Program Implementation and Tuning. NASA/CR-2005-213746
19. Telban, R.J., Frank M. Cardullo. (b) (2005): Motion Cueing Algorithm Development: Human-Centered Linear and Nonlinear Approaches. NASA/CR-2005-213747
20. Terrestrial Environment (Climatic) Criteria Handbook for Use in Aerospace Vehicle Development. NASA-HDBK-1001. August 11, 2000
21. Zaychik, Kirill B. (2009): Intelligent Systems Approach for Automated Identification of Individual Control Behavior of a Human Operator. PhD Thesis, Binghamton University, State University of New York. New York

REPORT DOCUMENTATION PAGE

*Form Approved
OMB No. 0704-0188*

The public reporting burden for this collection of information is estimated to average 1 hour per response, including the time for reviewing instructions, searching existing data sources, gathering and maintaining the data needed, and completing and reviewing the collection of information. Send comments regarding this burden estimate or any other aspect of this collection of information, including suggestions for reducing this burden, to Department of Defense, Washington Headquarters Services, Directorate for Information Operations and Reports (0704-0188), 1215 Jefferson Davis Highway, Suite 1204, Arlington, VA 22202-4302. Respondents should be aware that notwithstanding any other provision of law, no person shall be subject to any penalty for failing to comply with a collection of information if it does not display a currently valid OMB control number.
PLEASE DO NOT RETURN YOUR FORM TO THE ABOVE ADDRESS.

| | | | | | | |
|---|--------------------|---------------------|---|----------------------------|--|--|
| 1. REPORT DATE (DD-MM-YYYY) 01-08 - 2012 | | | 2. REPORT TYPE Technical Memorandum | | 3. DATES COVERED (From - To) | |
| 4. TITLE AND SUBTITLE Algorithm for Simulating Atmospheric Turbulence and Aeroelastic Effects on Simulator Motion Systems | | | | | 5a. CONTRACT NUMBER | |
| | | | | | 5b. GRANT NUMBER | |
| | | | | | 5c. PROGRAM ELEMENT NUMBER | |
| 6. AUTHOR(S) Ercole, Anthony V.; Cardullo, Frank M.; Kelly, Lon C.; Houck, Jacob A. | | | | | 5d. PROJECT NUMBER | |
| | | | | | 5e. TASK NUMBER | |
| | | | | | 5f. WORK UNIT NUMBER 160961.01.01.01 | |
| 7. PERFORMING ORGANIZATION NAME(S) AND ADDRESS(ES) NASA Langley Research Center Hampton, VA 23681-2199 | | | | | 8. PERFORMING ORGANIZATION REPORT NUMBER L-20173 | |
| 9. SPONSORING/MONITORING AGENCY NAME(S) AND ADDRESS(ES) National Aeronautics and Space Administration Washington, DC 20546-0001 | | | | | 10. SPONSOR/MONITOR'S ACRONYM(S) NASA | |
| | | | | | 11. SPONSOR/MONITOR'S REPORT NUMBER(S) NASA/TM-2012-217601 | |
| 12. DISTRIBUTION/AVAILABILITY STATEMENT Unclassified - Unlimited Subject Category 54 Availability: NASA CASI (443) 757-5802 | | | | | | |
| 13. SUPPLEMENTARY NOTES | | | | | | |
| 14. ABSTRACT Atmospheric turbulence produces high frequency accelerations in aircraft, typically greater than the response to pilot input. Motion system equipped flight simulators must present cues representative of the aircraft response to turbulence in order to maintain the integrity of the simulation. Currently, turbulence motion cueing produced by flight simulator motion systems has been less than satisfactory because the turbulence profiles have been attenuated by the motion cueing algorithms. This report presents a new turbulence motion cueing algorithm, referred to as the augmented turbulence channel. Like the previous turbulence algorithms, the output of the channel only augments the vertical degree of freedom of motion. This algorithm employs a parallel aircraft model and an optional high bandwidth cueing filter. Simulation of aeroelastic effects is also an area where frequency content must be preserved by the cueing algorithm. The current aeroelastic implementation uses a similar secondary channel that supplements the primary motion cue. Two studies were conducted using the NASA Langley Visual Motion Simulator and Cockpit Motion Facility to evaluate the effect of the turbulence channel and aeroelastic model on pilot control input. Results indicate that the pilot is better correlated with the aircraft response, when the augmented channel is in place. | | | | | | |
| 15. SUBJECT TERMS Aeroelastic; Cueing algorithms; Flight simulator; Motion systems; Turbulence | | | | | | |
| 16. SECURITY CLASSIFICATION OF: | | | 17. LIMITATION OF ABSTRACT | 18. NUMBER OF PAGES | 19a. NAME OF RESPONSIBLE PERSON | |
| a. REPORT | b. ABSTRACT | c. THIS PAGE | | | STI Help Desk (email: help@sti.nasa.gov) | |
| U | U | U | UU | 174 | 19b. TELEPHONE NUMBER (Include area code) (443) 757-5802 | |